Predictive Chemical Kinetics for Auto Ignition of Fuel Blends

by

Nathan W. Yee

M.S., Chemical Engineering Practice
Massachusetts Institute of Technology, 2016
B.S., Chemical and Biomolecular Engineering
University of Illinois at Urbana-Champaign, 2011

SUBMITTED TO THE DEPARTMENT OF CHEMICAL ENGINEERING IN PARTIAL
FULFILLMENT OF THE REQUIREMENTS FOR THE DEGREE OF
DOCTOR OF PHILOSOPHY IN CHEMICAL ENGINEERING
AT THE
MASSACHUSETTS INSTITUTES OF TECHNOLOGY

FEBRUARY 2018

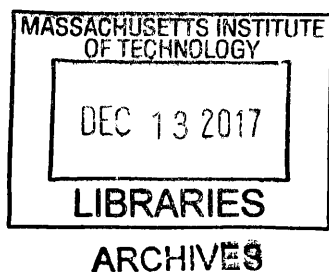Signature of Author: __ **Signature redacted** _____

Department of Chemical Engineering
November 15, 2017

Certified by: _____ **Signature redacted** _____

William H. Green
Hoyt C. Hottel Professor of Chemical Engineering
Thesis Supervisor

Accepted by: _____ **Signature redacted** _____

Patrick S. Doyle
Robert T. Haslam (1911) Professor of Chemical Engineering
Chairman, Committee for Graduate Students

Predictive Chemical Kinetics for Auto Ignition of Fuel Blends

by

Nathan W. Yee

Submitted to the Department of Chemical Engineering

on November 15, 2017 in Partial Fulfillment of the

Requirements for the Degree of Doctor of Philosophy

in Chemical Engineering

Abstract

Predictive chemical kinetics plays an important part in the study of chemical systems by reducing the need for expensive experiments. The size and complexity of modern chemical mechanisms increasingly require the use of automated mechanism generators, such as the Reaction Mechanism Generator (RMG). Use of these automated generators for creating quality chemical mechanisms necessitates accurate reaction rates. Unfortunately, the vast majority of kinetic parameters governing rate constants are not known. The goals of this thesis are the accurate estimation of kinetic parameters and its application to the prediction of auto ignition in fuel blends.

At the molecular scale, quantum chemical methods can give kinetic coefficients with accuracy nearing those of experiments. Even when specific kinetic parameters are unavailable, rates can be evaluated by analogy to similar molecules. RMG uses an averaging scheme based on arranging functional groups in a hierarchical tree structure. We have been able to continue expansion of the database to species with nitrogen and sulfur, improve methods for structural representation, and showcase validation for thermochemistry and kinetic parameter estimates.

Studying kinetics at the mechanistic level allows insight into the interaction between chemical reactions. Specifically, we have been interested in finding and analyzing the reaction pathways relevant to auto ignition, simplifying well-studied fuel mechanisms for propane and methanol. We were able to define clear stages of ignition and report the controlling chemistry during each stage. Understanding of these base fuels provides the basis to analyzing ignition for larger and more novel fuels.

Finally, from a macroscopic perspective we studied ignition for blends of phenolic additives in gasoline. Chemical mechanisms generated by RMG were modeled in a variable volume reactor that emulate end gas conditions of the CRF engine used to evaluate Research Octane Number (RON). We predicted the effect each additive has on the timing of ignition, which were later proven to be reasonably accurate by experimental validation. The chemical pathways that affect the ignition were analyzed and discussed. Finally, we developed a framework for predicting several different aspects of potential fuel additives, which could help eliminate costly experiments by identifying unsuitable candidates before they are even synthesized.

Thesis Supervisor: William H. Green
Title: Hoyt C. Hottel Professor of Chemical Engineering

Dedication

This thesis is dedicated to my parents Ah-Lyan and Yein-Khee Yee, whose

hard work gave me the opportunity and inspired me

to pursue this work.

Acknowledgements

First and foremost, I would like to acknowledge Prof. Bill Green for his constant advice and support during my thesis work. He has always given me a great deal of freedom in pursing my own projects. Despite a busy schedule, Bill has always been accessible, whether in person or e-mail, and is always ready with useful insight into the many problems we explored together. Finally, Bill sincerely cares about the well-being and success of his students even outside the scope of the thesis work. I have been truly blessed to have him as my thesis advisor.

I am also grateful to my thesis committee members, Prof. Jesse Kroll and Prof. Heather Kulik. Their helpful discussion and enthusiasm have been an immense help.

The Green group is a wonderful environment where everybody is willing to help one another. Dr. Greg Magoon was my first mentor who introduced me to many aspects of mechanism development as well as my first foray into Python coding. Dr. Josh Allen's impressive knowledge of computer science was instrumental in guiding many of implementations of RMG features. Dr. Shamel Merchant and I worked on many similar projects, and I have always benefited from his kind and excellent advice. Dr. Aäron Vandeputte and Dr. Amrit Jalan taught me everything I know about running quantum chemical calculations. Dr. Connie Gao was a delight to work with in the transition of from RMG-Java to RMG-Py. Dr. Soumya Gudiyella was always a rare and cherished source of positivity for our group. Prof. Richard West has been both tireless and relentless in improving the testing and quality of code for RMG. His influence has saved hours of painful debugging for all current and future developers. I gratefully acknowledge Zachary Buras for his many useful discussions and for being my closest confidante in the group.

I thank Kehang Han, Max Liu, Jim Chu, Dr. Soumya Gudiyella, and Zach Buras for working on aromatic and polycyclics estimates in RMG, which yielded profound improvements to many of my projects. I acknowledge Mark Goldman for collaborating with me on the work in methanol+propane work in Chapter 3, and appreciate his pragmatic approach to problem solving. I'm grateful to Alon Grinberg Dana for his constant positive attitude and contributions for including nitrogen and sulfur in RMG. Thank you to Matt Johnson for helping me with database maintenance and thermochemical validations. I would like to acknowledge Lawrence Lai and Mark Payne for collaborating with me on experiments in the feasibility screening of bio-oils. None of this work would have been possible without the painstaking maintenance of our servers by Dr. Ray Speth, Kehang Han, Dr. Phalgun Lolur, Collin Grambow, and Mark Payne. I apologize in advance to Alan Long, who will succeed me in frustrating

7

administrative duties of the Rainier server. Thank you to the rest of the current and former Green group members for embarking on this journey with me.

I have been very fortunate to have been sponsored by British Petroleum P.L.C. for a large part of my thesis work. I would like to specifically thank Casey Hetrick, Jim Simnick, George Huff, John Shabaker, and Sorin Filip for their guidance and many useful discussions. I am grateful to Randall Field for the facilitating meetings with BP as well as tutoring me in some of the more advanced usages of the Aspen Program.

The administration and staff at MIT have my gratitude for their services in facilitating many aspects of the work. With no exaggeration, I acknowledge Gwen Wilcox as the most ruthlessly efficient and organized administrative assistant I have ever witnessed. In addition to being amazingly fast, she is incredibly kind and always willing to help make a student's life a little bit easier. I would also like to thank former and current members of the Course 10 Student Office: Suzanne Maguire, Joel Dashnaw, Suzanne Ronkin, and Eileen Demarkles for always being ready with a smile and informative advice for the many confusing bureaucratic hurdles in the department.

I would like to thank my many friends who made my experience at MIT that much brighter. My hot pot and board gaming group, Alex, Sakul, Dariusz, Winston, Natasha, Yi, Connie, Wenjing, and Shireen shared many delicious meals together. Thank you to the many sharks at the Draper Bridge Club for constantly humbling and teaching me.

Finally, I would like to thank my parents, Ah-Lyan and Yein-Khee Yee for their unwavering love and support. For my entire life, they have led by example and I still look to them for guidance to this day.

The work presented in Chapters 4 and 5 was funded by BP P.L.C. I also acknowledge the National Science Foundation and the Department of Energy for funding throughout various parts of my thesis. Some calculations for this work also used computational resources from the National Energy Research Scientific Computing Center, a Department of Energy Office of Science User Facility.

Table of Contents

Table of Figures

13

14

Table of Tables

Chapter 1

Introduction

1.1 Background and Motivation

Improvements to the efficiency and reduction to environmental impact of fuels requires a fundamental understanding of their combustion chemistry. A full detailed kinetic mechanism is one component to making realistic models with predictive capability. However, a major difficulty is the size of the mechanisms: modern chemical mechanisms can reach thousands of species and tens of thousands of reactions [1]. All species require several thermochemistry parameters, and all reactions require Arrhenius parameters to calculate their rate coefficients. To make matters worse, the vast majority of these parameters are unknown and must be estimated using empirical schemes. Manual construction for these mechanisms is error-prone and tedious. Fortunately, the difficulties in manual construction are more easily handled by computers. Modern computing power allows the inclusion of a much larger number of species. Additionally, algorithms can quickly query for or estimate the many parameters, although the final mechanism will still be limited by the overall accuracy of the estimates. As a result, many pieces of software for the automatic generation of mechanisms have been developed [2], [3].

The Reaction Mechanism Generator [4] is the automatic generator developed in the Green Group. The original implementation was written in Java by Dr. Jing Song [5], but more recently was

rewritten in Python by Dr. Joshua Allen [6] and Prof. Richard West. The main defining feature of RMG, which sets it apart from other mechanism generators, is its unique approach to filtering of species. RMG iteratively includes species with the highest calculated flux based on isobaric, isothermal simulations of the system. As a result, it is particularly important for RMG to make reasonable estimates for thermodynamics and reaction coefficients because the estimates decide which chemical pathways are explored. Thermochemistry is estimated using a Benson group additivity scheme [7] with additional corrections for ring-strain and some long-range interactions. Reaction coefficients are estimated by generalizing reactions to specific families and averaging the Arrhenius parameters of chemically similar reactions. To our knowledge, RMG is also the only automatic generator that considers pressure-dependent networks and resonance structures.

The RMG database, which stores Benson group values and training data for rate coefficients, is completely separated from the main code. This enables outside user to apply their own chemical knowledge without extensive understanding of the algorithms or Python code. The data is stored in a hierarchical tree structure that allows groups to be roughly ordered by chemical similarity.

1.2 Motivation and Outline of Thesis

The U.S. Energy Information Administration does not project a significant decrease in the use of liquid fuels in the energy sector for the next 20 years [8]. Therefore, there is significant environmental and economic pressure for cleaner and more efficient formulations. One of the limiting factors for the efficiency of an internal combustion engine is the auto ignition behavior, measured by octane rating in spark ignition engines [9]. Adding ethanol to gasoline slows down auto ignition, leading to better efficiency. Following this example, researchers have considered many other biologically derived oxygenates as potential fuel components. Unfortunately, even a trained kineticist is hard-pressed to predict the induced auto ignition effects from chemical structure alone. The contrast between tert-butyl ether, which slows down auto ignition [10], and dimethyl ether, which speeds it up [11], exemplifies this difficulty. Despite both possessing ether groups, they have opposite effects on auto ignition!

Luckily, RMG is particularly useful for the determining the controlling chemistry of these novel fuel components. RMG will exhaustively apply every reaction family in the database to the fuel component but keep only the fastest pathways. Ideally, it will create a mechanism that captures all the important chemistry and, occasionally, even suggest correct chemical pathways that would never be imagined by a human. More often than not, poor thermochemistry estimation leads RMG to include unphysical intermediates. It is common for the users to cycle between using RMG to create mechanisms

and improving the database performance before gaining a successful model. Therefore, it is still imperative that the user have some chemical intuition to interpret RMG's output.

The first part of thesis focused on improvements for the structure, accuracy, and user-friendliness of the RMG database. A great deal of time was spent making previous entries in the database consistent in their chemical representation and accessible throughout the trees. Many unit tests were developed with Dr. Connie Gao to ensure that past mistakes are not repeated when current users contribute to the database. We also added the capability to represent many types of nitrogen and sulfur atoms in RMG. Although training data has been added by Dr. Alon Grinberg, Dr. Caleb Class, Dr. Beat Buesser, and Ryan Gillis, there is still not quite enough to make accurate estimates for many nitrogen and sulfur-containing species. Finally, RMG's thermochemistry and rate coefficient estimates were validated against larger test sets than in any other previous attempt.

The main application studied in this thesis was auto ignition for various fuel blends. In the first project, we closely studied mechanisms of methanol and propane blends at low temperatures. The purpose of this work was to simplify the auto ignition effect to either a reduced mechanism or analytical equations. As propane is representative model compound for alkanes, which appear in both diesel and gasoline, this work helped establish the chemical knowledge needed to model more complex fuels. We next applied RMG to creating mechanisms for the auto ignition of butane blended with substituted phenols. After obtaining mechanisms, we developed a volume profile to model the end gas conditions in a CFR engine used to calculate the research octane number. This relatively simple model gave surprisingly accurate results for ranking each fuel blend's research octane number, being a large improvement over both constant-volume and rapid compression machine-like simulations.

The same procedures for predicting research octane number were applied to gasoline blends with model compounds from lignin-derived bio-oil. In addition, pre-experimental screens for other blend attributes that could be induced by additives were developed or compiled. These attributes include tendency to produce soot, fuel/water solubility for the additives, and elastomer swelling. While the test for soot production used chemical kinetics, the other two screens were compiled from various methods in literature. This work represents a first attempt at developing a cost-saving framework for screening of potential fuel candidates.

1.3 Thesis Overview by Chapter

1.3.1 RMG Database: Accuracy and Improvements

This chapter presents the most-up-to-date overview of the structure and features of the Reaction Mechanism Generator (RMG) database. Descriptions of the molecular structure represented as graph data structures is shown along with updated atom types for carbon, oxygen, nitrogen, and sulfur. Detailed explanation for the storage of Benson group additive values in hierarchical trees is given. We subsequently validate RMG estimates of thermochemistry, which shows on average about 7 kcal/mol enthalpy of formation error for species of carbon, hydrogen, and oxygen, but significantly more error for nitrogenated species. A description of the reaction families along with their more complex tree structures and estimation scheme is given. We discuss best practice guidelines for the writing of entries to guide future users in making contributions to the database. The reaction rates were also validated showing an average multiplicative error of 22. Unfortunately, the process for users to contribute to the database is somewhat tedious and opaque. A number of unit tests have been implemented into RMG to catch bugs and help users correctly input their data. The chapter wraps up with description of these unit tests.

1.3.2 Understanding the Low-T ignition of Propane+Methanol blends

Modeling low temperature auto-ignition is challenging because the governing chemistry is complex, occurring in multiple stages and involving a large number of intermediate species. This is particularly true for fuel blends where we traditionally account for the potential of cross reaction between intermediates. In this chapter, we characterize the low temperature ignition of methanol and propane as simple archetypes for alkanes and alcohols. We find that each stage of ignition is governed by only a few key reaction cycles that are only first or zero-order in fuel species. Additionally, we observe that the alkane chemistry, although appearing much more complex, has striking parallels to that of alcohols. Overall, we find that the ignition delay can be predicted with only a few reaction cycles producing small radicals, OH and HO_2, and a few classes of exothermic reactions. From our analysis of pre-ignition chemistry, we construct reduced mechanisms for methanol and propane ignition, which are less than 10% the size of the full detailed model but still predict ignition delay with reasonable accuracy. Adding only minimal cross reactions, we combine the two mechanisms for the modeling of a propane/methanol blend. It is observed that this "sum-of-parts" model's prediction of ignition delay has good agreement with models which consider all intermediate cross reactions. The agreement suggests that the pre-ignition reaction paths are largely non-interacting. This simplification has potential in making future analysis of fuel blends much more manageable.

1.3.3 Modeling Study of Substituted Phenols in Engine-like Conditions

This chapter presents kinetic modeling efforts to evaluate the anti-knock tendency of several substituted phenols if used as gasoline additives. They are p-cresol, m-cresol, o-cresol, 2,4-xylenol, 2-ethylphenol, and guaiacol. A detailed kinetic model was constructed to predict the ignition of blends of the phenols in n-butane with the help of RMG, an open-source software package. The resulting model, which has 1465 species and 27428 reactions, was validated against literature n-butane ignition data in the low-to-intermediate temperature range. To rank the anti-knock tendency of the additives, engine-like simulations were performed in a closed adiabatic homogenous batch reactor with a volume history derived from the pressure profile of a real Research Octane Number engine test. The ignition timings of the additive blends were compared to that of Primary Reference Fuels to quantitatively predict the anti-knock ability. The chemical pathways involved in the auto ignition effects were studied using rate of production and sensitivity analysis. The model predictions agree well with experimental determinations of the changes in Research Octane Number induced by the additives.

1.3.4 Pre-experimental Framework for the Broad Screening of Drop-in Fuel Additives

A wide variety of molecules, many formed from biomass, have been proposed as fuel components or fuel additives. Before introducing a new fuel component or fuel additive into fuels, it is prudent to verify it satisfies many performance metrics: ignition chemistry, sooting tendency, aqueous solubility, toxicity, heating value, material compatibility, and many others. However, experimental testing of each of these attributes of every proposed new fuel component is time intensive and expensive. This work presents pre-experimental computer screening methods for four important fuel attributes: ignition delay and RON, tendency to produce polycyclic-aromatic hydrocarbon precursors, fuel/water partition coefficient, and elastomer swelling from fuel contact. The additives tested were phenol, anisole, furan, and furfural, model compounds of species in bio-oil from fast pyrolysis of lignin. The former two screening tests use detailed kinetic mechanisms constructed with use of the Reaction Mechanism Generator, while the latter two apply existing theoretical models. The results from each of these inexpensive screening tests on the computer are accurate enough that they could be used to eliminate some proposed fuel components from consideration before they were even synthesized.

1.4 References

[1]   T. Lu and C. K. Law, "Toward accommodating realistic fuel chemistry in large-scale computations," *Prog. Energy Combust. Sci.*, vol. 35, no. 2, pp. 192–215, Apr. 2009.

[2]   R. Van de Vijver *et al.*, "Automatic Mechanism and Kinetic Model Generation for Gas- and Solution-Phase Processes: A Perspective on Best Practices, Recent Advances, and Future Challenges," *Int. J. Chem. Kinet.*, vol. 47, no. 4, pp. 199–231, Apr. 2015.

[3]   E. Blurock, F. Battin-Leclerc, T. Faravelli, and W. H. Green, "Automatic Generation of Detailed Mechanisms," in *Cleaner Combustion*, Springer, London, 2013, pp. 59–92.

[4]   C. W. Gao, J. W. Allen, W. H. Green, and R. H. West, "Reaction Mechanism Generator: Automatic construction of chemical kinetic mechanisms," *Comput. Phys. Commun.*, vol. 203, pp. 212–225, Jun. 2016.

[5]   J. Song, "Building robust chemical reaction mechanisms: next generation of automatic model construction software," Thesis, Massachusetts Institute of Technology, 2004.

[6]   J. W. (Joshua W. Allen, "Predictive chemical kinetics: enabling automatic mechanism generation and evaluation," Thesis, Massachusetts Institute of Technology, 2013.

[7]   Benson, Sidney W., *Thermochemical kinetics: Methods for the Estimation of Thermochemical Data and Rate Parameters*, 2nd ed. Wiley, 1976.

[8]   U.S. Energy Information Agency, "EIA - Annual Energy Outlook 2017," 2017.

[9]   J. B. Heywood, *Internal Combustion Engines Fundamentals*. New York: McGraw-Hill, 1988.

[10]   İ. Sezer and A. Bilgin, "Effects of Methyl tert-Butyl Ether Addition to Base Gasoline on the Performance and CO Emissions of a Spark Ignition Engine," *Energy Fuels*, vol. 22, no. 2, pp. 1341–1348, Mar. 2008.

[11]   E. E. Dames, A. S. Rosen, B. W. Weber, C. W. Gao, C.-J. Sung, and W. H. Green, "A detailed combined experimental and theoretical study on dimethyl ether/propane blended oxidation," *Combust. Flame*, vol. 168, no. Supplement C, pp. 310–330, Jun. 2016.

Chapter 2

RMG Database: Accuracy and

Improvements

2.1 Introduction

Many fields including combustion, atmospheric chemistry, astrophysics, and systems biology commonly use detailed chemical kinetics to model their systems. However, in combustion it is rare to find complete and reliable mechanisms for many fuels, as they are both difficult and time-intensive to create. One of the major difficulties is that hundreds of intermediate radical reactions are necessary, especially because number of reactions scales super -linearly with the number of intermediates [1], whereas very of the rate coefficients are known.

Previously, most mechanisms were constructed by hand, painstakingly recording all parameters and adding relevant reactions through expert knowledge. Luckily, the main difficulties to manual generation are handled easily by computers. Ideally, an automatic mechanism will comprehensively consider all chemistry it has been taught and never incorrectly apply parameters from its database. Realizing the potential to this approach, researchers have

developed many automatic mechanism generators: NETGEN [2], RMG [3], EXGAS [4], Genesys [5], RING [6], MAMOX [7], and REACTION [8] to name a few modern ones with a combustion focus. Several excellent review articles discuss main challenges of automatic generation and each software in great detail [9,10].

The Reaction Mechanism Generator (RMG) is the open-source suite of programs for automatic mechanism generation developed in the Green Group. The minimum input required by the user is the concentration of initial species, the initial conditions for any number of reactors used for simulation, and a flux tolerance, ε, usually between 0.01 and 0.1. The initial species are placed in the mechanism "core". RMG will then iteratively repeat the following steps:

1. Generate possible reactions which use core species as reactants. If product species of these reactions are not in core, then they are placed in the mechanism "edge".

2. Estimate the reaction rates and thermochemistry for species in the edge

3. Run isothermal, isobaric simulations of the mechanism using the inputted reactors, tracking the chemical flux toward edge species

4. When an edge species's flux exceeds the absolute value of all core fluxes multiplied by the ε, it is recognized as an important intermediate and included in the core. The entire algorithm is then repeated starting with step 1.

The main RMG algorithm continues until a finishing criteria, usually a simulation end-time or reactant conversion rate is reached. The final output is a chemical mechanism written in Chemkin or Cantera format and a species dictionary with adjacency lists.

During the generation, reactions based on pre-programmed rules are exhaustively explored and then optionally filtered based on a wide range of criteria depending on the software. RMG is unique from other automatic generator because it calculates the species with largest flux to determine the reactions to include in the mechanism. Therefore, the estimation of reaction rates is especially crucial, not simply to have correct rate coefficients in the final mechanism, but to direct the software on what chemistry to include. To enable mechanism generation, a great deal of effort has been applied to training the RMG database to quickly and accurately make estimates. Thus, a powerful stand-alone tool for estimating thermochemistry and kinetic rate parameters has, almost inadvertently, emerged.

RMG implements Benson group additivity [11] to calculate the thermochemistry of species. Many databases which record experimentally measured or calculated values of

thermochemistry exists: CRC handbook [12], ATcT [13], NIST Chemical WebBook [14], Burcat's 3rd millennium database [15], and THERM [16] to name a few. Databases for kinetic rate parameters are even rarer: NIST Kinetics Database [17] and PrIME [18], although the latter has many more applications than simply being a kinetics database. While kinetic parameters are available in a variety of published mechanisms, it is tedious for users to search these, and even more tedious to track down the sources of each number. Of these databases, only RMG provides automated estimates for unknown rate parameters, while THERM, a NIST tool, RMG, and some commercial software all provide estimates for unknown thermochemistry.

This chapter first presents updated explanations of features and the structure of the database for RMG. It also shows validation for accuracy of the thermochemistry and kinetic estimations provided by the current methods implemented in RMG. Finally, it describes the suite of unit tests developed to maintain consistency and compatibility across the database.

2.2 Representation of Chemical Structures

In RMG, the adjacency list ("adjlist" for short) is a graph data structure of the atoms and connecting bonds used to represent chemical structures in two dimensions. There are three data classes that are represented with adjlists: molecules, species, and groups. A molecule object is a complete chemical structure and is always associated with *one* adjlist. A species object contains a label, thermochemistry, and a set of molecule objects representing the resonance structures of the species. For a given species, RMG automatically generates the list of resonance structures. An example adjacency list for a methoxy radical is shown in Figure 2-1. RMG generates all molecule adjlists with explicit hydrogens, but the user may omit any number of hydrogens for convenience.

```
species label        CH3O
species multiplicity multiplicity 2
                     1 C u0 p0 c0 {2,S} {3,S} {4,S} {5,S}
                     2 O u1 p2 c0 {1,S}
                     3 H u0 p0 c0 {1,S}
                     4 H u0 p0 c0 {1,S}
                     5 H u0 p0 c0 {1,S}

        atom index ──┘ │ │ │ │ │ │
          element ─────┘ │ │ │ │ │
unpaired electrons ──────┘ │ │ │ │
        lone pairs ────────┘ │ │ │
            charge ──────────┘ │ │
   bond atom index ────────────┘ │
        bond order ──────────────┘
```
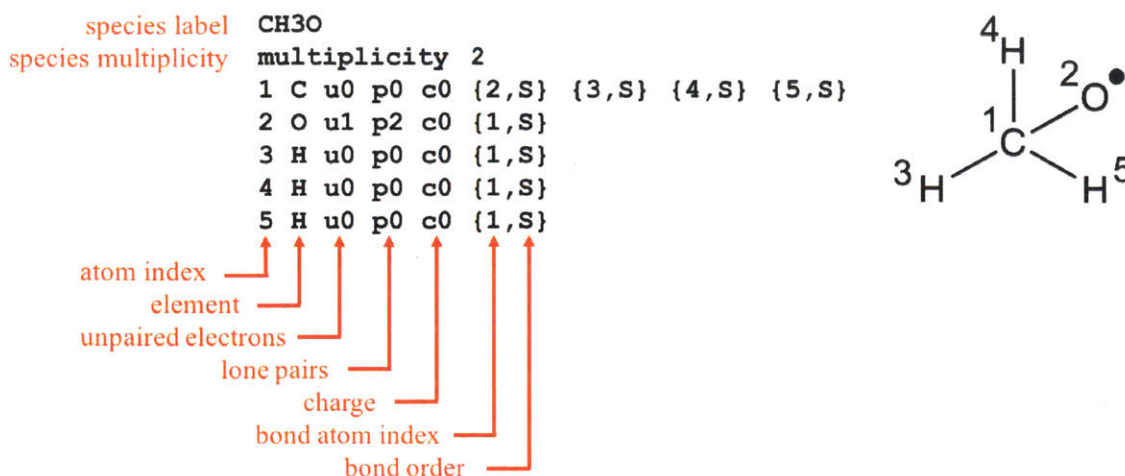
Figure 2-1 Adjacency list and Lewis structure for methoxy radical

For the molecule adjlist, the optional first line is the species label, the name given to the species in RMG. The second line gives the total multiplicity of the chemical structure. The second line gives the total multiplicity of the chemical structure. Each subsequent line describes each atom with the following syntax: the first column is the atom's index, the second column is the element, the third column denoted, "u", is the number of unpaired electrons, the fourth column denoted, "p", is the number of lone pairs, the fifth column denoted by, "c", is the formal charge, and, finally, each bracketed pair represents a bond involving the atom. For the bond brackets, the number indicates the bonded atom's index and the letter gives the bond order: S for single, D for double, T for triple, and B for benzene. Benzene bonds refer to any bonds with aromatic character, including bonds that appear in species such as naphthalene, furan, and pyridine. Finally, it is worth noting that O_2 should always be represented in its ground state triplet form (single bonded and one radical per oxygen atom), to react properly in RMG.

The group class, christened for its application in Benson groups or functional groups, is used to represent fragments of a full molecule. There are several major differences between the adjlist of a group and that of a molecule which make them immediately distinguishable. The molecule's multiplicity is omitted for adjacency lists of groups because a substructure does not necessarily give enough information to determine it. Unpaired radicals, lone pairs, and charge attributes can be sets in a group instead of a defined value. Either the value "x" or the absence of the attribute counts as a wildcard, indicating any value allowed, for these attributes. Bond order can also be defined as a set inside square brackets, but does not use the wildcard 'x'. Because

groups represent fragments, atoms in a group adjlist may have an incomplete valence. Missing valence on atom A can be bonded to any atom, subject to A's atom type restrictions. An additional attribute called "atom label" is optionally inserted after the atom index. The atom label marks specific atoms of interest such as the center of a Benson group or the atoms which participate in a reaction. Although not all atoms require an atom label, all current applications require at least one atom label in a group.

The final major difference between the adjlists of groups and molecules is that elements are replaced by a set of "atom types". Atom types categorizes atom using some subset of the following criteria: number of valence electrons, element, number of lone pairs, charge, and bonding requirements. A list of all atom types is given in Table 2-1.

Table 2-1 Definition of atom types implemented in RMG.
An "--" indicates that there is no requirement in the category for the atom type. Unless otherwise specified, bond order requirements assume 0 double, 0 triple, 0 benzene, and any number of single bonds. Any bond order requirements for double, triple, and benzene bonds must be matched exactly as opposed to being a minimum value.

Atom type	Element	Lone Pairs	Charge	Bond Order Requirements
R	Any	--	--	--
R!H	Not H	--	--	--
Val4	C, Si	--	--	--
Val5	N	--	--	--
Val6	O,S	--	--	--
Val7	Cl	--	--	--
H	H	--	--	--
He	He	--	--	--
Ne	Ne	--	--	--
Ar	Ar	--	--	--
Cl	Cl	--	--	--
C	C	--	--	--
Ca	C	2	0	No bonds
Cs	C	--	--	Only single
Csc	C	--	-1	Only single
Cd	C	0	--	1 double to atom other than oxygen or sulfur
CO	C	0	--	1 double to oxygen
CS	C	0	--	1 double to sulfur
Cdc	C	0	-1	1 double
Cdd	C	0	0	2 double
Ct	C	0	0	1 triple
Ctc	C	0	-1	1 triple
Cb	C	0	0	1 or 2 benzene
Cbf	C	--	--	3 benzene
C2s	C	1	0	Only single
C2sc	C	0	-1	Only single
C2d	C	1	0	1 double
C2dc	C	1	-1	1 double
C2tc	C	1	-1	1 triple
O	O	--	--	--
Oa	O	3	0	No bonds
O0sc	O	3	-1	No bonds
O0dc	O	3	-2	1 double
O2s	O	2	0	Only single
O2sp	O	2	+1	Only single
O2sn	O	2	-1	Only single
O2d	O	2	0	1 double
O2dc	O	2	-1	1 double
O2tc	O	2	-1	1 triple

Atom type	Element	Lone Pairs	Charge	Bond Order Requirements
O4sc	O	1	+1	Only single
O4dc	O	1	+1	1 double
O4tc	O	1	+1	1 triple
N	N	--	--	--
N0sc	N	3	-2	All single
N1s	N	2	0	All single
N1sc	N	2	-1	All single
N1dc	N	2	-1	1 double
N3s	N	1	0	All single
N3d	N	1	0	1 double
N3t	N	1	0	1 triple
N3b	N	1	0	2 benzene
N5sc	N	0	+1, +2	All single
N5dc	N	0	+1	1 double
N5dc2	N	0	+2	1 double
N5dd	N	0	0	2 double
N5ddc	N	0	+1	2 double
N5tc	N	0	+1	1 triple
N5td	N	0	0	1 triple, 1 double
N5b	N	0	0, +1	1 benzene
Si	Si	--	--	--
Sis	Si	--	--	All single
SiO	Si	--	--	1 double to oxygen
Sid	Si	--	--	1 double
Sidd	Si	--	--	2 double
Sit	Si	--	--	1 triple
Sib	Si	--	--	2 benzene
Sibf	Si	--	--	3 benzene
S	S	--	--	--
Sa	S	3	0	No bonds
S0s	S	3	0	All single
S2s	S	2	0	All single
S2sp	S	2	+1	All single
S2sn	S	2	-1	All single
S2d	S	2	0	1 double
S2dc	S	2	-1	1 double
S4s	S	1	0	All single
S4sc	S	1	+1	All single
S4d	S	1	0	1 double
S4dc	S	1	+1	1 double
S4b	S	1	0	2 benzene
S4dd	S	1	0	2 double
S4ddc	S	1	-1	2 double

Atom type	Element	Lone Pairs	Charge	Bond Order Requirements
S4t	S	1	0	1 triple
S4tc	S	1	+1	1 triple
S6s	S	0	0	All single
S6d	S	0	0	1 double
S6dc	S	0	+1, +2	1 double
S6dd	S	0	0	2 double
S6ddc	S	0	+1	2 double
S6ddd	S	0	0	3 double
S6t	S	0	0	1 triple
S6tc	S	0	+1	1 triple
S6td	S	0	0	1 triple, 1 double
S6tdc	S	0	+1	1 triple, 1 double
S6tt	S	0	0	2 triple

Using atom types both speeds up matching and allows more concise adjlists for groups. When all explicit lines of the group adjacency list are represented in a molecule list, the group is said to be subgraph isomorphic, or matched for short, to the molecule. An example of a group adjlist and possible matches is shown in Figure 2-2.
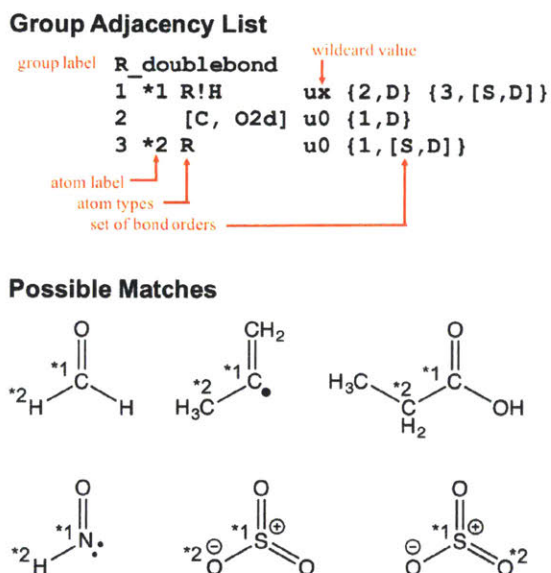
Figure 2-2 Example of adjacency list for group and possible matching molecular structures
Values that are omitted number of lone pairs or charge are assumed to be wildcard. Note that there may be several ways to match the same structure as shown with sulfur trioxide

2.3 Thermochemistry database

2.3.1 Base structure and groups

Benson group additivity estimates the thermodynamics of a given molecule by assuming that thermodynamic parameters can be calculated based on summing contributions from each individual atom in a given molecule. Value for an individual atom can depend on what types of bonds that atom has, what it is bonded to and its local molecular structure in general. In practice these values are usually generated from linear fits of molecules with known thermodynamic parameters.

Within RMG individual atom contributions are determined by descending a structured tree with an example shown in Figure 2-3. At each node within RMG trees, a local group structure is defined. A molecule with the given atom label descends the tree by starting at the top node to check whether the group object is subgraph isomorphic to the molecule. If so, it will then perform subgraph isomorphism for each child of the top node in the order they are listed. Once matched, that child node becomes the current node and its children are searched for matches. This process ends either when none of the child nodes matches the molecule or the end of the tree is reached. This type of tree transversal is known as a post-order search.
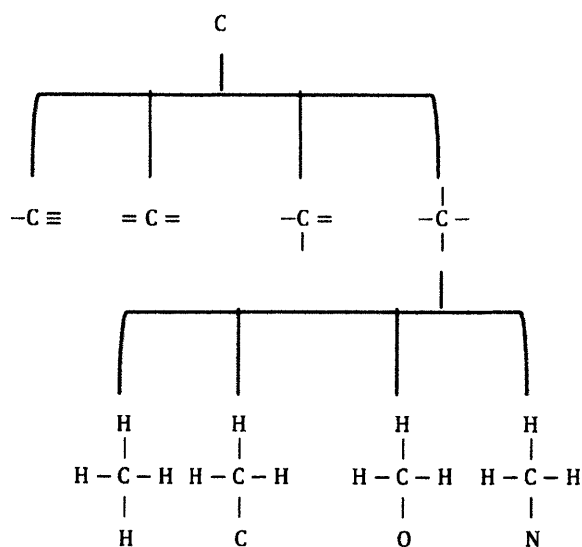
Figure 2-3 Example of RMG tree for matching groups

Many of these nodes do not have data directly associated with them. In these cases that node is instead referenced to another node, which will either have data or another reference. The database is constructed such that following the references from any node will eventually hit appropriate data.

```
entry(
    index = 50,
    label = "Cds",
    group =
"""
1 * [Cd,CO,CS] u0
""",
    thermo = u'Cds-CdsCsCs',
    shortDesc = u"""""",
    longDesc =
u"""

""",
)

entry(
    index = 1823,
    label = "Cds-OdN3sH",
    group =
"""
1 * CO   u0 {2,S} {3,S} {4,D}
2   N3s  u0 {1,S}
3   H    u0 {1,S}
4   Od   u0 {1,D}
""",
    thermo = ThermoData(
        Tdata = ([300,400,500,600,800,1000,1500],'K'),
        Cpdata = ([7.03,7.87,8.82,9.68,11.16,12.2,14.8],'cal/(mol*K)'),
        H298 = (-29.6,'kcal/mol'),
        S298 = (34.93,'cal/(mol*K)'),
    ),
    shortDesc = u"""""",
    longDesc =
u"""

""",
)
```

Figure 2-4 Example of entries for thermochemistry groups in RMG.
The Cds node points to the Cds-CdsCsCs node for its thermo data, while the Cds-OdN3sH node contains its own thermochemistry data.

After summing up the individual atomic contributions RMG adds a number of corrections. The first is the hydrogen bond increment (HBI) correction. If the molecule is a radical the Benson group additivity is applied to the saturated molecule rather than the actual molecule. Then the HBI corrections following the methods of Lay et al are applied [19]. The enthalpy correction is expressed as:

$$HBI(\Delta_f H^o_{298}) = \Delta_f H^o_{298}(R^*) - \Delta_f H^o_{298}(R-H) = BDE(R-H) - \Delta_f H^o_{298}(H^*) \qquad \textbf{(1)}$$

where *BDE* denotes a bond dissociation energy and H^* denotes a hydrogen radical. Note that the entries in the database are for *HBI* corrections, not the more commonly reported *BDE*; the algorithm automatically subtracts the enthalpy of the H atom. Much like the group additivity tree for a given atom, HBI corrections are estimated using an RMG tree.

Cyclic molecules have additional corrections for the ring strain. If there are no fused rings, the thermodynamic contribution of the strain induced by each individual ring is applied to the molecule. This follows exactly the same matching algorithm as the standard groups and HBI correction. Molecules with fused polycyclic rings have a separate tree of ring-strain corrections, but there are many more possible combinations, not all of which have available data. Therefore, when no match is found, a heuristic has been implemented which combines existing data to estimate the missing ring corrections, described in detailed by Han et al [20].

Finally, additional corrections are added for non-next-nearest neighbor interactions (NNI). These interactions occur between two atoms that are at least three bonds apart. These are calculated separately depending if the molecule is cyclic or non-cyclic. The non-cyclic tree provides corrections for gauche(1,4), and gauche(1,5) interactions. The cyclic tree provides corrections for ortho/meta/para interactions on the ring.

2.3.2 Resonance structures and application to thermochemistry

The estimate of thermochemical parameters considers all resonance structures of a species. For RMG this involves applying several resonance recipes, all shown in Figure 2-5. The most common is radical allyl shift, but the algorithm also accounts for radical shifts with a lone pair and lone pair shifts in azide groups. Additional resonance structures are also generated for aromatic species. The full aromatic structure gives all aromatic rings benzene bonds, while kekulized structures convert all of the benzene bonds into single/double bonds. When generating resonance isomers, combinations of these isomerization recipes are also considered. After Benson group additivity and corrections are applied, the thermodynamic parameters for the resonance isomer with the lowest 298K enthalpy are used to represent the species.
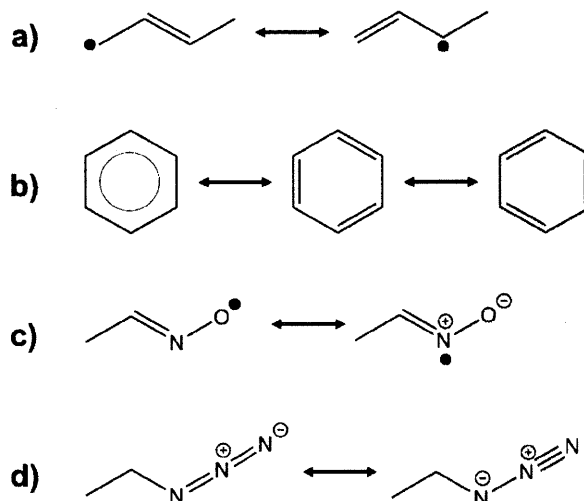
Figure 2-5 Examples of all resonance isomerizations recipes implemented in RMG
(a) allyl/radical shift; (b) aromatic kekulization; (c) radical lone pair shift; (d) azide lone pair/lone pair shift.

2.3.3 Validation of enthalpy estimates in RMG-database

The RMG's estimates of enthalpy of formation at 298K were validated against a large database of CBS-QB3 calculated molecules [21]. CBS-QB3 calculations are generally accurate within 2 kcal/mol, with occasional lapses to as much as 10 kcal/mol, for enthalpy calculations at 298K [22]. Figure 2-6 shows a histogram of errors between [21] and estimates generated by RMG for species with only carbon, oxygen, and hydrogen. This validation shows that the vast amount of RMG estimates for oxygenates have an average error of 5.96 kcal, agreeing well within the estimated error of the quantum calculations. When considering cyclic species, we see a slightly larger average error, 6.49 kcal/mol, although the comparison is still quite reasonable.
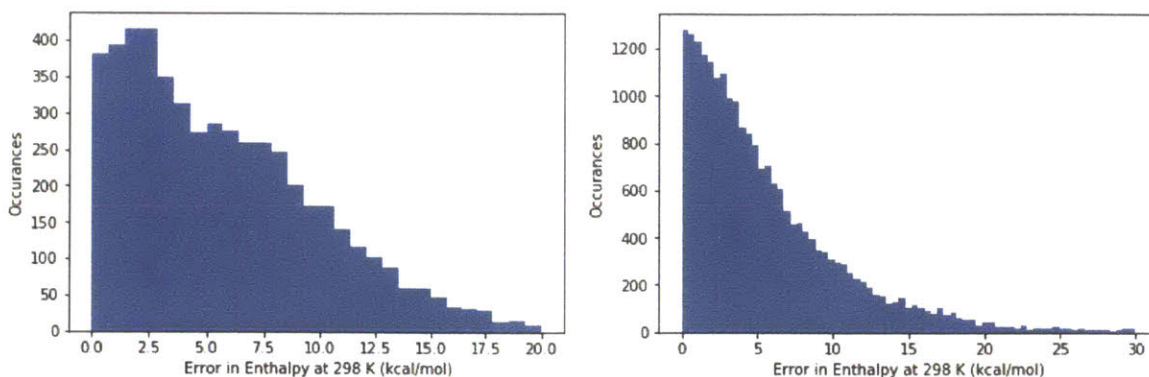
Figure 2-6 Histogram of error of ΔH_f at 298K between RMG estimates and values reported in [21] for oxygenates and hydrocarbons
The left-hand plot compares only non-cyclic species and the right-hand plot only cyclics and polycyclics. Note the change in scale between the two figures.

Figure 2-7 shows the validation errors for nitrogen containing compounds. These non-cyclic species have an average error of 23.24 kcal/mol, and the cyclics have 14.06 kcal/mol. The bulge seen in the histogram for non-cyclics around 25 - 45 kcal/mol coincides with many species with carbon triple bonded to nitrogen. While the current database has some data for groups with triple bonded nitrogen, not all cases are covered, and the most general triple bonded nitrogen has no correction. Further addition of nitrogen groups is recommended. The histogram for cyclic errors in Figure 2-7 does not show any abnormal spurt in error because triple bonded nitrogen atoms are unlikely to appear in cyclic species. Most of the ring corrections in RMG are for hydrocarbons or oxygenates, which, at most, may be generalized to other atoms. Thus, it is unsurprising to see a greater degree of error for the cyclic species with nitrogen, compared with the oxygenates and hydrocarbons.

37
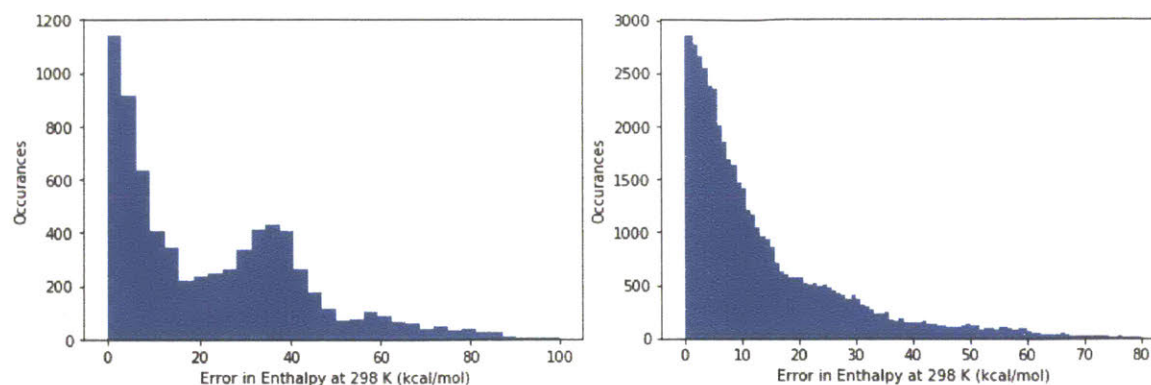
Figure 2-7 Histogram of error of *ΔH_f* at 298K between RMG estimates and the values reported in [21] for nitrogen containing species
The left-hand plot compares only non-cyclic species and the right-hand plot only cyclics and polycyclics

Finally, errors for compounds containing sulfur are shown below. Because [21] does not contain any sulfur compounds, the test set for this data was actually the group of molecules used to train the group values. This includes about only 10 species which are cyclic and 180 which are non-cyclic. Because we do not have a distinct test set, we cannot obtain a good estimate of the accuracy of RMG's predictions for the thermochemistry of sulfur compounds, but this comparison is still useful for giving error intrinsic to the RMG's approach. It was found that the mean error was approximately 1.39 kcal/mol.
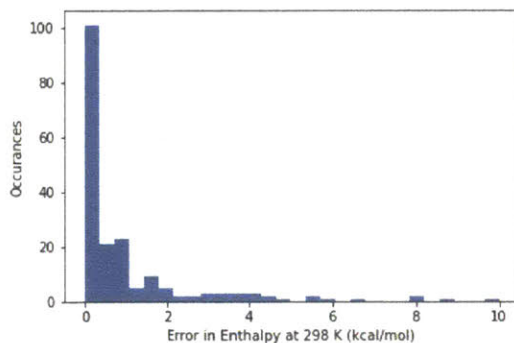
Figure 2-8 Histogram of error of *ΔH_f* at 298K of RMG estimates for sulfur containing species
Because the test set was the same as the training set used to create the groups, this comparison gives a measure of the consistency of RMG's approach.

38

A summary of the mean error for each type of species in the validation is given in Table 2-2.

Table 2-2 Summary for validation of RMG estimates on ΔH_f at 298K.
*The test for the sulfur-containing species used test data which was the same as the training data for the groups.

Compound Type	Number of test points	Mean Error (kcal/mol)	Standard Deviation (kcal/mol)
Non-Cyclic Oxygenates and Hydrocarbons	5201	5.96	4.48
Non-Cyclic Species with Nitrogen	7269	23.24	20.69
Species containing Sulfur*	195	(1.39)	(3.12)
Cyclic Oxygenates	49976	6.49	7.66
Cyclic Species with Nitrogen	22734	14.06	14.96

2.4 Reaction and Kinetics database

The most common format to save kinetics parameters is the modified Arrhenius form

$$k(T) = A \left(\frac{T}{1\,K} \right)^n \exp \left(-\frac{E_a}{RT} \right) \tag{1}$$

where A is the pre-exponential factor, T is temperature, n is the temperature exponential factor, E_a is the activation energy, and R is the gas constant. The activation energy is made more flexible by adding an Evans-Polanyi correction, but it is also subject to the constraint:

$$E_a = \max(0, \Delta H_{rxn}, \alpha \Delta H_{rxn} + E_0) \tag{2}$$

where ΔH_{rxn} is the enthalpy of reaction, α is the Evans-Polanyi correction, and E_0 is the base activation energy. The maximum constraint implements two sanity checks: the activation energy cannot be negative and the activation energy of an endothermic reaction is at least as large as its enthalpy of reaction. For the reaction families, all kinetic parameters are at the high-pressure

limit. Pressure-dependent effects can be calculated subsequently using RMG's internal master equation solver, which converts k(T) to k(E) using Inverse Laplace Transform methods [23].

2.4.1 Reaction families

55 reaction families give templates for the possible chemistry considered by RMG. The recipe for a reaction family describes the chemical reaction. The families cover a wide range of predominantly radical chemistry. While some families are extremely well-studied with over a hundred training data points, many represent fairly niche-case reactions, such as the Korcek reaction [24] where few parameters are available. Figure 2-9 shows an example of the recipe for H-abstraction, the largest family in RMG. Recipe actions include gaining radical, losing radical, forming bond, breaking bond, incrementing bond, decrementing bond, gaining lone pairs, and losing lone pairs. Changes in formal charge are not specifically indicated in the recipe, but each atom's formal charge is recalculated from its valence after the entire recipe is applied.
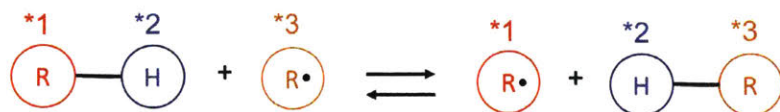
Reaction Recipe   Break bond   {*1, 1, *2}
                      Form bond   {*2, 1, *3}
                      Gain radical {*1, 1}
                      Lose radical {*3, 1}

Figure 2-9 Graphical representation and reaction recipe for H-abstraction family

Similar to the thermochemistry database, functional groups for the reaction families are organized into trees, which grow in specificity during descent. However, because there are always at least two reacting atoms, each family has a separate tree for the reacting sites. The simplest case are the bimolecular families, which have two trees. A simplified example tree is given for the H-abstraction family in Figure 2-10. Two groups, one from the XH tree and one from the Y rad tree are needed to describe the reacting sites of the reactants. The combination of groups is known as a "template". For example, methane, a primary carbon, reacting with hydroxyl radical would have a template of [C pri, OH] in the sample trees.
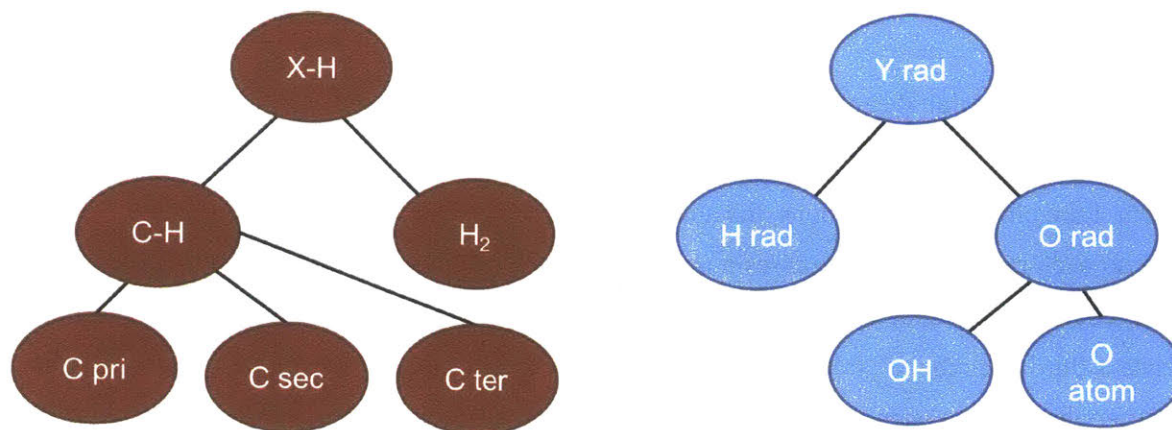
Figure 2-10 Example of simple trees for the H-abstraction family
Each tree represents one of the necessary reacting sites, a bonded hydrogen and a radical.

When kinetic parameters are applied directly to a template, the resulting entry is called a "rule". Kinetic rules are most appropriate when the parameters are generalized from several similar functional groups, such as Dean et al [25]. Because the group representation lacks symmetry information, all kinetic rules must have an A-factor assuming a degeneracy of one (RMG will then estimate the degeneracy/symmetry factors). However, some of the kinetic rules in the database were derived from literature data including degeneracy factors; instead these numbers which are for specific reactions not general functional groups should be stored as training reactions rather than in the rate estimation tree.

A second way to assign kinetic parameters to a rule is through training reactions. The training reactions of family is the database of kinetic parameters assigned to fully defined reactions; that is, the training reactions use species instead of groups as their entry key. When initializing the database, RMG descends a family's tree and assigns a training reaction to the most specific rule that matches the reactants. Training reactions written in the reverse direction are also compatible. An advantageous trait of the training reaction is its independence from tree structure. If groups in the tree are edited, rules must be manually checked to ensure they still apply to the template. However, training reactions are immune to this error since they are matched to templates by descending the tree. As a result, users are strongly encouraged to store kinetic parameters in training reactions instead of rules whenever possible. In contrast to the A-factor for a rule, A-factors in the training reaction include degeneracy from symmetry, as it most intuitive for a user to assign the experimentally observed or commonly reported rate coefficient.

2.4.2 Unimolecular Reaction Families

Reactions which are unimolecular pose unique difficulties when performing a template match. Like bimolecular reactions, the atoms which react can have a strong effect on the reaction rate, so each reacting "end" requires a tree in the family. In many cases, however, the length of the cyclic transition state has an equal or larger effect on the reaction rate. Therefore, the family needs a third "backbone" tree which describes both the length and functional groups of atoms between the reacting ends. An example of three adjlists and their labels are shown for an intra-H-migration family.

To ensure consistent and correct usage of the unimolecular trees, several constraints are placed on the definition of backbone and end groups. Under these guidelines, any template should be valid. Figure 2-11 shows an example of a valid template for the unimolecular reaction of 1-oxy,2-butanone.

Template

```
O_rad_out1       R5H_CCC(O2d)C                          Cs_H_out_2H
*1 O u1          1 *1 R!H  u1 {2,S}                     1 *2 Cs u0 {2,S} {3,S} {4,S}
                 2 *4 C    u0 {1,S} {3,S}               2 *3 H  u0 {1,S}
                 3 *6 CO   u0 {2,S} {4,S} {7,D}         3    H  u0 {1,S}
                 4 *5 C    u0 {3,S} {5,S}               4    H  u0 {1,S}
                 5 *2 R!H  u0 {4,S} {6,S}
                 6 *3 H    u0 {5,S}
                 7    O2d  u0 {3,D}
```

Reaction
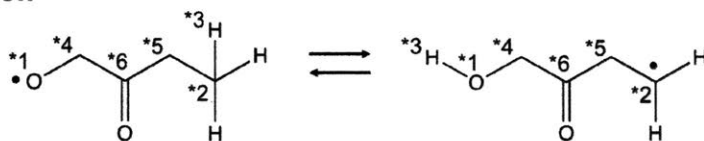
Figure 2-11 Example of template for intra-H migration in 1-oxy,3-butanone
All template adjacency lists are correct in that they conform to labeling restriction of end groups and backbone groups.

Constraints on end groups
1. End groups may only contain labels which appear in the family recipe
2. The two end groups in a valid rule must contain all labels which appear in the family recipe

3. End groups are meant to define reacting sites and relevant features local to the reacting sites. No attempt to define the backbones should be included. Any additional unlabeled atoms on an end group are assumed to exclude the backbone.

Constraints on backbone groups
   1. Every backbone group should include all labels in the family recipe
   2. End groups should be defined as the root of their respective subtrees, such that no backbone defines any aspect of the end groups other than how they connect to the backbone
   3. All atoms connecting the atoms labeled in the end group must all be labelled with numbers greater than the labels in the recipe. The numbering of the atoms should be consistent when descending the tree.
   4. All unlabeled atoms are meant to describe other relevant features of the backbone. No unlabeled atoms should be attached to the end group atoms.

The 2D nature of graphs creates complications when defining backbone groups for cyclic species. For a linear species, the current notation unambiguously defines the length of the transition state as a nth-member transition state where n is the number of labeled atoms. However, a cyclic species has a transition state that reaches across the ring, resulting in a very different transition state from its linear analog. Currently the groups may not differentiate between the linear and cyclic case since groups rely on a subgraph isomorphism. To further complicate matters, a mono-cyclic species can enumerate backbone atoms in two different directions, clockwise and counter-clockwise, which erroneously results in two separate rate estimates. A polycyclic species may have even more than two valid enumerations of backbones. Some solution that are currently in development include splitting families into linear and cyclic versions, adding a ring attribute to atoms in the adjacency lists, and judicious restructure of current trees.

2.4.3 Estimation of kinetic parameters in families

All trees of the family are descended to determine the most specific template matching the reactants. If a rule or training reaction has been assigned to the template, the match is

designated an "exact match", and the appropriate kinetic data is used as an estimate. If there are multiple rules or training reactions, the one with the highest rank is chosen. One exception to the rank priority is when the reaction is identical to a training reaction, in which case the training reaction is used regardless of rank.

The combinatorial nature of the rate rules creates a very large set of valid rules in each family. It is rare that the set of templates is even 1% populated with rules or training reactions. When no kinetic data is available for the matched template, RMG designates the match as an "averaged match" and reverts to an averaging algorithm to determine the values of kinetic parameters. Assume a reaction has matched template, [A, B], but no rule or training reaction has been assigned to this template. Using [A, B] as the origin for the 2D space for the two trees, RMG will search the space for a replacement template [A', B'], with kinetic parameters and the smallest 2-norm distance. Once an appropriate [A', B'] is found its kinetic parameters are substituted in for [A, B]. Of course, unimolecular families have template of three nodes, so a 3D space is used, but the principle remains the same. If multiple valid templates are found to have the same minimum 2-norm, then kinetic parameters are estimated as the means for the kinetic parameters. In the case of n, α, and E_a the standard mean of values from each valid template is used. Because the A-factor can span a very large order of magnitude, a geometric mean is used instead.

By default, each parent-child distance between nodes is considered to have a length of one when calculating the norms. The developers recognize that the tree structures are arbitrary, such that a uniform edge length may give minimum norms that do not conform with chemical similarity. For example, in intra-H-migration, the length of the transition state is one of the most important factors for estimating the kinetics, more so than the element that the radical resides on. Thus, the most chemically correct minimum distance would weigh distances on the backbone tree to be smaller, than the distances on the end group trees. In anticipation of the result, all nodal lengths are customizable on an individual basis or by tree. In the future, optimization of nodal lengths could lead to vastly improved accuracy on averaged matches.

Two separate validations were performed for the reaction families. First, exact matches were tested against a training set of reactions data-mined from the NIST kinetics database [17]. In this validation test, points with outliers greater than 10^{15} were discarded, as they are most likely explained by unit errors in the NIST database. The accuracy of the averaged matches was

tested internally using the leave-one-out cross validation (LOOCV) test. In the LOOCV, the test set is each template with a training reaction of rule. The training set is the entire database minus the current template being tested. Thus, the database creates an averaged match for data point A when data A is not present. This type of cross-validation provides an estimate for how much error is introduced when RMG creates an averaged match. A parity plot for the NIST validation and LOOCV for H-Abstraction is given in Figure 2-12.
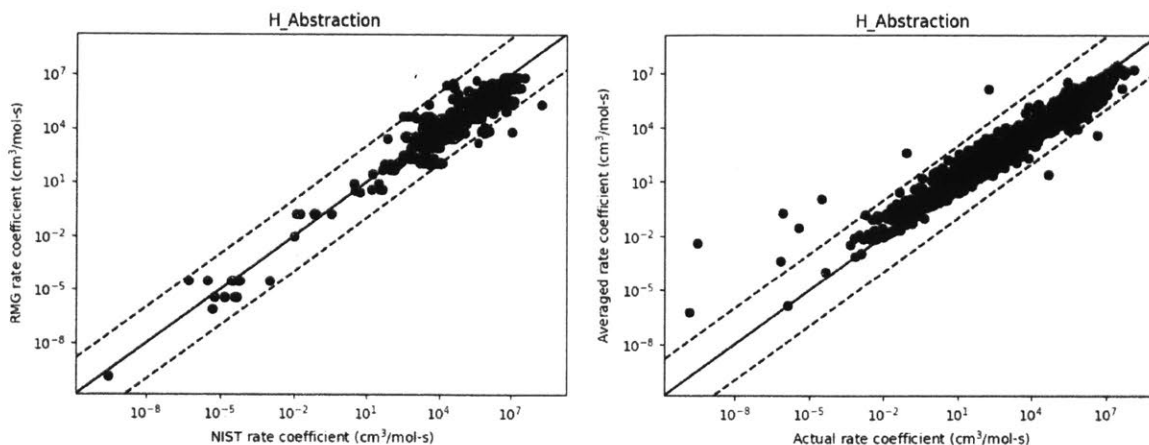
Figure 2-12. Parity plots for validation of H-Abstraction rate coefficients at 1000K in RMG.
Dotted lines enclose the space that correspond accuracy within two orders of magnitude. The left-hand figure shows validation for exact matches with the NIST chemical kinetics database [17]. The right-hand figures validation against a LOOCV

For both the NIST validation and LOOCV, the mean averaged error (MAE) and root mean square error (RMSE) for the base 10 logarithm of rate coefficient at T = 1000K is reported:

$$MAE = \frac{1}{N} \sum_i \left| \log k_{i,test} - \log k_{i,training} \right| \tag{3}$$

$$RMSE = \sqrt[2]{\frac{1}{N} \sum_i \left[\left(\log k_{i,test} \right)^2 - \left(\log k_{i,training} \right)^2 \right]} \tag{4}$$

where N is the total number of data points tested. The RMSE differs from MAE in that it is more sensitive to outliers.

Table 2-3 Validation of log10 of rate coefficients at 1000K estimated by RMG vs. NIST kinetics database.

Only families which matched at least one reaction from the NIST database are shown. *Because the LOOCV was performed for all families, the reported mean includes values not shown. **The mean for large families only includes families with more than 100 training reactions.

Family	Number of rules	Number of Exact comparisons	Exact Match RMSE	Exact Match MAE	LOOCV RMSE	LOOCV MAE
1,3 Insertion CO2	6	5	0.83	0.67	0.21	0.10
1,3 Insertion ROR	24	45	1.64	1.03	0.22	0.13
Cyclic Ether Formation	38	3	4.42	4.42	1.00	0.85
Diels-alder addition	19	13	0.45	0.33	0.37	0.17
Disproportionation	140	65	1.45	1.19	0.39	0.16
H-abstraction	2841	645	0.79	0.63	0.50	0.32
HO2 Elimination from Peroxy Radical	16	6	1.41	1.18	1.11	0.55
Intra H-migration	331	40	1.87	1.53	1.03	0.48
Intra R Add Endocyclic	724	9	1.09	0.89	0.92	0.31
R Addition Multiple Bond	2642	378	0.90	0.64	0.39	0.26
R Recombination	101	390	1.38	0.78	1.37	0.52
Overall mean	-	-	1.48	1.21	0.66*	0.40*
Mean for large families**	-	-	1.25	0.94	0.80*	0.40*

Table 2-3 gives an overview of the validation for families which matched reactions in the NIST database. Families for which there is a small amount of training data do not provide a good assessment of accuracy. Given only a few points of training data, the error could be either over-estimated or under-estimated depending on the chemical similarity of the test data to the training data. Therefore, the best comparison uses the last line of Table 2-3, which only includes families with a hundred or more points of training data. For these large families, the MAE is 0.94 for exact matches, indicating that RMG estimates rate coefficients with an order of magnitude error when data is available (exact matches). The MAE for the LOOCV is 0.40 which approximately

corresponds to multiplicative error of 2.5. The MAE for LOOCV corresponds to additional error incurred when RMG uses its averaging scheme. Therefore, one would expect an averaged rate coefficient from RMG to have a total MAE = 1.34, combining the MAE from the exact matches and the LOOCV, which results in a total multiplicative error of ~22. Interestingly, it can be seen from Figure 2-12 that the LOOCV tends to have more outliers outside of the two order of magnitude bounds shown in dotted lines. Although on average, RMG's averaging scheme adds less error than the exact matches, it occasionally adds a large amount. This probably occurs when there is no training data within a close 2-norm to the template of interest.

2.4.4 Reaction library

Reaction libraries are user-defined lists of reactions and kinetic parameters, meant to supplement the core reaction families. All species are defined in RMG dictionary format. Reactions are written as Python-style entries and assigned kinetic parameters with degeneracy factored into the A-factor, similar to training reactions. Kinetic parameters defined in a library replace those estimated by the reaction families. However, these parameters will only be used for the exact reaction to which they are assigned. No averaging or generalization for these parameters will be considered for similar reactions. In contrast to the reaction families, pressure-dependent networks can be defined inside reaction libraries using Troe [26] or Chebyshev form [27]. One drawback to defining pressure dependence in a reaction library is that RMG considers the pressure-dependent network complete and will not attempt to incorporate newly discovered reactions into the same network; this typically causes the RMG model to omit minor product channels of the chemically-activated reactions in the library.

2.5 Unit tests for RMG database

Previously users adding to the database would often make mistakes that would make their training data inaccessible to RMG. It cannot be stressed enough that a prudent user should run quick test jobs to ensure that data they've added emerges in their models. To help alleviate these frustrations, unit tests have been implemented that automatically check for common mistakes when modifying the rate estimation database. In this new framework, failing a unit test prevent the user from pushing such changes to the master branch of RMG. During the implementation of the unit tests all offending database entries were corrected. Unless specifically stated otherwise, all unit tests apply to both the thermochemistry and reaction families.

Many of the unit tests are self-explanatory: checkNodesFoundInTree ensures that each group exists in the tree, checkGroupsNonidentical makes sure that no two groups are exactly isomorphic, checkChildParentRelationships makes sure that each child is indeed subgraph isomorphic to its parent. The test checkSiblingsForParents has a little more complexity. Imagine group A which is a parent to group B and group C, with group B appearing first in the tree i.e. B is an older sibling to C. Because RMG uses post-order tree transversal, B will always be matched before C. If C is subgraph isomorphic to B, then C can never be reached. Thus, checkSiblingsForParents will throw an error whenever it finds an instance that a younger sibling is sub-graph isomorphic to an older one. It does *not* check if B is subgraph isomorphic to C because including that restriction would limit the flexibility of tree design.

The next test, checkCdAtomType, is a misnomer; it actually checks several atom types: 'Cd', 'CO', 'Cdd', and 'CS'. As can be seen in Table 2-1, each of these atom types is a carbon atom with very specific requirements on the bonding. For example, Cd must have exactly one double bond to an atom that is not sulfur or oxygen. It is possible for a user to create a group with an atom typed as Cd but which cannot actually fulfill the atom type requirements. For instance, if a Cd atom is shown to have three or more single bonds, it cannot have a double bond. This group would never match any molecules. (As an aside, a Cd atom with two single bonds and no other explicitly bonds would still be valid because any unwritten bonds are assumed to be wildcard.) The checkCdAtomType ensures that the four atom types listed above fulfill all bonding requirements. It is somewhat outdated because many more atom types should be tested in this way.

The test checkSampleDescendsToGroup is a generalized accessibility test that ensures every group can be reached by some molecule. All mistakes found by all previously described tests are subsets of mistakes checkSampleDescendsToGroup will catch. However, they are not completely redundant. The unit test, checkSampleDescendsToGroup, will only tell the user when an entry is inaccessible, but not *why* it is inaccessible. Regardless, this unit test is a powerful tool for finding the novel and unexpected mistakes users can make. In fact, the development of this unit test aided in the development of the many rules applied to unimolecular reactions listed in section 4.2.

For each group A in a tree, checkSampleDescendsToGroup will create a sample molecule object B. Then it will descend the tree searching for the best post-order match for the created

molecule B, eventually settling on some matched group C. The test then asserts that C must either be A itself or have A as an ancestor. When creating the sample molecule, the test creates the simplest molecule that fulfills bonding requirements for each atom type in the group and then saturates all unfilled valences with hydrogen atoms. Due to the complexity of polycyclic aromatics, the algorithm cannot create any sample molecule with more than two fused aromatic rings, throwing a warning instead. Additional complications arise when creating sample molecules for end groups in unimolecular families. If one created the sample molecule solely from the end group, it would result in a molecule that would never react in family. To create a functional sample molecule, the end group must be merged with a backbone group. For simplicity, the top backbone group is always chosen.

Finally, there are two unit tests which are only applied to reaction families. The checkReactantAndProductTemplate checks that reversible families have the same product and reaction top level node, and that non-reversible families have different reactant and product nodes. The checkUnimolecularGroups tests that groups in unimolecular families follow the rules outlined in section 4.2.

2.6 Conclusions

The RMG database is an essential feature for mechanism generation which provides estimates for the thermochemistry and kinetic parameters. The most current version is compatible with species composed of hydrogen, carbon, oxygen, nitrogen, and sulfur. Molecular structure is represented using graph data structures called adjacency lists. These adjacency lists are used to match species with groups in the database. For thermochemistry, the matched groups each have associated Benson group additivity values, which are used to provide the estimates. The groups are organized in a hierarchical tree data structure with increasing specificity with descent. This approach yields estimates for free energy at 298K which have a mean error of 5.96 kcal/mol for non-cyclic oxygenates and 23.24 kcal/mol for non-cyclic nitrogen-containing species. The large error for nitrogen-containing species appears to arise from missing data for key groups that appear in the test set. Estimates for cyclic species are usually a little bit poorer than for aliphatics: 6.49 kcal/mol for cyclic oxygenates and 14.06 kcal/mol for nitrogen containing cyclics.

The other main function of the database is to provide kinetic estimates of reactions. The database stores 55 reaction families, recipes for possible chemical reactions. Like the thermochemistry groups, each family categorizes its reacting sites with hierarchical tree data structures. When estimating a reaction rate, the subtrees in the family are descended (in post-order) to find the most specifically matched groups, generating a template. In some cases, the matched template has assigned kinetic parameters in the form a rate rule or training reaction. More commonly, the reaction rate will be estimated by averaging the closest templates with kinetic parameters. Overall, this approach leads to reaction coefficients at 1000 K which are generally within 2 orders of magnitude of experiment, having an average multiplicative error of ~10 when no averaging algorithm is required and a factor of 22 when averaging is required.

The ability to provide estimates of thermochemistry and kinetic parameters gives it wide application in the field of chemical kinetics. In the future, the potential uses of the tool will only grow with increased usage, data, and functionality.

2.7 References

[1]   Lu, T., and Law, C. K., 2009, "Toward Accommodating Realistic Fuel Chemistry in Large-Scale Computations," Prog. Energy Combust. Sci., 35(2), pp. 192–215.

[2]   Broadbelt, L. J., Stark, S. M., and Klein, M. T., 1994, "Computer Generated Pyrolysis Modeling: On-the-Fly Generation of Species, Reactions, and Rates," Ind. Eng. Chem. Res., 33(4), pp. 790–799.

[3]   Gao, C. W., Allen, J. W., Green, W. H., and West, R. H., 2016, "Reaction Mechanism Generator: Automatic Construction of Chemical Kinetic Mechanisms," Comput. Phys. Commun., 203, pp. 212–225.

[4]   Warth, V., Battin-Leclerc, F., Fournet, R., Glaude, P. A., Côme, G. M., and Scacchi, G., 2000, "Computer Based Generation of Reaction Mechanisms for Gas-Phase Oxidation," Comput. Chem., 24(5), pp. 541–560.

[5]   Vandewiele, N. M., Van Geem, K. M., Reyniers, M.-F., and Marin, G. B., 2012, "Genesys: Kinetic Model Construction Using Chemo-Informatics," Chem. Eng. J., 207–208(Supplement C), pp. 526–538.

[6]   Rangarajan, S., Bhan, A., and Daoutidis, P., 2012, "Language-Oriented Rule-Based Reaction Network Generation and Analysis: Description of RING," Comput. Chem. Eng., 45(Supplement C), pp. 114–123.

[7]   Ranzi, E., Dente, M., Goldaniga, A., Bozzano, G., and Faravelli, T., 2001, "Lumping Procedures in Detailed Kinetic Modeling of Gasification, Pyrolysis, Partial Oxidation and Combustion of Hydrocarbon Mixtures," Prog. Energy Combust. Sci., 27(1), pp. 99–139.

[8]   Blurock, E. S., 1995, "Reaction: System for Modeling Chemical Reactions," J. Chem. Inf. Comput. Sci., 35(3), pp. 607–616.

[9]   Blurock, E., Battin-Leclerc, F., Faravelli, T., and Green, W. H., 2013, "Automatic Generation of Detailed Mechanisms," Cleaner Combustion, Springer, London, pp. 59–92.

[10]   Van de Vijver, R., Vandewiele, N. M., Bhoorasingh, P. L., Slakman, B. L., Seyedzadeh Khanshan, F., Carstensen, H.-H., Reyniers, M.-F., Marin, G. B., West, R. H., and Van Geem, K. M., 2015, "Automatic Mechanism and Kinetic Model Generation for Gas- and Solution-Phase Processes: A Perspective on Best Practices, Recent Advances, and Future Challenges," Int. J. Chem. Kinet., 47(4), pp. 199–231.

[11]   Benson, Sidney W., 1976, Thermochemical Kinetics: Methods for the Estimation of Thermochemical Data and Rate Parameters, Wiley.

[12]   Lide, D. R., and Kehiaian, H. V., 1994, CRC Handbook of Thermophysical and Thermochemical Data, CRC Press, Boca Raton.

[13]   Ruscic, B., Pinzon, R. E., Laszewski, G. von, Kodeboyina, D., Burcat, A., David Leahy, Montoy, D., and Wagner, A. F., 2005, "Active Thermochemical Tables: Thermochemistry for the 21st Century," J. Phys. Conf. Ser., 16(1), p. 561.

[14]   Linstrom, P. J., and Mallard, W. G., Eds., "NIST Chemistry WebBook, NIST Standard Reference Database Number 69, National Institute of Standards and Technology, Gaithersburg MD, 20899" [Online]. Available: http://webbook.nist.gov/chemistry/.

[15]   Goos, E., Burcat, A., and Ruscic, B., 2009, "Third Millennium Ideal Gas and Condensed Phase Thermochemical Database for Combustion," URL Httpgarfield Chem Elte HuBurcatburcat Html.

[16]   Ritter, E. R., and Bozzelli, J. W., 1991, "THERM: Thermodynamic Property Estimation for Gas Phase Radicals and Molecules," Int. J. Chem. Kinet., 23(9), pp. 767–778.

[17]   Manion, J. A., Huie, R. E., Levin, R. D., Burgess Jr., D. R., Orkin, V. L., Tsang, W., McGivern, W. S., Hudgens, J. W., Knayzev, V. D., Atkinson, D. B., Chai, E., Tereza, A. M., Lin, C.-Y., Allison, T. C., Mallard, W. G., Westly, F., Herron, J. T., Hampson, R. F., and Frizzell, D. H., 2015, "NIST Chemical Kinetics Database, NIST Standard Reference Database 17, Version 7.0 (Web Version), Release 1.6.8, Data Version 2015.12, National Institute of Standards and Technology, Gaithersburg, Maryland, 20899-8320." [Online]. Available: http://kinetics.nist.gov. [Accessed: 19-Oct-2017].

[18]   Frenklach, M., 2007, "Transforming Data into knowledge—Process Informatics for Combustion Chemistry," Proc. Combust. Inst., 31(1), pp. 125–140.

[19]   Lay, T. H., Bozzelli, J. W., Dean, A. M., and Ritter, E. R., 1995, "Hydrogen Atom Bond Increments for Calculation of Thermodynamic Properties of Hydrocarbon Radical Species," J. Phys. Chem., 99(39), pp. 14514–14527.

[20]   Han, K., Jamel, A., Grambow, C. A., Buras, Z. J., and Green, W. H., (submitted), "An Extended Group Additivity Method for Polycyclic Thermochemistry Estimation," INT J CHEM KINET.

[21]   Ramakrishnan, R., Dral, P. O., Rupp, M., and Lilienfeld, O. A. von, 2014, "Quantum Chemistry Structures and Properties of 134 Kilo Molecules," Sci. Data, 1, p. sdata201422.

[22]   Simmie, J. M., and Somers, K. P., 2015, "Benchmarking Compound Methods (CBS-QB3, CBS-APNO, G3, G4, W1BD) against the Active Thermochemical Tables: A Litmus Test for Cost-Effective Molecular Formation Enthalpies," J. Phys. Chem. A, 119(28), pp. 7235–7246.

[23]   Allen, J. W., Goldsmith, C. F., and Green, W. H., 2011, "Automatic Estimation of Pressure-Dependent Rate Coefficients," Phys. Chem. Chem. Phys., 14(3), pp. 1131–1155.

[24]   Jalan, A., Alecu, I. M., Meana-Pañeda, R., Aguilera-Iparraguirre, J., Yang, K. R., Merchant, S. S., Truhlar, D. G., and Green, W. H., 2013, "New Pathways for Formation of Acids and Carbonyl Products in Low-Temperature Oxidation: The Korcek Decomposition of γ-Ketohydroperoxides," J. Am. Chem. Soc., 135(30), pp. 11100–11114.

[25]   Carstensen, H.-H., and Dean, A. M., 2009, "Rate Constant Rules for the Automated Generation of Gas-Phase Reaction Mechanisms," J. Phys. Chem. A, 113(2), pp. 367–380.

[26]   Gilbert, R. G., Luther, K., and Troe, J., 1983, "Theory of Thermal Unimolecular Reactions in the Fall-off Range. II. Weak Collision Rate Constants," Berichte Bunsenges. Für Phys. Chem., 87(2), pp. 169–177.

[27]   Venkatesh, P. K., Dean, A. M., Cohen, M. H., and Carr, R. W., 2011, "CHEBYSHEV EXPANSIONS AND SENSITIVITY ANALYSIS FOR APPROXIMATING THE TEMPERATURE- AND PRESSURE-DEPENDENCE OF CHEMICALLY-ACTIVATED REACTIONS," Rev. Chem. Eng., 13(1), pp. 1–67.

Chapter 3

Understanding the low-T ignition of propane+methanol blends

3.1 Introduction

The development of detailed low-T ignition chemistry models is challenging because of the large number of intermediate species involved, particularly di-substituted peroxy intermediates such as hydroperoxyalkyl radicals and ketohydroperoxides (KHP). Existing models for pure single-component fuels often contain several hundred chemical species (even after some lumping). [1][2] Because of this complexity, only a few detailed models for low-T ignition of fuel blends have been constructed [3][4][5]; the number of potential cross-reactions between the different fuel species is already intimidating.

In this work, we study the ignition pathways for a blend of propane and methanol. These types of fuel exemplify differences in fuel chemistry. Propane, like larger alkanes [6], has low-temperature chemistry dominated by the chain-branching production of KHPs. After reaching around 700K, the KHP formation chemistry slows down relative to competing HO_2 producing channels, resulting in slower production of radicals. Therefore, propane experiences a negative temperature coefficient (NTC) region, characterized by slowing ignition with increasing initial temperature. Methanol, the simplest

53

representative alcohol, does not produce KHP at low temperatures [7], [8]. Because methanol has less chain branching at low temperatures, it has overall slower ignition delay and no NTC behavior. By combining these two fuels, we are able to analyze quantitatively how their low temperature chemistry is affected by one another.

In this work, detailed kinetic mechanisms of propane and methanol are reduced to pinpoint only the chemistry related to auto-ignition. By studying the reduced mechanism, we are able to sub-divide the ignition into different stages and identify controlling chemistry of each step. An analytical expression is derived for the transition between the first and second stage of ignition for methanol. Unfortunately, later stages of ignition chemistry in both propane and methanol prove too complex to simplify to an analytical expression. Finally, we show that these cross-reactions do not affect the ignition delay very much, so that fuel blend models can be constructed by combining models for each fuel. In fact, all the important reactions are zero-order or first-order in fuel species, suggesting that more simplifications are possible. To a large degree, particularly in stage 2, the chemistry is dominated by OH and HO2 reactions with fuel species and with small molecule products such as formaldehyde; the HO2 reactions with fuel are important because they form H2O2 and so lead to chain branching. Combining this information with an understanding of the different stages of pre-ignition chemistry and prior analyses of ignition kinetics [9][10][11] makes the problem of modeling ignition of fuel blends more manageable.

3.2 Mechanism creation

The full chemical mechanism for propane is taken from Merchant et al.[9]; key parameters were taken from high level ab-initio calculations [12],[13], the H2/O2 sub-mechanism of Li et al[14] and the methyl formate sub-mechanism of Dooley et al.[15] The methanol mechanism was generated by the Reaction Mechanism Generator(RMG) [16] using some thermochemistry and kinetic rate parameters from [15],[17]. The hydrogen abstraction from methanol by O2 and HO2 were updated by conventional TST calculations performed by the authors at the CBS-QB3 level using Gaussian 03[18]. A combined propane/methanol model was creating by first manually merging the two models, and then using RMG to fill in cross reactions between the two. Smaller reduced models were created by selecting reactions from the full model that were relevant to pre-ignition chemistry based on the analyses discussed below. All model simulations presented in this work are performed using Chemkin Pro [19].

3.3 Low Temperature Oxidation of Methanol

The pre-ignition chemistry of methanol is relatively simple compared to alkanes, following one major reaction pathway, which is a subset of an analogous pathway seen in alkanes, discussed below with Fig. 2. As a result of its simpler chemistry, methanol lacks both the two-stage ignition and the NTC region characteristic of alkane fuels. Figure 3-13 shows the concentration and temperature profile for methanol ignition.
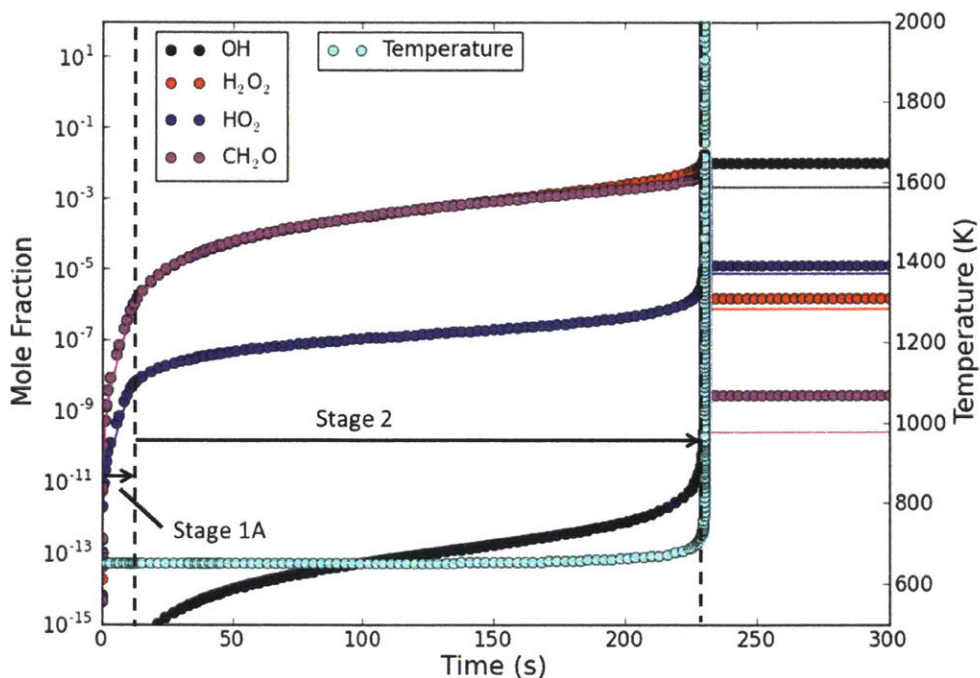
Figure 3-13 Temperature and concentration profile for key species in methanol ignition
The reactor is adiabatic and isochoric starting at T_0=650K and P_0=10 bar with stoichiometric air/fuel ratio. The solid line shows the profile generated from the reduced mechanism and the dots show results from the full mechanism.

In keeping with terminology defined in [9], the time period characterized by exponential growth is called stage 1A. The following time period, stage 2, observes a quasi-steady state for H2O2 and HO2. The temperature remains nearly constant throughout most of the pre-ignition period and experiences only one dramatic rise at the onset of ignition. Figure 3-14 summarizes the major reaction pathway for methanol pre-ignition.
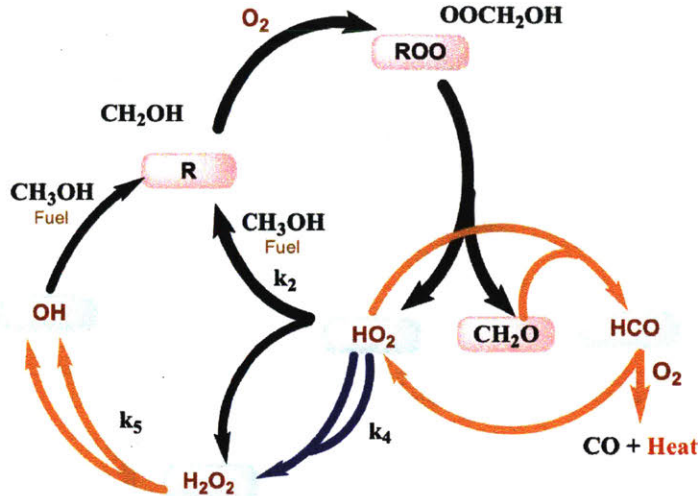
Figure 3-14 Major pathways during low temperature oxidation of methanol
Black arrows signify chemistry that is important during stage 1A, blue arrows reactions important in stage 2, and orange arrows reactions that become important just prior to the final ignition.

H-abstraction from methanol strongly favors the formation of CH2OH radical. This reacts with oxygen to form a peroxy radical, which decomposes to HO2 radical and formaldehyde. The HO2 forms H2O2 by reacting with fuel or by self-reaction. The resulting H2O2 slowly decomposes to two OH radicals which each immediately abstract hydrogen from the fuel, eventually leading to the formation of two more HO2 radicals.

During first stage ignition, ordinary differential equations can be written for the concentration of HO2 and H2O2. In the vector form:

$$\frac{dC}{dt} = \underline{\underline{M}}\,\underline{C} + \underline{R} \tag{1}$$

where C is the concentration vector, M is a matrix of coefficients and R is a vector of constants. Plugging in the correct coefficients gives:

$$\frac{d}{dt}\begin{bmatrix} H_2O_2 \\ HO_2 \end{bmatrix} = \begin{bmatrix} -k_5 & k_2[CH_3OH] \\ 2k_5 & 0 \end{bmatrix}\begin{bmatrix} H_2O_2 \\ HO_2 \end{bmatrix} + \begin{bmatrix} 0 \\ 2k_1[CH_3OH][O_2] \end{bmatrix} \tag{2}$$

The system of ODEs has the exact solution

$$\underline{C} = \underline{\underline{V}}exp\left(\underline{\underline{\Lambda}}t\right)\underline{\underline{V}}^{-1}\underline{C_0} + \underline{\underline{V}}\left(exp\left(\underline{\underline{\Lambda}}t\right) - \underline{\underline{I}}\right)\underline{\underline{\Lambda}}^{-1}\underline{\underline{V}}^{-1}\underline{R} \tag{3}$$

where V and Λ are the eigenvector and eigvenvalue matrices of M. Given two ODEs, two eigenvalues arise, one of which is always negative and the other always positive:

56

$$\lambda_- = -k_5 - (k_5^2 + 8k_2k_5[CH_3OH])^{-\frac{1}{2}} \tag{4}$$

$$\lambda_+ = -k_5 + (k_5^2 + 8k_2k_5[CH_3OH])^{-\frac{1}{2}} \tag{5}$$

Including the induction period, this can be solved exactly:

$$[H_2O_2]_{stage\ 1A} = \frac{2k_1[CH_3OH][O_2]\lambda_-}{\lambda_- - \lambda_+} \times \left(\frac{1}{\lambda_-} - \frac{1}{\lambda_+} - \frac{\exp(\lambda_-t)}{\lambda_-} + \frac{\exp(\lambda_+t)}{\lambda_+} \right) \tag{6}$$

$$[HO_2]_{stage\ 1A} = \frac{k_1[CH_3OH][O_2]}{2k_5^2(\lambda_- - \lambda_+)} \times \left(\frac{\lambda_+}{\lambda_-} - \frac{\lambda_-}{\lambda_+} - \frac{\lambda_+\exp(\lambda_1t)}{\lambda_-} + \frac{\lambda_-\exp(\lambda_+t)}{\lambda_+} \right) \tag{7}$$

However, because there is only one positive eigenvalue, the last term in each equation will eventually dominate, making the following very good approximations:

$$[H_2O_2]_{stage\ 1A} \approx \frac{2k_1[CH_3OH][O_2]\lambda_-}{\lambda_+(\lambda_- - \lambda_+)} \times \exp(\lambda_+t) \tag{8}$$

$$[HO_2]_{stage\ 1A} \approx \frac{k_1[CH_3OH][O_2]\lambda_-}{2k_5^2\lambda_+(\lambda_- - \lambda_+)} \times \exp(\lambda_+t) \tag{9}$$

Although OH radical is generally thought to drive pre-ignition chemistry, it is actually HO2 the leads to chain branching in methanol. Every radical of HO2 that abstracts from methanol eventually forms another HO2 from the hydroxymethyl radical and two OH radicals from the decomposition of H2O2.

The transition from stage 1A to stage 2 occurs when HO2 self-reaction becomes competitive with H-abstraction by HO2. The differential equations of importance are:

$$\frac{d}{dt}[H_2O_2] = -k_5[H_2O_2] + k_2[CH_3OH][HO_2] + k_p[CH_2O][HO_2] + k_4[HO_2]^2 \cong 0 \tag{10}$$

$$\frac{d}{dt}[HO_2] = 2k_5[H_2O_2] - 2k_4[HO_2]^2 \cong 0 \tag{11}$$

Combining Eq. 8, 9, and 11 results in the following expression for the transition time to stage 2 is derived

57

$$t_{1B} = \frac{\ln\left(\frac{k_2[CH3OH]}{k_4[HO_2]}\right)}{\lambda} \qquad (12)$$

These two equations can be solved simultaneously showing that HO_2 is proportional to the square root of H_2O_2.

$$\frac{[HO_2]_{stage2}}{\left([H_2O_2]_{stage2}\right)^{1/2}} = \left(\frac{k_5}{k_4}\right)^{1/2} \qquad (13)$$

Further manipulation, gives a final expression for HO_2:

$$[HO_2]_{stage2} = 2\frac{k_5}{k_4}(k_2[CH_3OH] + k_9[CH_2O])t + constant \qquad (14)$$

Ignition occurs only when there is a sufficient concentration of formaldehyde that the orange reaction pathway shown in Figure 3-14 becomes competitive with the others. The reaction $O_2 + HCO \rightarrow CO + HO_2$ is highly exothermic due to the formation of carbon monoxide. Once this reaction becomes significant, a positive feedback loop between temperature and increased radical production (from H_2O_2) begins, quickly consuming all fuel.

A reduced mechanism was created for methanol using only the chemistry presented above, resulting in a total of 12 reactions. The reduced mechanism is given in Table 3-4.

Table 3-4 Reduced mechanism for methanol oxidation

Label	Reaction	Rate coefficient	Reference
R1	$CH_3OH + O_2 = HO_2 + CH_2OH$	k_1	This study
R2	$CH_3OH + OH = H_2O + CH_2OH$	k_2	[20]
R3	$CH_3OH + HO_2 = H_2O_2 + CH_2OH$	k_3	This study
R4	$HO_2 + HO_2 = O_2 + H_2O_2$	k_4	[17]
R5	$H_2O_2 = 2OH$	k_5	[17]
R6	$O_2 + CH_2OH = HO_2 + CH_2O$	k_6	[21]
R7	$O_2 + CH_2OH = OOCH_2OH$	k_7	[16]
R8	$OOCH_2OH = HO_2 + CH_2O$	k_8	[16]
R9	$HO_2 + CH_2O = H_2O_2 + HCO$	k_9	[22]
R10	$O_2 + CH_2O = HO_2 + HCO$	k_{10}	[23]
R11	$OH + CH_2O = H_2O + HCO$	k_{11}	[24]
R12	$O_2 + HCO = CO + HO_2$	k_{12}	[25]

A comparison of the reduced and full models is given in Figure 3-13. The temperature and species concentration match almost exactly during the pre-ignition chemistry, with the ignition delay being predicted with less than 5% error for a variety of initial temperatures. However, the reduced model does not predict the correct ignition temperature because many of the high temperature oxidation reactions (such as CO_2 formation) are missing. This drawback is acceptable as the goal of the reduced model is to predict the timing of the ignition without necessarily predicting the post-ignition conditions.

3.4 Low Temperature Oxidation of Propane

Historically, alkane fuels were said to ignite in two stage manner, observed experimentally by an initial temperature rise (stage 1 ignition) followed by a relatively isothermal induction period prior to the final ignition event. As seen in Figure 3-15, the first stage can be further divided into stage 1A and stage 1B, which is only observable when tracking the radical concentrations as opposed to temperature or pressure. A detailed schematic showing the oxidation chemistry for propane is presented in Figure 3-16.
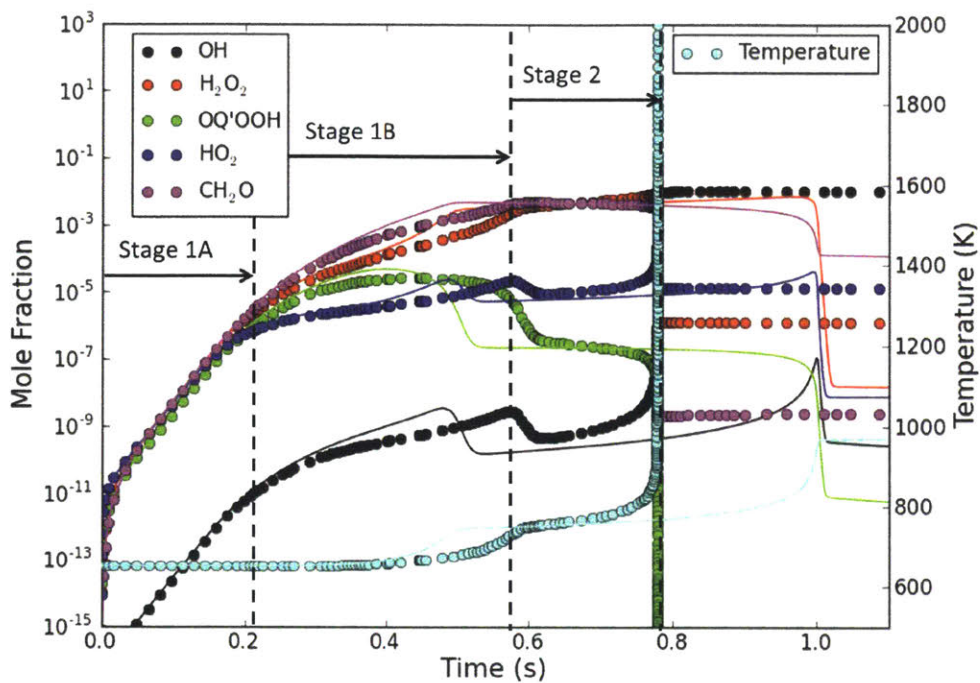
Figure 3-15 Temperature and concentration profile for key species for propane oxidation
The reactors is isochoric adiabatic starting at 650K, 10 bar and stoichiometric air/fuel ratio. The solid lines show results of a reduced mechanism and the dots show the full detailed mechanism
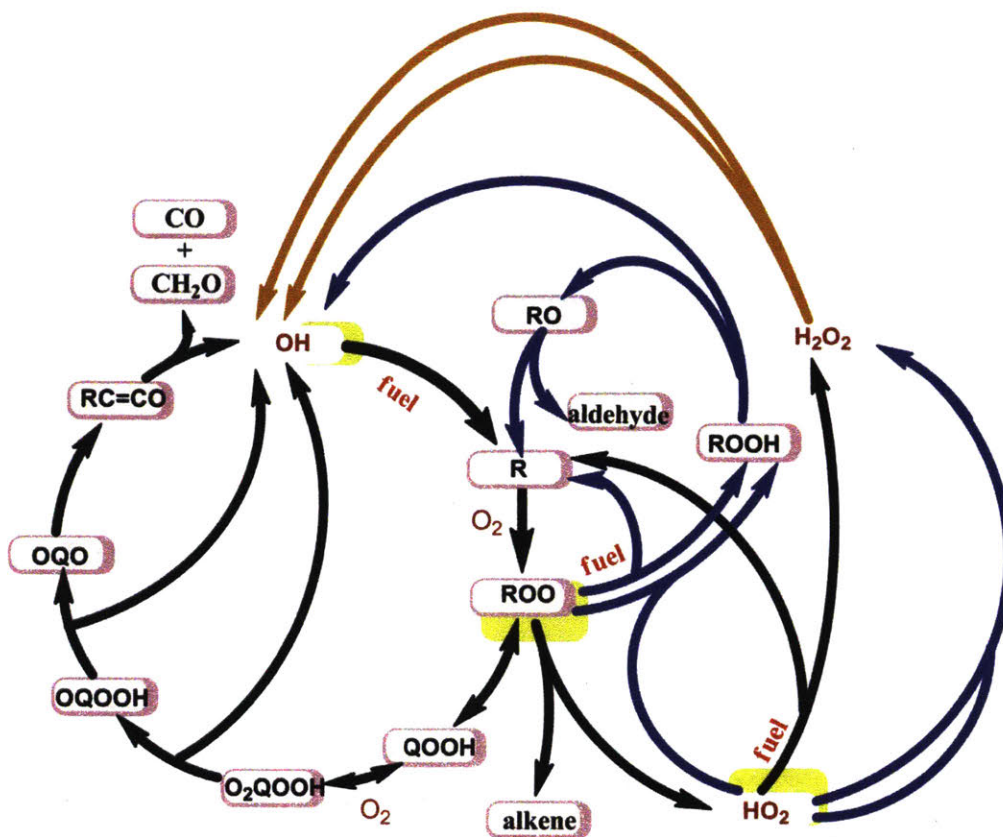
Figure 3-16 Schematic of major reaction pathways for oxidation of propane
The pathways shown in black arrow are significant during stage 1A, the blue arrows during stage 1B, and the orange arrows during stage 2. Key branching ratios are highlighted.

The ketohydroperoxide cycle shown on the left in black arrows in Figure 3-16 has been discussed in detail in [9]. The overall feedback cycle gives rise to 3 OH radicals and results an in exponential rise in radicals during stage 1A. In this study, we add the coupling with the H_2O_2 and ROOH cycles which become important at the end of stage 1B and throughout stage 2.

During stage 1A of ignition, the HO_2 radicals contribute significantly to the hydrogen abstraction of the fuel, resulting in some production of H_2O_2. Similarly to methanol, the transition from stage 1A to 1B occurs when a sufficient concentration of HO_2 has built up, such that HO_2 self-reaction overtakes hydrogen abstraction by HO_2. This effect dampens the exponential rise causing the concentration profiles in Figure 3-15 to level off. Additionally, the HO_2 can react with RO_2 to form ROOH, which will decompose to OH and alkoxy radical (RO) at a similar rate to OQ'OOH decomposition. The n-propyl alkoxy radicals (nRO) beta scission to formaldehyde and a smaller R' radical, which continues on a similar reaction paths as R. Alkoxy radicals from nRO may continually decompose until a formaldehyde

is formed for each carbon. The overall reaction when n-propyl peroxy (nRO$_2$) follows this decomposition path all the way through is:

$$nRO_2 + 3HO_2 \rightarrow 3OH + 3CH_2O + H + O_2 \tag{15}$$
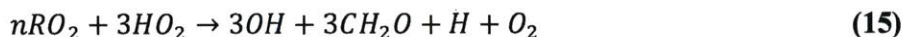
Although the overall ROO+HO2 reaction path is chain propagating, it increases the reactivity of the system because it converts three less reactive HO$_2$ into three OH radicals. By contrast, iso-propyl alkoxy radicals (iRO) beta scission directly to methyl radical and ethanal, with weaker kinetic effects. A rate of production (ROP) analysis of OH is presented in Figure 3-17. The QOOH pathway dominates OH production until beginning of stage 1B, but the RO$_2$+HO$_2$ pathways become comparable around the time of first stage ignition. In fact, for a brief period, the decomposition of CH$_3$OOH (resulting from methyl radical from both iRO and nRO beta-scission) becomes more significant than the QOOH cycle. After the QOOH cycle shuts down due to increased temperature, OH is produced primarily by H$_2$O$_2$ via the cycle described above for methanol.
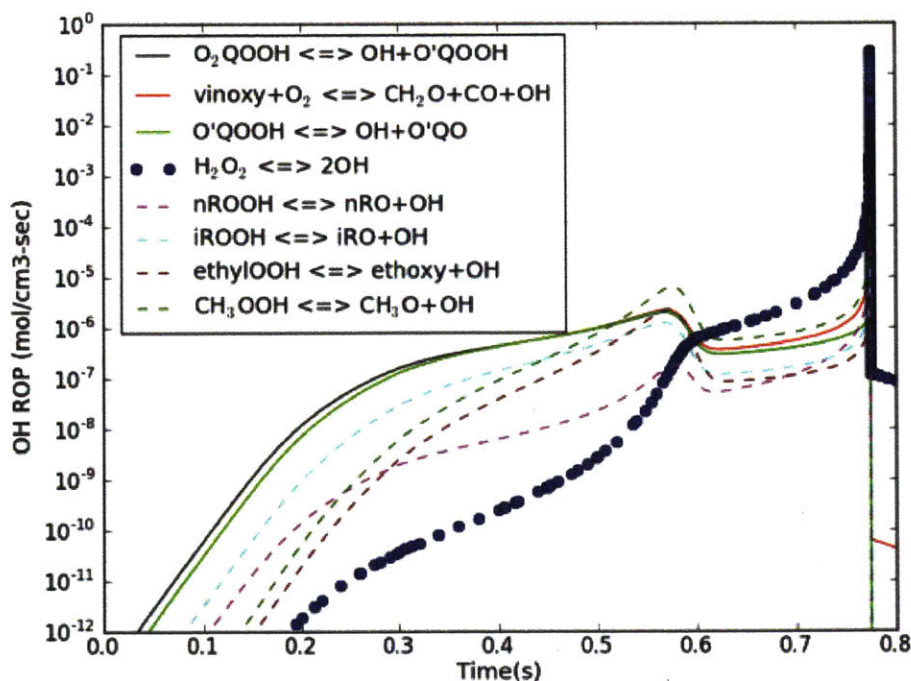
Figure 3-17 OH radical ROP from key reactions during different stages of ignition.
The solid lines show reactions associated with the low temperature ketohydroperoxide chain branching cycle. The dashed lines show reactions arising from beta scissions that become important at first ignition. The dotted line shows the decomposition of H2O2 important during stage 2.

Figure 3-18 presents an analysis on the heat production during propane oxidation. Many reactions contribute to the temperature release, but they all belong to just a few reaction classes. One of

the most exothermic classes is $R+O_2 \rightarrow RO_2$. Because the secondary radicals contribute non-negligibly to temperature rise, it becomes even more critical to include the $RO_2 + HO_2$ pathways. Other classes that significantly affect the temperature are O'QOOH decomposition, H-abstraction from fuel by OH, and H-abstraction from HO_2 by RO_2. A special case of the last class is the self-reaction of HO_2, which is important in almost all oxidation systems.
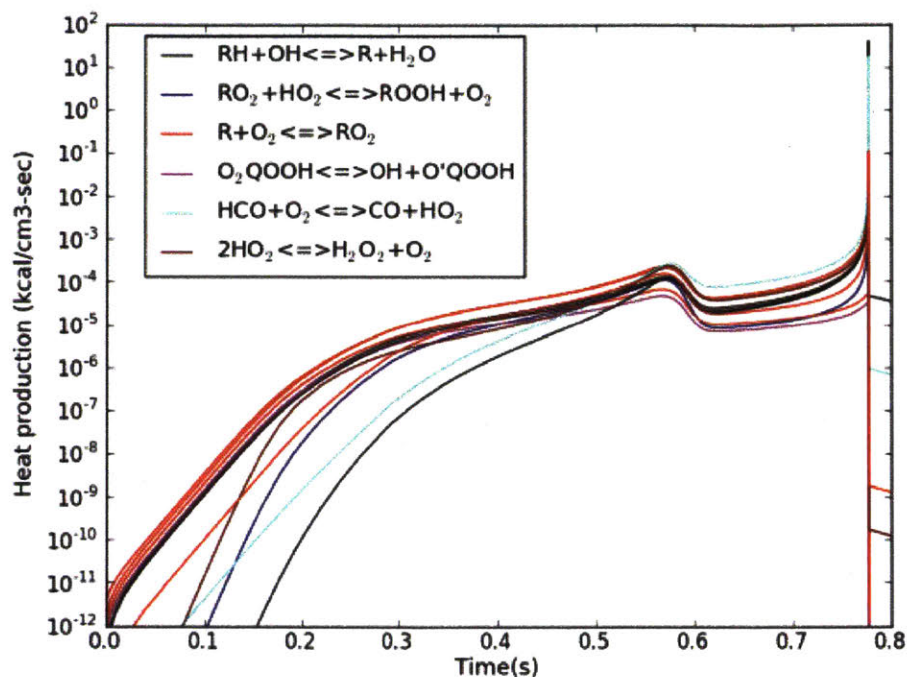
Figure 3-18 Heat produced per reaction for propane oxidation
Initial Conditions are 650K, 10 bar and stoichiometric conditions. While many reactions contribute non-negligibly to the heat release, they can be classified into just a few classes of reactions.

As the temperature rises the key branching ratio $RO_2 \rightarrow HO_2$ + alkene versus $RO_2 \rightarrow$ OQ'OOH changes significantly, due to the higher Ea for the first reaction and the reversibility of several steps between ROO and OQ'OOH. As a result, the left-hand cycle in Fig. 4 no longer has gain > 1, and the OQ'OOH concentration drops sharply. This change marks the transition from stage 1 to stage 2. Assuming negligible secondary chemistry, Merchant et al [9] calculated a critical temperature, $T_{stage1,max}$, above which the system enters stage 2. For stoichiometric oxidation of propane in 10 bar, the $T_{stage1,max}$=690K; longer n-alkanes have higher transition temperatures.[1] Finally, it was found that OH concentration was sensitive to hydrogen abstraction from fuel by RO_2 during the transition from stage1B to stage 2. The increase in temperature and the drop in $[HO_2]$ causes more RO_2 + fuel to become competitive with $RO_2 + HO_2$.

With lower OH production, all chemistry slows down, resulting in the point of inflection in dT/dt characteristic of first stage ignition. As seen in Figure 3-17, the majority of OH during stage 2 is produced by the decomposition of H_2O_2, whose concentration increases due to HO_2+RH. The stage 2 chemistry of propane is completely analogous to the stage 2 chemistry of methanol. As seen in Figure 3-18, second-stage ignition is even driven by the same exothermic reaction: H-abstraction from H_2CO forming carbon monoxide via HCO.

A reduced mechanism was formed using the chemistry discussed above. The reduced mechanism has 50 reactions whereas the full detailed mechanism had over 500. A comparison of the reduced model to the full model is shown in Figure 3-15 for stoichiometric oxidation at 650K and 10 bar. The reduced model slightly under-predicts first stage ignition, most likely because of missing side channels involving combinations of different RO_2 radicals. The error is compounded because the reduced model does not capture all heat rise. Throughout stage 2, the reduced model captures 87%-91% of the heat release of the full model, capturing less near the ignition as more secondary products appear. However, the timing of ignition is still captured within a factor of 2, despite the fact that more than 90% of the reactions in the full model have been deleted.

3.5 Reduced Mechanism for Propane/Methanol Blends

If the intermediates of initial radicals do not cross react significantly, then chemistry of fuel blends can be modeled as just the sum of individual mechanisms. Based on the analysis above, the important intermediates in pre-ignition chemistry only react significantly with small molecules (e.g. HO_2, OH) , fuel and O_2. To further test the theory, the reduced methanol and reduced propane mechanism were combined into a single mechanism. The only cross reactions added were the hydrogen abstractions of fuel and primary RO_2 (e.g. nRO_2 + methanol). These cross reactions do not add much complexity to the modeling. A comparison of the ignition delay predicted by the full model and the reduced model is presented in Figure 3-19. The comparison at 650K, which is most appropriate for low temperature, shows interesting behavior. For pure propane, the reduced model over-predicts ignition delay. The difference decreases until, at a 50% fuel mixture, the reduced model actually under-predicts ignition delay. The under-prediction becomes worse at 60% methanol, and improves for higher methanol blends until disappearing entirely at pure methanol. This trend suggests that some cross reactions missing in the reduced model have small impact on the ignition delay. However, the difference in the predicted ignition delays is always less than a factor of 1.5x (for comparison the ignition delays increase by more than a factor of 300x as mixture composition is varied), so the assumption of separable reaction pathways is usefully accurate.
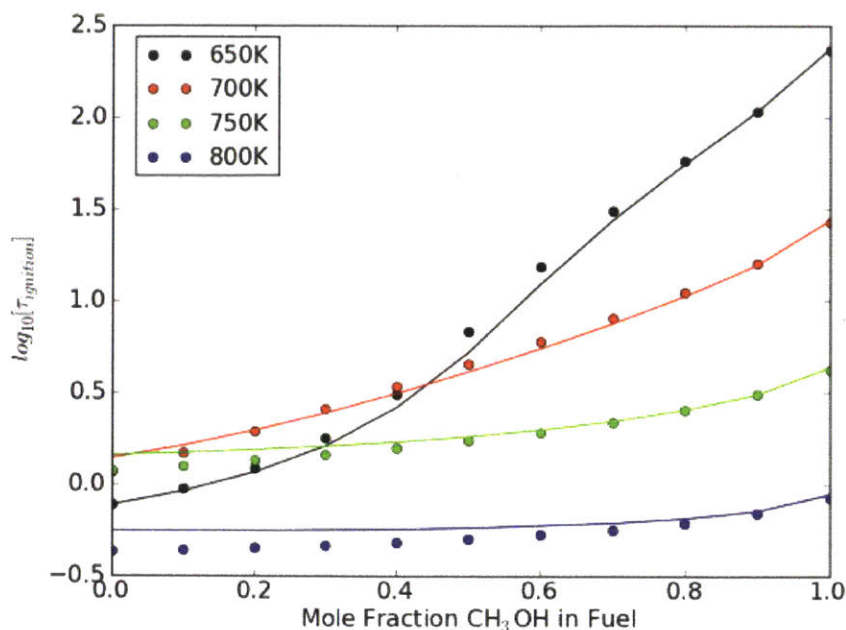
Figure 3-19 Comparison between reduced and full models' ignition delays for propane and methanol blends
All conditions were stoichiometric and at P=10 bar. The solid line shows the reduced model while the dots show the full model.

For all other temperatures, the largest discrepancies are for pure propane, with the reduced model becoming more accurate as the amount of methanol is increased, suggesting that cross reactions have an almost imperceptible effect at these temperatures

3.6 Conclusion

Using detailed modeling we analyze the controlling chemistry for methanol combustion. We find that while methanol is experimentally classified as a "one stage" fuel, the pre-ignition chemistry can be divided into two stages. In stage 1A, radicals rise exponentially based on a time constant, λ, which only depends on a few key rate constants and initial conditions. Stage 2 begins when HO_2 self-reaction overtakes abstraction from fuel, resulting in a dampening effect on the radical rise and leading to an approximately linear rise in HO_2. The main chain branching comes from decomposition of H_2O_2, itself a product of HO_2 abstractions. The final ignition event is preceded by heat production from the oxidation of formaldehyde.

We also build upon the work of [9] in the understanding of propane chemistry, principally adding coupling of HO_2 chemistry and successive RO2 + HO2 reactions, as well as an analysis of the

heat rise during ignition. ROOH decomposition becomes a non-negligible source of OH at the end of stage 1B. Also, we find that various $R+O_2 \rightarrow RO_2$ reactions contribute significantly to the temperature rise during the entire ignition, underscoring the need to track production of secondary R radicals. The chemistry changes drastically between stage 1 and stage 2 due to increased temperature, causing the gain of the ketohydroperoxide chemical amplifier to drop drastically. It was found that stage 2 chemistry in propane is parallel to stage 2 in methanol, with HO_2 + fuel = H_2O_2 driving the chain branching and even igniting due to the same exothermic sequence arising from CH_2O.

The above analysis allowed the creation of reduced mechanisms which predict ignition behavior within a factor of 2 using approximately 10% of the reactions in the full detailed model. We also constructed a combined mechanism from the reduced methanol and propane sub-mechanisms, which was simply the sum of the two sub-mechanisms with additional primary RO_2 + fuel reactions. The ignition delay from the combined reduced mechanisms agreed reasonably well with the ignition delay from full detailed mechanism of the fuel blend. This suggests that the fundamental chemistry is largely non-interacting, except through the chemistry of a few small molecules. This discovery has the potential to drastically simplify prediction of low temperature ignition of fuel blends.

3.7 References

[1]   H. J. Curran, P. Gaffuri, W. J. Pitz, and C. K. Westbrook, "A Comprehensive Modeling Study of n-Heptane Oxidation," *Combust. Flame*, vol. 114, no. 1–2, pp. 149–177, Jul. 1998.

[2]   O. Herbinet, W. J. Pitz, and C. K. Westbrook, "Detailed chemical kinetic oxidation mechanism for a biodiesel surrogate," *Combust. Flame*, vol. 154, no. 3, pp. 507–528, 2008.

[3]   O. Herbinet, W. J. Pitz, and C. K. Westbrook, "Detailed chemical kinetic mechanism for the oxidation of biodiesel fuels blend surrogate," *Combust. Flame*, vol. 157, no. 5, pp. 893–908, 2010.

[4]   S. M. Sarathy, M. J. Thomson, C. Togbé, P. Dagaut, F. Halter, and C. Mounaim-rousselle, "An experimental and kinetic modeling study of n -butanol combustion," *Combust. Flame*, vol. 156, no. 4, pp. 852–864, 2009.

[5]   Y. Sakai, A. Miyoshi, M. Koshi, and W. J. Pitz, "A kinetic modeling study on the oxidation of primary reference fuel – toluene mixtures including cross reactions between aromatics and aliphatics," *Proc. Combust. Inst.*, vol. 32, no. 1, pp. 411–418, 2009.

[6]   F. Buda, R. Bounaceur, V. Warth, P. A. Glaude, R. Fournet, and F. Battin-Leclerc, "Progress toward a unified detailed kinetic model for the autoignition of alkanes from C4 to C10 between 600 and 1200 K," *Combust. Flame*, vol. 142, no. 1, pp. 170–186, Jul. 2005.

[7]   U. Burke, W. K. Metcalfe, S. M. Burke, K. A. Heufer, P. Dagaut, and H. J. Curran, "A detailed chemical kinetic modeling, ignition delay time and jet-stirred reactor study of methanol oxidation," *Combust. Flame*, vol. 165, no. Supplement C, pp. 125–136, Mar. 2016.

[8]   C. L. Rasmussen, K. H. Wassard, K. Dam-Johansen, and P. Glarborg, "Methanol oxidation in a flow reactor: Implications for the branching ratio of the CH3OH+OH reaction," *Int. J. Chem. Kinet.*, vol. 40, no. 7, pp. 423–441, Jul. 2008.

[9]   S. S. Merchant, C. F. Goldsmith, A. G. Vandeputte, M. P. Burke, S. J. Klippenstein, and W. H. Green, "Understanding low-temperature first-stage ignition delay: Propane," *Combust. Flame*, vol. 162, no. 10, pp. 3658–3673, Aug. 2015.

[10]   N. Peters, G. Paczko, R. Seiser, and K. Seshadri, "Temperature Cross-Over and Non-Thermal Runaway at Two-Stage Ignition of N-Heptane," *Combust. Flame*, vol. 128, no. 1, pp. 38–59, 2002.

[11]   C. Sang, T. Lu, J. H. Chen, and C. K. Law, "Direct numerical simulations of ignition of a lean n -heptane / air mixture with temperature inhomogeneities at constant volume : Parametric study," *Combust. Flame*, vol. 158, no. 9, pp. 1727–1741, 2011.

[12]   C. F. Goldsmith, W. H. Green, and S. J. Klippenstein, "Role of O2 + QOOH in low-temperature ignition of propane. 1. temperature and pressure dependent rate coefficients," *J. Phys. Chem. A*, vol. 116, no. 13, pp. 3325–3346, 2012.

[13]   J. a. Miller and S. J. Klippenstein, "The reaction between ethyl and molecular oxygen II: Further analysis," *Int. J. Chem. Kinet.*, vol. 33, no. 11, pp. 654–668, 2001.

[14]   J. Li, Z. Zhao, A. Kazakov, and F. L. Dryer, "An updated comprehensive kinetic model of hydrogen combustion," *Int. J. Chem. Kinet.*, vol. 36, no. 10, pp. 566–575, 2004.

[15]   S. Dooley *et al.*, "Modeling the combustion of high molecular weight fuels by a functional group approach," *Int. J. Chem. Kinet.*, vol. 44, no. 9, pp. 257–276, 2010.

[16]   C. W. Gao, J. W. Allen, W. H. Green, and R. H. West, "Reaction Mechanism Generator: automatic construction of chemical kinetic mechanisms," *Comput. Phys. Commun.*

[17]   M. P. Burke, M. Chaos, Y. Ju, F. L. Dryer, and S. J. Klippenstein, "Comprehensive H2/O2 kinetic model for high-pressure combustion," *Int. J. Chem. Kinet.*, vol. 44, no. 7, pp. 444–474, 2012.

[18]   M. J. Frisch *et al.*, "Gaussion 03." Gaussian Inc., Pittsburgh, 2003.

[19]   "CHEMKIN-PRO 15131, Reaction Design: San Diego, 2013."

[20]   J. E. Bott and N. Cohen, "A Shock Tube Study of the Reaction of Methyl Radicals with Hydroxyl Radicals," *Int J Chem Kinet*, vol. 23, no. November 1990, pp. 1017–1033, 1991.

[21]   H. Grotheer, G. Riekert, D. Walter, and T. Just, "Non-Arrhenius Behavior of the Reaction of Hydroxymethyl Radicals with Molecular Oxygen," *J. Phys. Chem.*, vol. 92, no. 13, pp. 4028–4030, 1988.

[22]   B. Eiteneer, C.-L. Yu, M. Goldenberg, and M. Frenklach, "Determination of Rate Coefficients for Reactions of Formaldehyde Pyrolysis and Oxidation in the Gas Phase," *J. Phys. Chem. A*, vol. 102, no. 27, pp. 5196–5205, 1998.

[23]   Y. Hidaka, T. Taniguchi, and H. Tanaka, "Shock-tube study of CH 2 O pyrolysis and oxidation," *Combust. Flame*, vol. 376, no. 4, pp. 365–376, 1993.

[24]   W. Tsang and R. F. Hampson, "Chemical kinetic data base for combustion chemistry. Part I. Methane and related compounds," *J. Phys. Chem. Ref. Data*, vol. 15, no. 3, pp. 1087–1279, 1986.

[25]   R. S. Timonen, E. Ratajczak, and D. Gutman, "Kinetics of the reactions of the formyl radical with oxygen, nitrogen dioxide, chlorine, and bromine," *J. Phys. Chem.*, vol. 92, no. 3, pp. 651–655, 1988.

Chapter 4

Modeling Study of Substituted Phenols in Engine-like Conditions

4.1 Introduction

Engine knock, an undesirable combustion phenomena caused by the auto-ignition of the unburned mixture (end gas), significantly limits the efficiency of spark-ignition engines [1]. Therefore, the anti-knock tendency, which is described by octane number (ON), is a good criterion to screen the candidates in the development of additives and drop-in fuels. However the standard octane rating procedures, including the rating of research octane number (RON) [2] and motor octane number (MON) [3], are capital and time intensive. First, the new proposed additives must be synthesized and purified, and then it requires a trained technician to operate a specially made cooperative fuel research (CFR) engine following a complicated empirical rating protocol [2,3]. After all of those efforts, the only result is a single number without revealing any mechanistic information. Although there are some studies trying to correlate the ON with other observables such as infrared spectroscopy [4], distillation curve [5], and dielectric spectroscopy

[6], these methods are developed by fitting the existing ON database; no studies have reported a method for accurately predicting the ON of fuel mixtures containing additives not yet synthesized. Even a perfect method for predicting ON would not provide perfect ranking of fuels, since fuels which have the same ON can have very different ignition behavior in modern engines [7,8]. An ideal model would be able to predict the ignition delay of any fuel mixture at any engine-relevant condition.

In an engine, the end gas is compressed by the piston motion and by the flame propagation around top-dead-center (TDC). Knocking will occur if the end-gas auto-ignites before being consumed by the flame [9–11]. Therefore, the anti-knock tendency is mainly determined by the ignition delay time and the flame speed, which are both controlled by the combustion kinetics of the fuel. Consequently, the anti-knock tendency of an additive can be studied by simulation if 1) its combustion kinetics is known and 2) one can accurately estimate the conditions that the end gas experienced in the CFR test.

The former problem and the need for a model accurate at many reaction conditions can be solved by the reaction mechanism generator (RMG) [12], which is an open-source software package designed to automatically construct kinetic models using a flux-based algorithm for model expansion. As demonstrated in previously published papers [13–15], a reasonable model can be obtained with minimal manual work, making it feasible to study a series of molecules in a short time. Moreover, with the help of the kinetic model, the chemical origin of the anti-knock tendency of specific species can be analyzed, which will benefit the design of fuel additives in the future.

To estimate conditions that the end gas experienced in the CFR test, some studies [16–18] simply correlated the ON with the ignition delay in a constant volume batch reactor. However, more rigorous treatment also considers the actual pressure and temperature history experienced by the end gas. Westbrook *et al* [19] suggested incorporating a pressure profile from a real engine test into a perfect stirred reactor (PSR) to study the relation between chemical structure and octane sensitivity. Similarly, Badra *et al.* [18] proposed a variable volume simulation, which incorporates a pressure-derived-volume profile into a homogenous batch reactor, to correlate the ignition timing with the RON and MON of the fuel. A variable volume similar to that suggested by Badra *et al*[18] is used in this work to study the anti-knock tendency of phenolics.

In the following sections, the above method will be applied to predict the anti-knock tendency of several substituted phenols, which are important products derived from the pyrolysis oil of lignocellulosic-biomass and have the potential to be used as drop-in fuels or fuel additives [20–22]. The methodology for model generation is introduced first. The base fuel model is validated with the literature data, and the effect variable volume condition has on base fuel chemistry is discussed. Next, the predicted changes in ignition delay at constant volume adiabatic conditions induced by adding each of the six phenols are presented. Then, the anti-knock performance for each phenol is predicted, and the predictions are compared with experimental RON data on these additives blended in gasoline. Finally, the mechanism of the of the anti-knock property for each substituted phenol is discussed.

Supplemental information includes derivations for equations used to calculate volume profiles used in the engine-like simulation, a table of said volume profile, and sensitivity analysis for phenolics not discussed in the main text. It also includes sample RMG input files used to generate mechanisms, chemkin files of the mechanism used in this work, and species dictionary of the mechanism.

4.2 Methodology

4.2.1 Detailed kinetic modeling
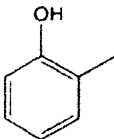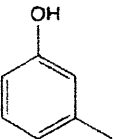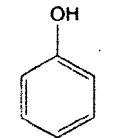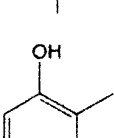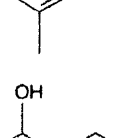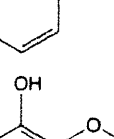
RMG [12] is an automated reaction mechanism generator using a flux-based model enlargement algorithm. First, it reacts inputted core species at specified conditions to propose possible reactions and products in the model edge. The importance of an edge species is judged by calculating the chemical flux of the core towards this edge species in homogenous isothermal reactors. When a certain chemical flux is exceeded, an edge species (and all associated reactions) are moved to the core to subsequently generate additional edge products and reactions. Then, the simulation is restarted with the revised core. This cycle of adding core species continues until some convergence criterion, usually conversion of a key reactant, is reached. The converged core model is then exported as an RMG generated detailed kinetic model. In the above process, the thermochemistry of the generated species are mainly estimated by the Benson group additivity scheme [23]. The kinetics of the generated reactions are estimated by mapping to rate rule templates or training reactions collected in the database. More details of RMG can be found in the literature [12,24].

71

The model used in this study was generated by RMG-Py (version 2.0.0) and RMG-database (version 2.0.0) with some additions. Special attention was paid to the thermochemistry estimation of substituted aromatics and the reactivity of the cyclic structures. Non-nearest-neighbor interactions for substituted aromatic compounds [25] and substituted aromatic radicals [26] were implemented into the Benson group additivity scheme to improve its accuracy. Samples of the RMG input files are included in the Supplemental Information. Other than the libraries listed below, no other special treatments of RMG or quantum calculations employed in this study. This ensures the method proposed in this study can be easily applied to the study of the anti-knock tendency of other compounds.

In this study, n-butane is selected as the base fuel because of its the relatively small size and moderate RON of 94 [27], which is similar to that of practical gasolines [27]. The n-butane model is generated in the high-pressure limit under the condition of 1 bar and 650-2000 K. Foundational Fuel Chemistry Model Version 1 [28] and the H2/O2 mechanism from Burke et al [29] were used as a seed mechanism to include pressure dependence for small species. Additionally, a few sub-mechanisms were used as libraries to provide relevant chemistry: the methyl formate mechanism of Dooley et al [30] to provide some of the low temperature chemistry for butane oxidation, calculated rates for phenol decomposition by Brezinsky et al [31], and calculated rates for cyclopentadienyl pyrolysis by Long et al [32].

The models for the blends of substituted phenols were generated using the aforementioned n-butane inputs as a base. Six individual sub-models were respectively generated for the additive/butane blends, each with 2% mole fraction of the additive. The reactor conditions were 20 bar and 650-2000 K, with equivalence ratio unity. The six sub-models were merged together to obtain a unified model, which will be used in the following analysis. Finally, some species (and corresponding reactions including these species) were manually removed from the final merged mechanism. The removed species included polycyclic species and bi-radicals whose thermochemistry the current version of RMG poorly estimates. The removal of these species had little effect on the results as there is generally little flux towards these species, but removing them speeds up simulations quite a bit. The model sizes of the sub-models and the merged model were shown in Table 4-5. The final merged model is provided in the supporting information.

Table 4-5 The size of the sub-models and the merged model.

Fuel Additive	Structure	Number of Species	Number of Reactions
p-cresol		353	10220
m-cresol		490	10092
o-cresol		328	6690
2,4-xylenol		406	7461
2-ethylphenol		459	10080
guaiacol		549	11607
Merged model	/	1465	27428

4.2.2 Engine-like simulation

The aim of this simulation is evaluating the effect on the reactivity when 2% percent of the fuel is replaced by the additives. A full engine CFD simulation is infeasible due to the size of the mechanism, but a constant volume adiabatic batch reactor would be too simple considering real engines have highly dynamic pressure and temperature profiles. Therefore, an engine-like

simulation is needed to keep the simplicity of the adiabatic batch reactor but include the pressure and temperature profile from the real engine test.

Such engine-like simulation is based on the understanding of a simplified in-cylinder scenario of the RON test. After the intake valve is closed in the RON test, the mixture is compressed to a high pressure, high temperature condition by the piston. Then the spark plug ignites the mixture, initiating a flame from the spark plug that propagates to the cylinder wall. Due to the flame propagation, the in-cylinder pressure continues increasing and compressing the end gas. Knocking occurs if the end gas auto-ignites before being consumed by the flame. Therefore, the critical condition would be the auto-ignition and the completion of fuel consumption by the flame occurring at the same time. It is assumed the laminar flame speed and the specific heat ratio of the tested mixtures are similar because of the similar fuel compositions. Consequently, the environment of the end gas can be characterized by a pressure profile from a RON test with the following assumptions:

1) Homogenous assumption: the end gas is spatially homogenous.
2) Adiabatic assumption: the end gas is adiabatically compressed by the piston motion and by the expansion of the burned gases in other parts of the cylinder.

Pressure profiles of RON tests of PRF100 was obtained from a CFR engine at UC Berkeley. The compression ratio is 9.21. The spark timing is 15 crank angle degrees (CAD) before top-dead-center (BTDC). The intake valve close timing is 34 CAD after bottom-dead-center (ABDC). Therefore, the pressure history from -146 CAD BTDC (i.e. 34 CAD ABDC) to 50 CAD ABDC is used in the following simulation. Figure 4-20 shows the pressure profile averaged from 500 cycles.

74
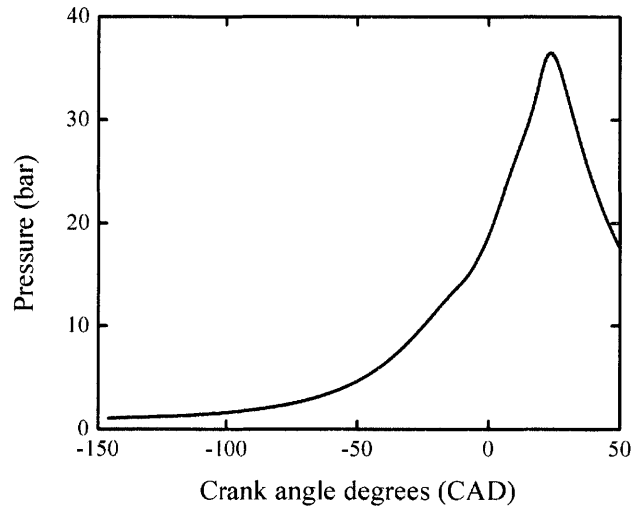
Figure 4-20 The pressure profile obtained from a RON test of PRF100 averaged over 500 cycles
This profile was used in the engine-like simulation.

The two equations used to convert a pressure profile to volume were:

$$\int_{T_0}^{T_c} \frac{\gamma}{\gamma - 1} \frac{dT}{T} = \ln\left(\frac{P_c}{P}\right) \tag{1}$$

$$\int_{T_0}^{T_c} \frac{1}{\gamma - 1} \frac{dT}{T} = \ln\left(\frac{V_c}{V}\right) \tag{2}$$

In the above equations, γ was calculated for a stoichiometric mixture of iso-octane and varied with temperature, but not composition, over time.

Derivation of Eq(1), starting from adiabatic relationship of pressure and temperature:

$$P^{1-\gamma}T^\gamma = constant \tag{3}$$

$$T^\gamma dP^{1-\gamma} + P^{1-\gamma}dT^\gamma = 0 \tag{4}$$

$$(1 - \gamma)P^{-\gamma}T^\gamma dP + \gamma T^{\gamma-1}P^{1-\gamma}dT = 0 \tag{5}$$

$$\frac{\gamma}{\gamma - 1} \frac{dT}{T} = \frac{dP}{P} \tag{6}$$

$$\int_{T_0}^{T_c} \frac{\gamma}{\gamma - 1} \frac{dT}{T} = \ln\left(\frac{P_c}{P_0}\right) \tag{7}$$

Derivation of Eq(2), starting from adiabatic relationship of volume and temperature:

75

$$TV^{\gamma-1} = constant \tag{8}$$

$$V^{\gamma-1}dT + TdV^{\gamma-1} = 0 \tag{9}$$

$$V^{\gamma-1}dT + (\gamma - 1)V^{\gamma-2}TdV = 0 \tag{10}$$

$$\frac{1}{\gamma - 1}\frac{dT}{T} = -\frac{dV}{V} \tag{11}$$

$$\int_{T_0}^{T_c} \frac{1}{\gamma - 1}\frac{dT}{T} = -\ln\left(\frac{V_C}{V_0}\right) = \ln(CR) \tag{12}$$

The total volume profile is provided in Appendix A. This profile was imported into an adiabatic batch reactor in Chemkin-PRO [34] to simulate the behavior of the end gas. In the simulation, the initial pressure was 1.09 bar, which was the experimental pressure at valve closing (-146 CAD BTDC). The initial temperature is not available from the experiment because the standard RON test protocol only ensures the intake air temperature is 325 K in the manifold; the temperature in the cylinder is not measured. Heat transfer from the residual gas and cylinder walls is expected to heat the intake air to a higher temperature around valve closing. Therefore, we tuned the initial temperature at -146 CAD BTDC in the PRF100 simulation to approximately match the simulated end gas's ignition time with the time of the maximum pressure in the experiment. The mechanism used in the tuning process is the PRF100 (i.e. iso-octane) mechanism from the Lawrence Livermore National Laboratory (LLNL) [35] and resulted in a tuned initial temperature of 400 K, which is used in all of the engine-like simulations in this study.

The timing of the ignition in the engine-like simulation is related to the RON of the fuel. While the compression ratios and pressure traces may vary with fuel composition, it is still relatively accurate to use these conditions for the study of the additives because the additive only account for 2% in the total fuel, and flame speed is known to be relatively insensitive to fuel composition [36]. It is assumed that longer ignition delays under these conditions result in better anti-knock behavior.

Figure 4-21 shows the computed ignition timing of PRFs and n-butane versus RON in this variable volume adiabatic batch reactor, using the LLNL PRF model [35] and the merged

76

butane model described in Section 2.1. As expected, the PRFs with lower RONs ignite faster than those with higher RONs. In the range of RON 90-100, the timing of the ignition varies linearly with RON. By interpolating the predicted ignition timing of n-butane with those of PRFs, the RON of n-butane can be predicted as 97.0, which is reasonably good comparison with its real RON of 94 [27], indicating the good consistency of the merged model and the LLNL PRF model.
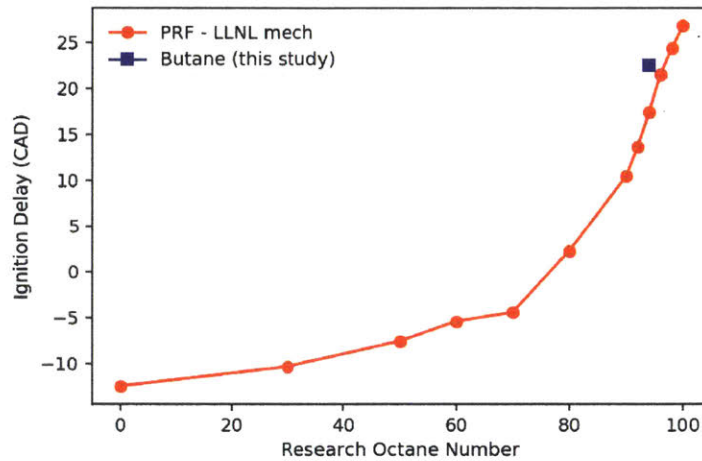
Figure 4-21 The computed time of ignition vs RON for PRFs and n-butane

4.3 Results and discussion

4.3.1 Prediction of the ignition of the base fuel

Figure 4-22 compares the experimental ignition delays of n-butane reported by Healy *et al* [37] with the prediction of the merged model at $\varphi = 1$ and diluent to oxygen ratio of 3.76. The experiments with ignition delay longer than 5 ms were conducted in a rapid compression machine (RCM) using nitrogen and argon blends as diluent. Data points with ignition delay shorter than 5 ms were conducted in a shock tube (ST) using nitrogen as diluent. The simulations were performed using Cantera [38] in a constant volume adiabatic homogenous batch reactor with nitrogen as a diluent without accounting for heat losses. The negative temperature coefficient (NTC) phenomena is successfully captured by the simulation, although it occurs at a lower temperature in the predictions than in experiments, likely because the prediction does not account for heat loss. The simulated ignition delays mostly agree within a factor of three with the

experimental data, which is reasonably good considering the simplified model, experimental uncertainties and many imperfectly known rate and thermochemistry parameters.
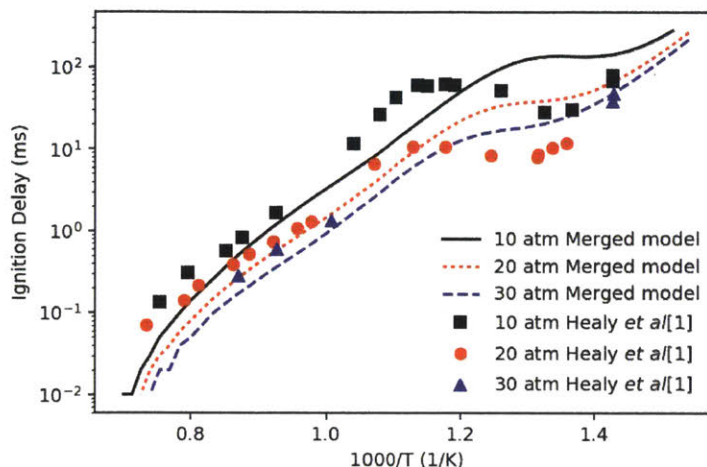
Figure 4-22 Comparison of the simulated ignition delays (lines) of n-butane with the experimental data (points) by Healy _et al._ [37].
Equivalence ratio is 1. Diluent to oxygen ratio is 3.76 corresponding to that of air. The diluent is nitrogen in both simulation and experiment.

The low temperature oxidation of butane is only briefly discussed here, but a more detailed discussion for analogous pathways in propane is given in Merchant _et al_ [39]. The main reaction pathways are outlined in Figure 4-23 to reveal the importance of the OH radical in driving the low temperature combustion chemistry. At temperatures below 800 K, the fuel consumption relies heavily on reactions with OH radical and to a much smaller degree HO_2 radical. In the low temperature regime, one OH radical is consumed to create the initial radical of the fuel, and then secondary chemistry can result in formation of up to three more OH radicals, as shown by the auto-catalytic cycle shown with the black arrows in Figure 4-23. Above ~690 K, this reaction pathway creates less than one OH for each OH inputted because two key reactions shift away from this cycle: QOOH begins to favor HO_2 + alkene formation, and O_2QOOH begins to decompose back to QOOH + O_2. From 690 K < T < 800 K, the system loses more OH than it produces which is the main cause of the NTC effect and two-stage ignition. At these temperatures, the reactions shown with blue arrows in Figure 4-23 become dominant. The net effect of these reactions is the build-up of H_2O_2 and the general build-up of heat from many exothermic reactions. After temperatures reach about 800 K, the decomposition of H_2O_2 to OH

78

becomes favorable enough that the net flux of OH becomes strongly positive. This influx of OH radicals propels the system to final ignition.
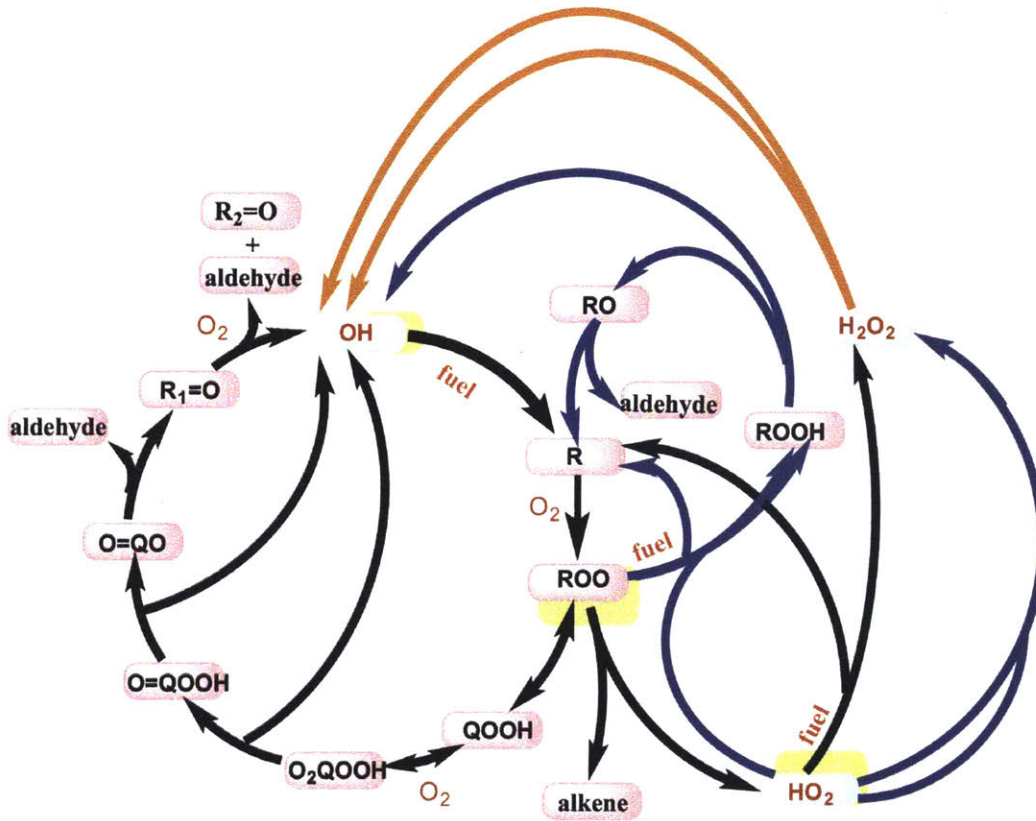
Figure 4-23 Main reaction pathways in the ignition for alkanes.
Black arrows show the chain branching ketohydroperoxide cycle that dominates below 690 K. Blue arrows show various heat-generating reactions for 690 K < T < 800 K. The orange arrows show the decomposition of H_2O_2 to OH radicals with predominantly occurs above 800 K.

4.3.2 Comparison of RCM and engine-like auto-ignition

While all three chemistry regimes discussed in section 3.1 are controlling at various times in a constant-volume reactor, it is unclear which, if any, regimes are rate-limiting for the engine-like simulation. Comparing a simulation of the analogous RCM to the engine-like simulation gives a good basis for discussion. The RCM simulation uses the same volume profile derived for the engine-like simulation but stops compression at -55 CAD (t = 32 ms), at which time the temperature is approximately T = 650 K. The engine-like simulation completes the full engine stroke (with additional compression from the burning gas after -15 CAD) through 50 CAD.

Figure 4-24(a) shows temperature profile of an RCM and engine-like simulation for pure butane. The RCM simulation takes approximately 10 times longer to ignite than the engine-like, and spends significantly more time below 800 K. In an RCM, the ignition is successively limited by the three cycles shown in Figure 4-23: chain-branching through ketohydroperoxide intermediates, heat generation by secondary chemistry, and finally OH dissociation from H_2O_2. On the other hand, the engine-like simulation seems to push past the first two regimes, as even pure nitrogen reaches a max temperature of ~1100 K in these conditions.

This contrast can be further seen in Figure 4-24(b), which presents the OH mole fraction as a function of temperature. For the RCM simulation, the OH mole fraction peaks around 750 K after the ketohydroperoxide cycle has become unfavorable, and does not start increasing again until after 800 K. Meanwhile in the engine-like simulation, the mole fraction of OH increases monotonically, but is much lower for 650 K < T < 800 K compared to RCM. Above 800 K, the OH mole fraction experiences similar increases in the two simulations. This comparison shows that the engine-like simulation rushes through the first two regimes, but experiences similar radical growth during the regime controlled by H_2O_2 dissociation. As a result, the engine-like simulation will build up less H_2O_2 prior to the third regime.
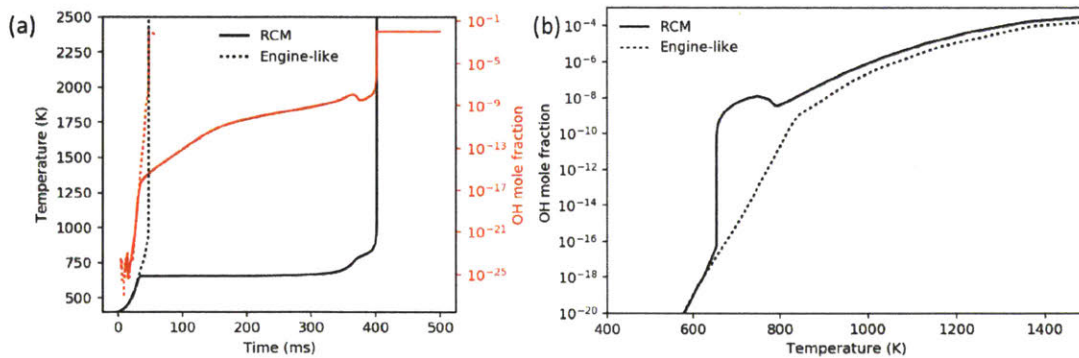
Figure 4-24 Comparison of temperature and OH mole fraction for engine-like simulation and RCM
(a) Temperature and OH mole fraction profile of RCM and engine-like simulations. (b) OH mole fraction concentration as a function of temperature in RCM and engine-like simulations.

Sensitivity analysis for the engine-like simulation of pure butane when T = 925K (just prior to ignition) is shown in Figure 4-25. The most sensitive reaction is the dissociation of H_2O_2, which agrees with the auto-ignition scheme shown Figure 4-23. Other reactions that create H_2O_2

also increase the amount of OH. The only H_2O_2 forming reactions which have negative sensitivity for OH production is the disproportionation of the 2-butyl radical to alkenes by HO_2. These compete with the chain-branching ketohydroperoxide cycle, which is dominate at low temperatures. Although that cycle is no longer the main source of OH radical at this temperature, the competition between alkene production and ketohydroperoxide production still exists.
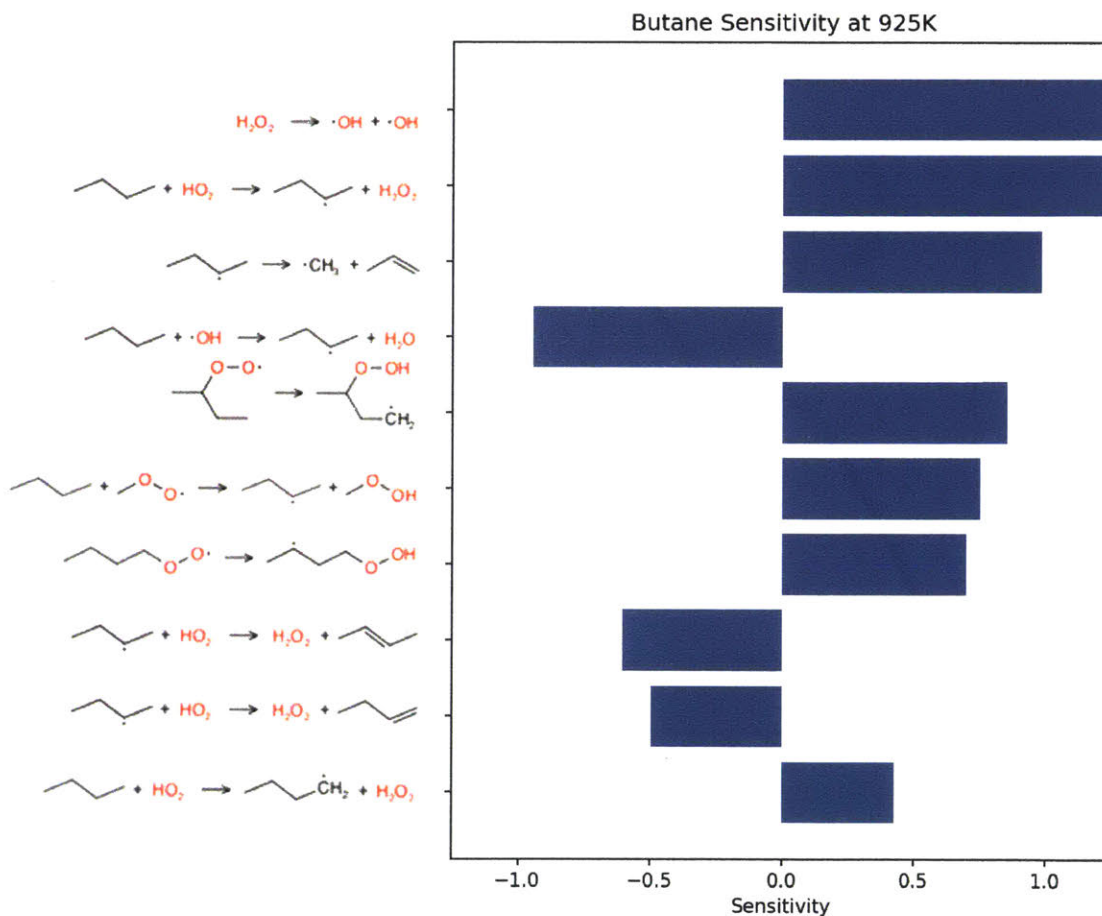
Figure 4-25 Sensitivity analysis for OH in in butane for the engine-like simulation
The time point was given at t = 4.62 ms and T = 925K. The top 50 sensitive reactions of pure butane were filtered out to underscore the reactions involving guaiacol.

4.3.3 Prediction of the anti-knock tendency

Figure 4-26 shows the simulated ignition delays of the different additive/n-butane blends with 2% additive in fuel. The simulation was conducted at the condition of 20 bar, 650-1000 K, and $\phi= 1$. M-cresol and ethylphenol is predicted to have very little effect on the ignition

throughout all temperature ranges. Guaiacol has ignition enhancing effects throughout all temperature ranges. The other three additives, p-cresol, o-cresol, and xylenol have a more complex effect. They enhance ignition for $T_0 < 780$ K. However, above 780 K these three additives providing anti-knock effect. Based solely on these simulation, it is unclear how to rank the anti-knock behavior of the additives. A real engine will cross the entire temperature range during a piston cycle, but analysis from section 3.1 suggests that the temperature range above 800 K is most relevant to the CRF engine.
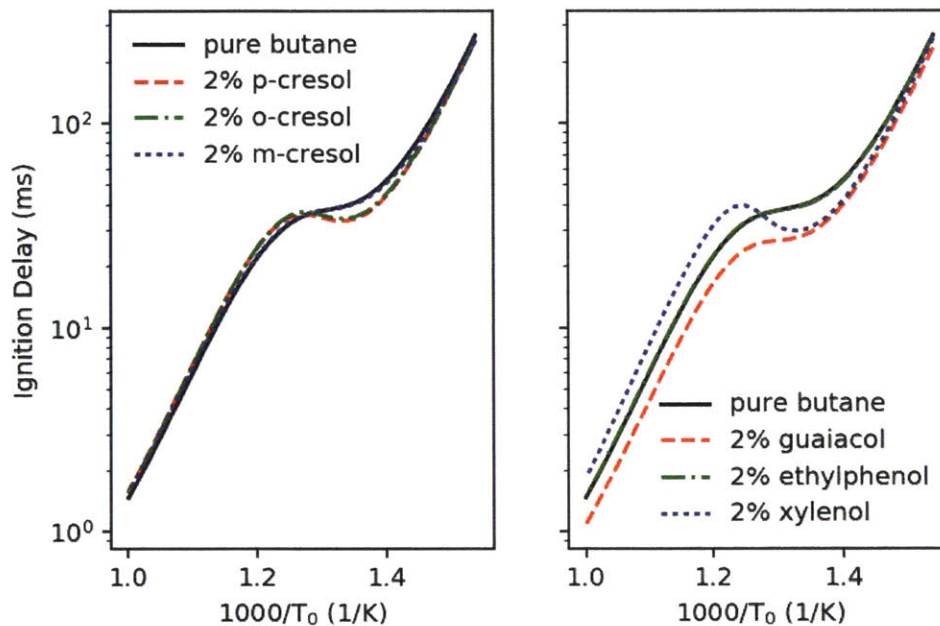
Figure 4-26 Simulated ignition delays of the additive/n-butane blends as a function of T_0
The reactor was a constant volume adiabatic homogenous batch reactor as a function of initial. The blend ratio is 2%, $\phi = 1$, and initial pressure is 20 bar.

To address the shortcomings of the constant-volume simulation, engine-like simulations following the methodology outlined in section 2.2 were performed to investigate the ignition timing of the mixture when being exposed to the end gas condition. All simulations were performed at $\phi = 1$, $T_0 = 400$ K, $P_0 = 1.09$ bar (taken from experimental CRF data) and a blending ratio of 2% mol additive in n-butane. Figure 4-27 shows the temperature history of the simulations. Guaiacol ignites fastest of all of the additive blends, which is consistent with the

constant volume simulation results. Both m-cresol and ethylphenol have the small effects, but do provide some anti-knock behavior. O-cresol and p-cresol have about the same anti-knock behavior which agrees well with the constant-volume simulation. Among all of the additive blends, 2,4-xylenol has the longest ignition delay, representing the best anti-knock capability. Based on Figure 4-27, the anti-knock tendency of the additives can be arranged as: 2,4-xylenol > p-cresol = o-cresol > m-cresol = 2-ethylphenol > guaiacol. This ranking suggests that constant-volume simulations starting above 800 K are more relevant to the RON when RON > 90.
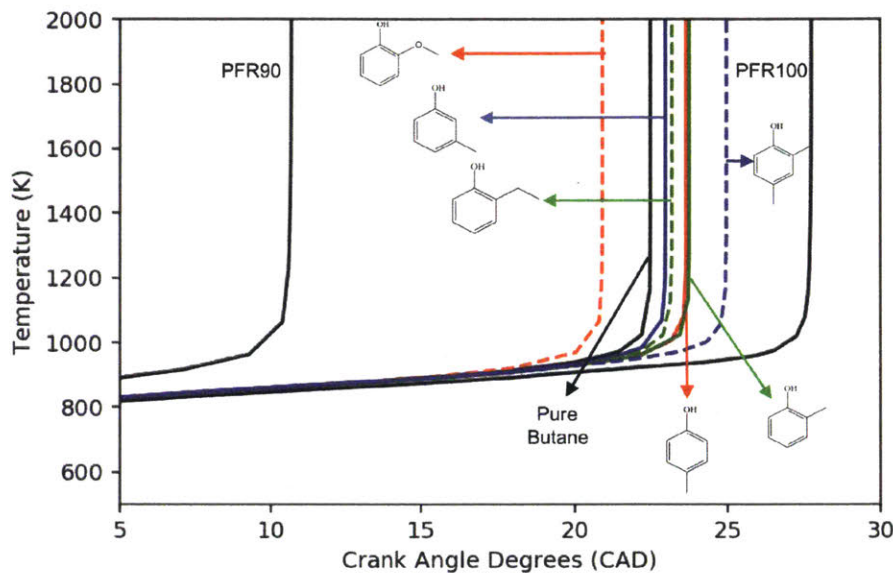
Figure 4-27 The predicted temperature history of the engine-like simulations using different fuel blends.
PRF90: 90% iso-octane/n-heptane; PRF100: pure iso-octane; pure n-butane; 2% additive/n-butane.
Conditions: $\phi = 1$, $T_0 = 400$ K, $P_0 = 1.09$ bar, adiabatic, effective V(t) defined by RON100 P(t).
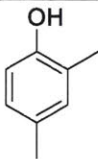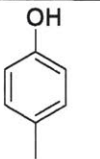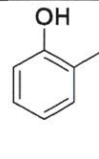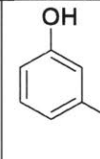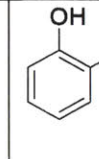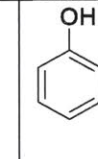
Following the RON test protocol, engine experiments were performed in a CFR engine to test the anti-knock tendency of the additives. Experimental RON's measured from the CFR test are summarized Table 4-6. The blends were tested over several days explaining the slight difference in base fuel RON. However, the base fuel was tested just before each blend to give accurate ΔRON. Based on these experiments, the additives from most to least anti-knock performance are: 2,4-xylenol > p-cresol > o-cresol > m-cresol > 2-ethylphenol > guaiacol. We note that experimental determinations of ΔRON between fuel blends have uncertainty of about ±0.5.

83

Quantitative predictions for the RON of additives blend can be made by interpolating the ignition timings of the additives into those of PRFs in Figure 4-21. There is some error in this prediction because the merged model does not exactly match the experimental RON 94 for pure butane. The predicted and experimentally determined changes in RON induced by additive are shown in Table 4-6.

Table 4-6 Comparison of predictions by engine-like simulation and experimentally determined ΔRON for fuel blends with additives.

The top set of data corresponds to prediction of standard RON engine-like simulations with 2% mole fraction phenol additives in butane. RON was computed by linear interpolation of calculations for different PRF fuels in our engine simulations, using the LLNL PRF mechanism, see Figure 4-21. The bottom set of data corresponds to standard RON experiments with 20g/L phenol additives in a gasoline.

	OH	OH	OH	OH	OH	OH
Computed Butane "RON"	97.0	97.0	97.0	97.0	97.0	97.0
Computed Blended "RON"	98.5	97.8	97.8	97.3	97.5	96.1
Computed Δ"RON"	1.5	0.8	0.8	0.3	0.5	-0.9
E0 base fuel RON	95.6	95.6	95.6	95.7	95.7	95.7
Blended RON	97.3	97.2	96.9	96.6	96.2	95.5
ΔRON	1.7	1.6	1.3	0.9	0.5	-0.2

Qualitatively, these predictions compare favorably with the experimental data predicting ΔRON for all six additives within 0.8 RON units and ranking the anti-knock behavior of the additives correctly except for switching m-cresol and ethylphenol.

4.3.4 Important reaction pathways of the additives

Figure 4-28 shows the main reaction pathway of o-cresol derived from the engine-like simulations with 2% mol o-cresol in butane. Analysis of all pathways were performed at the time corresponding to T = 925 K. This time point was chosen due to the results presented in section 3.2 and choosing a slightly closer time to the ignition. Only o-cresol related reactions are shown in the figure for readability. The consumption of o-cresol is initiated by hydrogen abstraction reactions. Free radicals, mainly OH radical and HO_2 radical, attack and abstract the hydrogen atom in the substituted methyl group and hydroxyl group, producing 2-methylphenoxy radical and 2-hydroxybenzyl radical. These two radicals then go through disproportionation reactions, consuming another radical and forming a conjugated ketone. These two steps are denoted as pathway P0 in Figure 4-28. The reaction sequence in P0 net destroys two radicals. This conjugated ketone is relatively stable, so the flux toward it is much higher than the secondary chemistry afterwards.

There are three main consumption pathways of the conjugated ketone, denoted as P1, P2, and P3 respectively in Figure 4-28. In the pathway P1, the ketone adds a methyl radical to its terminal carbon and disproportionates. Next, HO_2 abstracts to form H_2O_2, which at this temperature quickly dissociates into OH radicals. The P2 pathway adds methyl radical to the benzene ring instead. The resulting alkoxy radical performs intramolecular hydrogen migration moving the radical to carbon at the ortho position. Finally, oxygen disproportionates the alkyl radical to form another conjugated ketone and the lower reactivity radical HO_2. The P3 pathway adds H radical to the benzene ring and is followed by addition of oxygen to form peroxy radicals. Including the two radicals terminated by P0, the P1 pathway is radical neutral, P2 consumes 2 radicals, and P3 consumes 3 radicals.
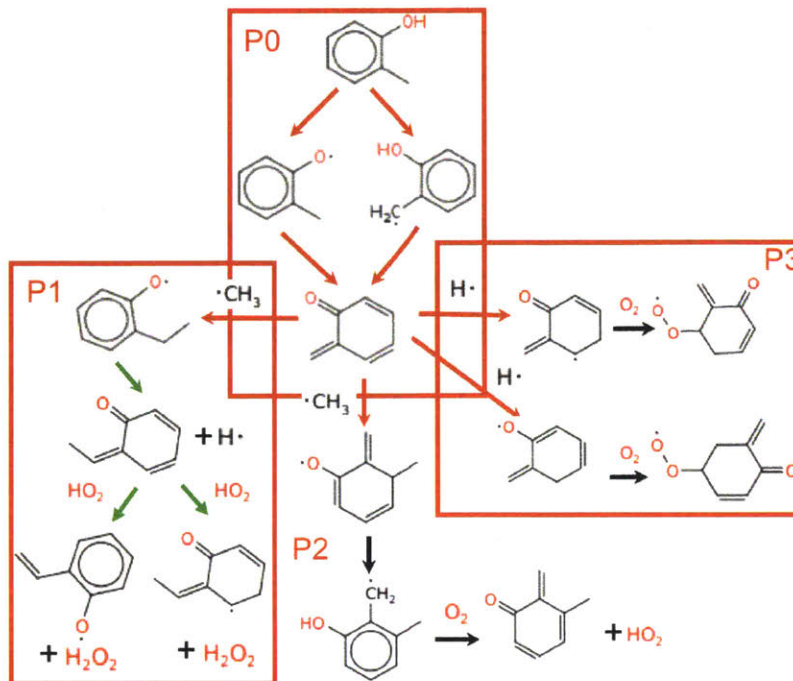
Figure 4-28 The reaction pathways of o-cresol in the engine-like simulation prior to final ignition
Taken at t = 46.2 ms and T = 925 K. Red arrows signify reactions that consume radicals, black arrows are radical neutral, and green arrows produce radicals.

Sensitivity analysis for OH radical was performed at the same conditions and time point. Because the phenolic compounds are in low concentration, the most sensitive reactions in the blend coincide with those of pure butane. To emphasize the contribution of the additives, the 50 most sensitive reactions from butane were removed from consideration. The remaining sensitive reactions are shown in Figure 4-29. The three most sensitive reactions occur on the P0 pathway. The remaining reactions only show secondary reactions of butane. It follows that the secondary chemistry of o-cresol has a much smaller effect on the ignition than the initial P0 pathway.

Figure 4-29 Sensitivity analysis for OH in a 2% mol o-cresol blend in butane for the engine-like simulation

Time point taken at t = 4.62 ms and T = 925K. The top 50 sensitive reactions of pure butane were filtered out to underscore the reactions involving o-cresol.

The main reaction pathways for p-cresol, 2,4-xylenol, and ethylphenol are analogous to o-cresol. As shown in Figure 4-30, their consumption also starts with the hydrogen abstraction reaction and is followed by disproportionation, resulting in conjugated ketones; their own version of the P0 pathway. The secondary chemistry is not shown as, similarly to o-cresol, it has a much lower effect than the P0 pathways featured. Because 2,4-xylenol has two methyl groups, either of which can form conjugated ketones, its P0 sequence has a higher reaction rate and stronger anti-knock effect than either p-cresol or o-cresol
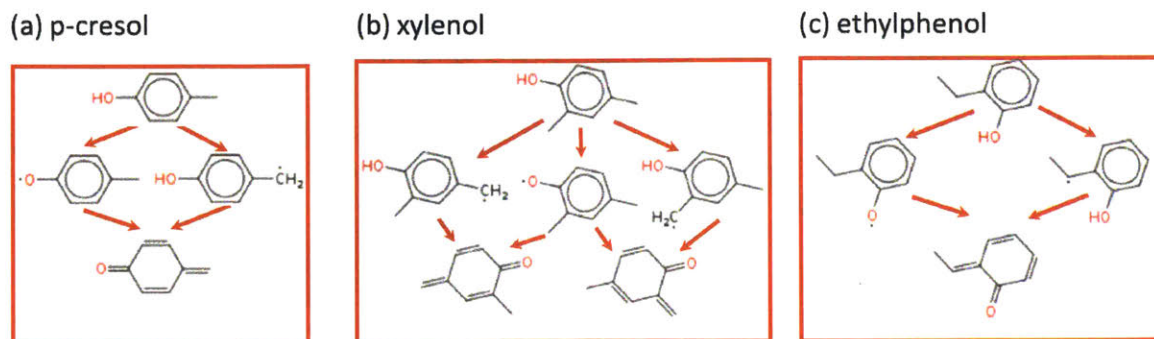
Figure 4-30 The P0 reaction pathways of p-cresol, 2,4-xylenol, and xylenol

Local sensitivity for these three additives were also is taken at T = 925K and shown in Figure 4-31 - Figure 4-33. For the additive blends, the top 50 most sensitive reactions from pure butane are filtered out to emphasize the effect of the additives. Reactions are drawn in the direction which they proceed at the given time point. Note that the range for the x-axis is not constant between figures. In general, the sensitive reactions for p-cresol, xylenol, and ethylphenol indicate that the P0 pathway has the largest impact on auto-ignition chemistry.
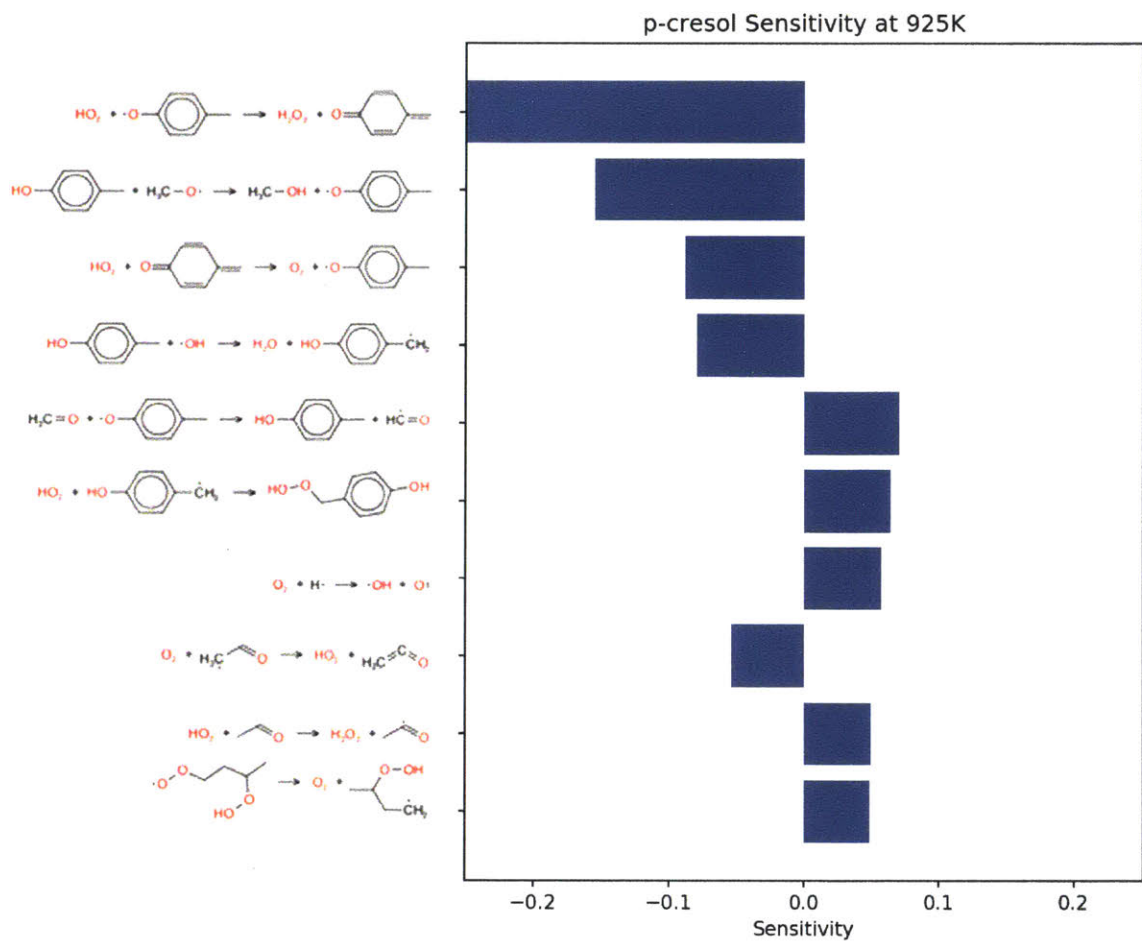
Figure 4-31 Sensitivity analysis for OH in a 2% mol p-cresol blend in butane for the engine-like simulation

Time point taken at t = 4.62 ms and T = 925K. The top 50 sensitive reactions of pure butane were filtered out to underscore the reactions involving p-cresol.
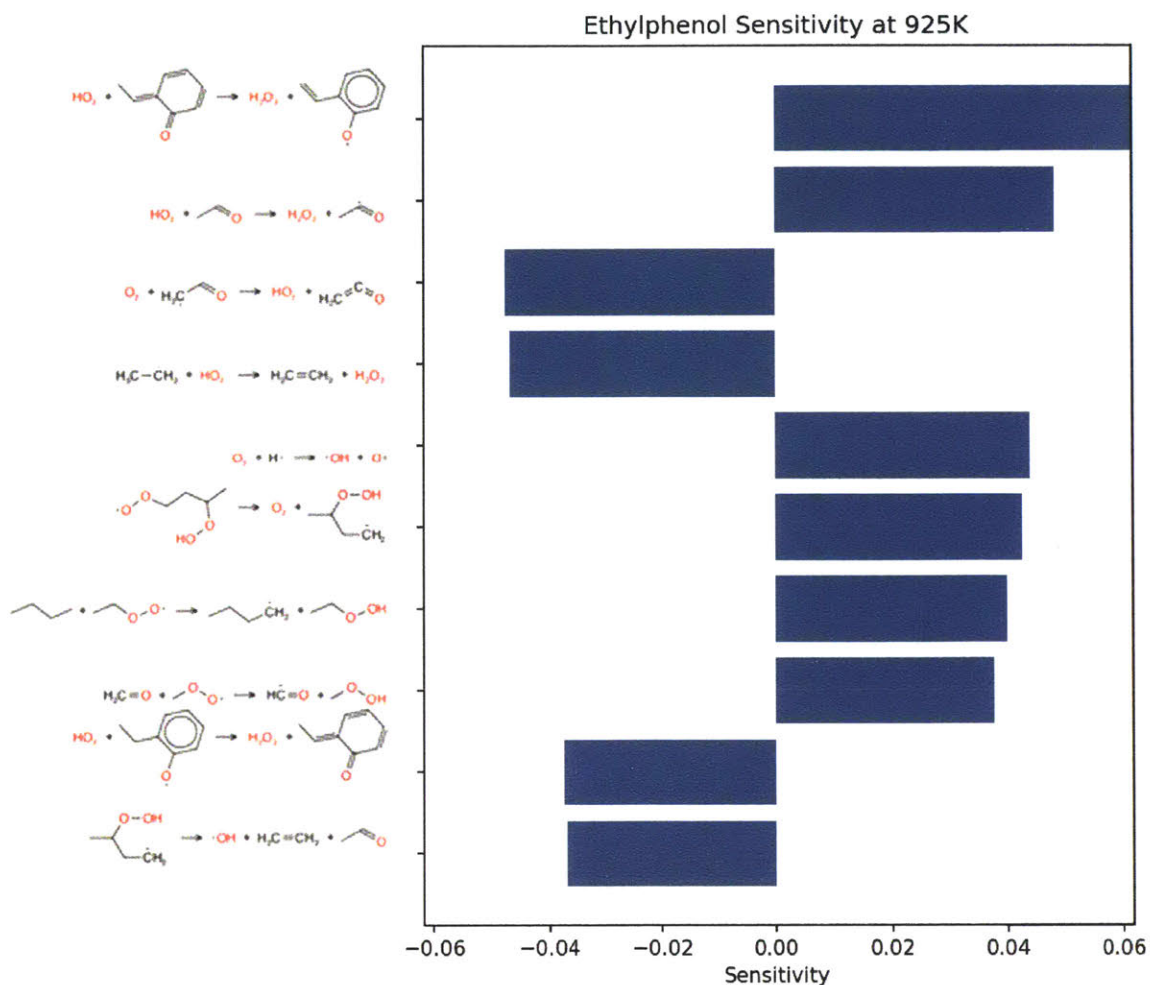
Figure 4-32 Sensitivity analysis for OH in a 2% mol ethylphenol blend in butane for the engine-like simulation

Time point taken at t = 4.62 ms and T = 925K. The top 50 sensitive reactions of pure butane were filtered out to underscore the reactions involving ethylphenol..
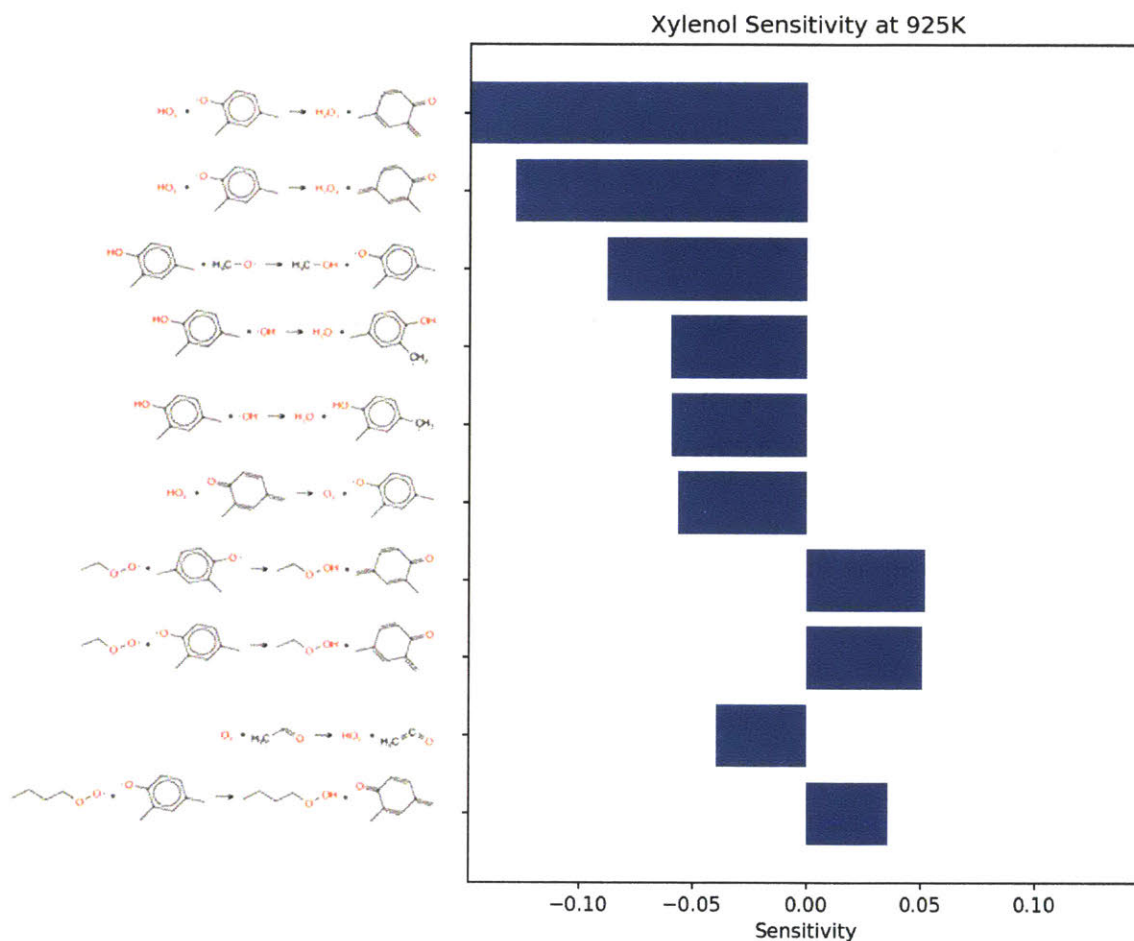
Figure 4-33 Sensitivity analysis for OH in a 2% mol xylenol blend in butane for the engine-like simulation
Time point taken at t = 4.62 ms and T = 925K. The top 50 sensitive reactions of pure butane were filtered out to underscore the reactions involving xylenol.

The main reaction pathway for guaiacol at 925K is direct dissociation to methyl radical and alkoxy radical as shown in Figure 4-34. This one reaction is the largest contributor to its cetane boosting effect at the conditions shown. Some of the o-hydroxy phenoxyl radicals formed abstract H atoms, further accelerating ignition, but some recombine or disproportionate with O_2 or other radicals reducing the reactivity. Two secondary pathways of guaiacol are also significant. H-abstraction from the phenol group induces O-C cleavage, so it is radical neutral. H-abstraction from the methyl group accelerates ignition by adding O_2 at low T, or by releasing formaldehyde and a reactive hydroxyl phenol radical as shown on the right side of Figure 4-34.

91
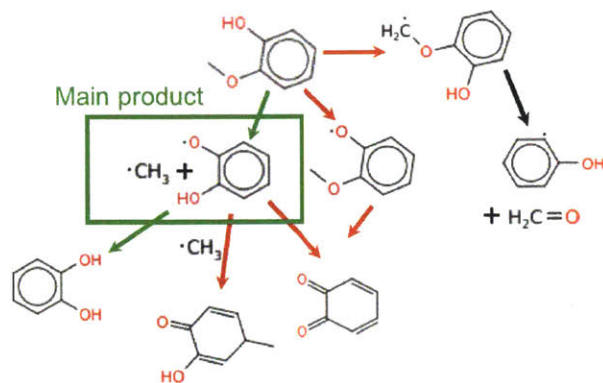
Figure 4-34 The main reaction pathways of guaiacol in the engine-like simulation at t = 46.2 ms and T = 925K

Sensitivity analysis shown in Figure 4-35 shows the bond dissociation pathway having the largest influence on OH concentration. At this time point, the HO_2 disproportionation to form conjugated ketone, reacts in the reverse direction. This gives a large negative sensitivity coefficient as HO_2 forms O_2 instead of H_2O_2 in this sequence. At earlier time points, the conjugated ketone is formed in the forward direction, netting one HO_2 radical. The third most sensitive reaction shows methyl peroxy radical disproportionating o-hydorxy phenoxy to form conjugated ketone. This gives positive sensitivity for OH sensitivity because the resulting methylperoxide will dissociate to methoxy and OH.
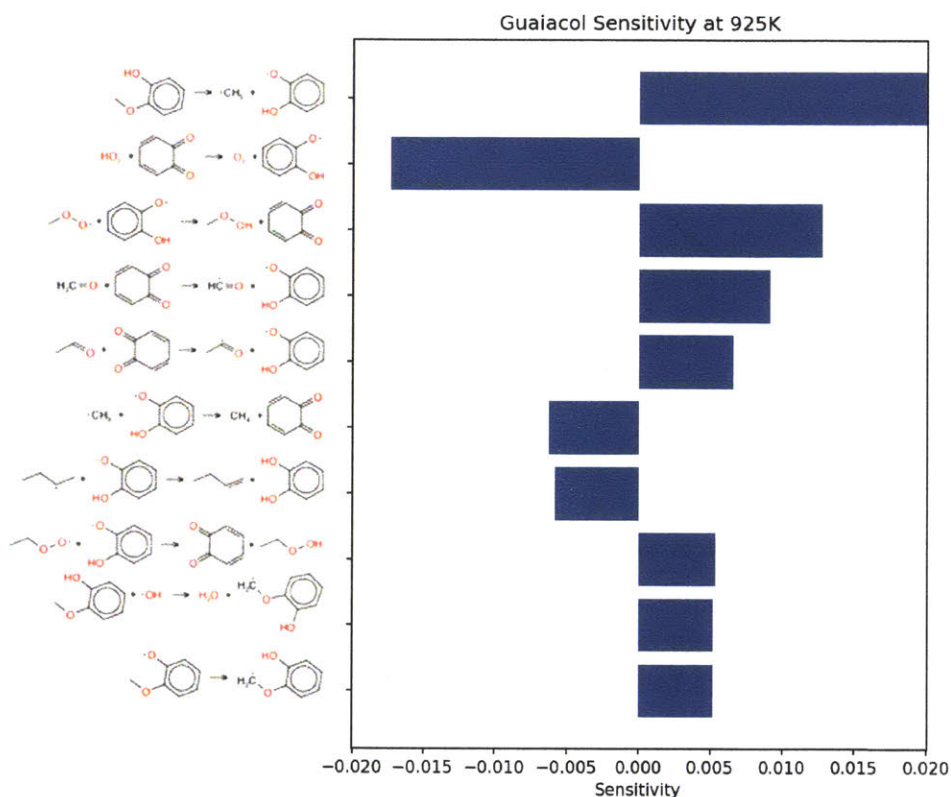
Figure 4-35 Sensitivity analysis for OH in a 2% mol guaiacol blend in butane given at t = 46.2 ms and T = 925K.
The top 50 sensitive reactions of pure butane were filtered out to underscore the reactions involving guaiacol.

The reaction pathway of m-cresol is different from those of the other five additives as it cannot follow the P0 pathway. After the hydrogen abstraction from the methyl site, 3-hydroxylbenzyl radical cannot produce the conjugated ketone through disproportion reaction because of the positioning of the methyl group. Instead, the 3-hydroxybenzyl radical will combine with HO_2. The resulting hydroperoxy breaks down to OH radical at these temperatures. The 3-methylphenoxy radical, the other likely product, can still form conjugated ketones but only by adding a radical, and there are only three conjugated bonds as opposed to the four seen for all the other additives. The reduced conjugation of its intermediates and secondary pathway forming OH, gives meta-cresol a lower octane-boosting effect than the previous additives.

93
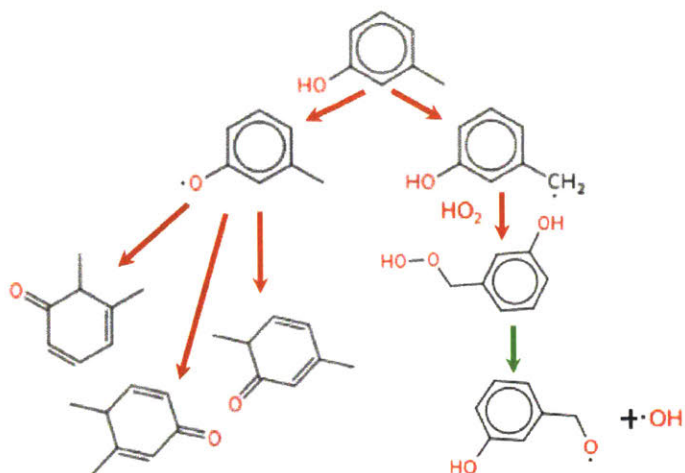
Figure 4-36 The main reaction pathways of m-cresol

Sensitivity analysis for m-cresol is shown in Figure 4-37 below. Even after filtering the top 50 reactions associated with butane sensitivity, many of the leftover reactions do now show m-cresol or any of its intermediates. In fact, the only reaction that does appear in the sensitivity is the first hydrogen abstraction to the alkoxy radical. This indicates that in the current mechanism very few of m-cresols reactions affect the OH concentration.
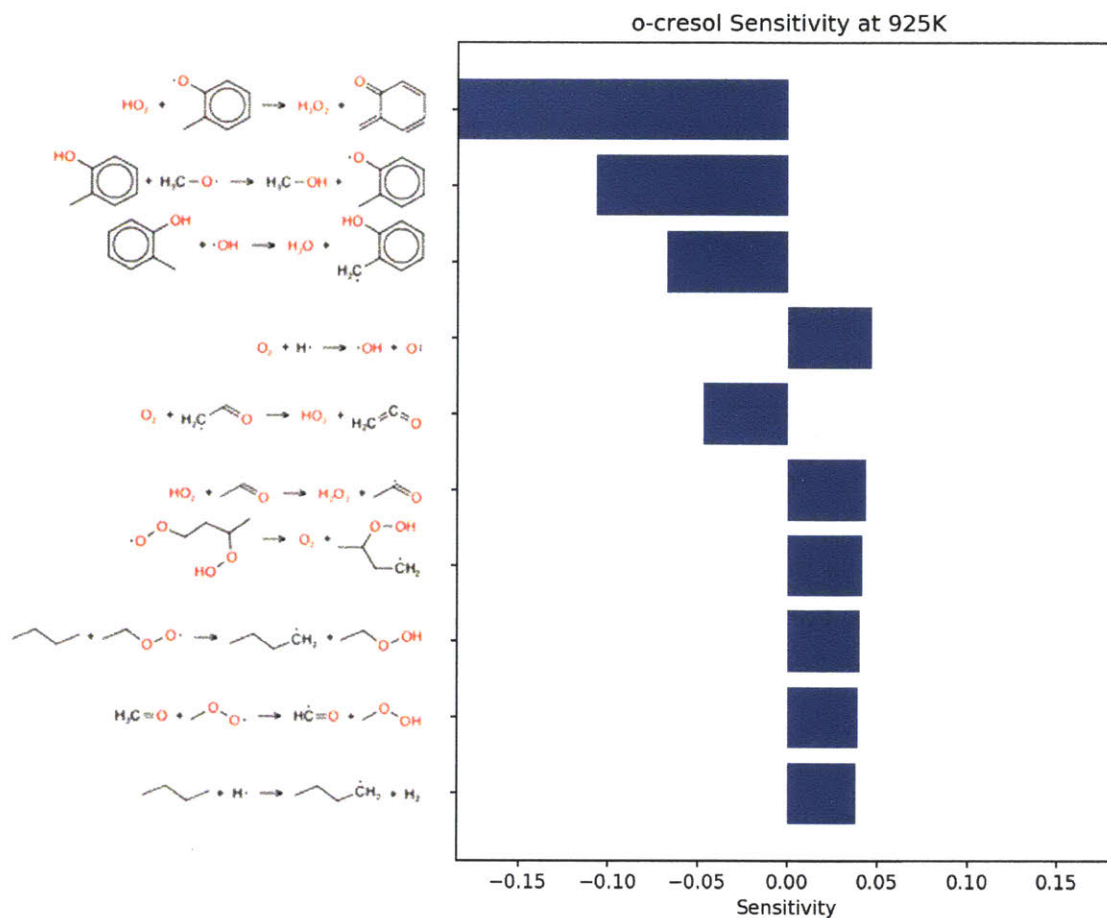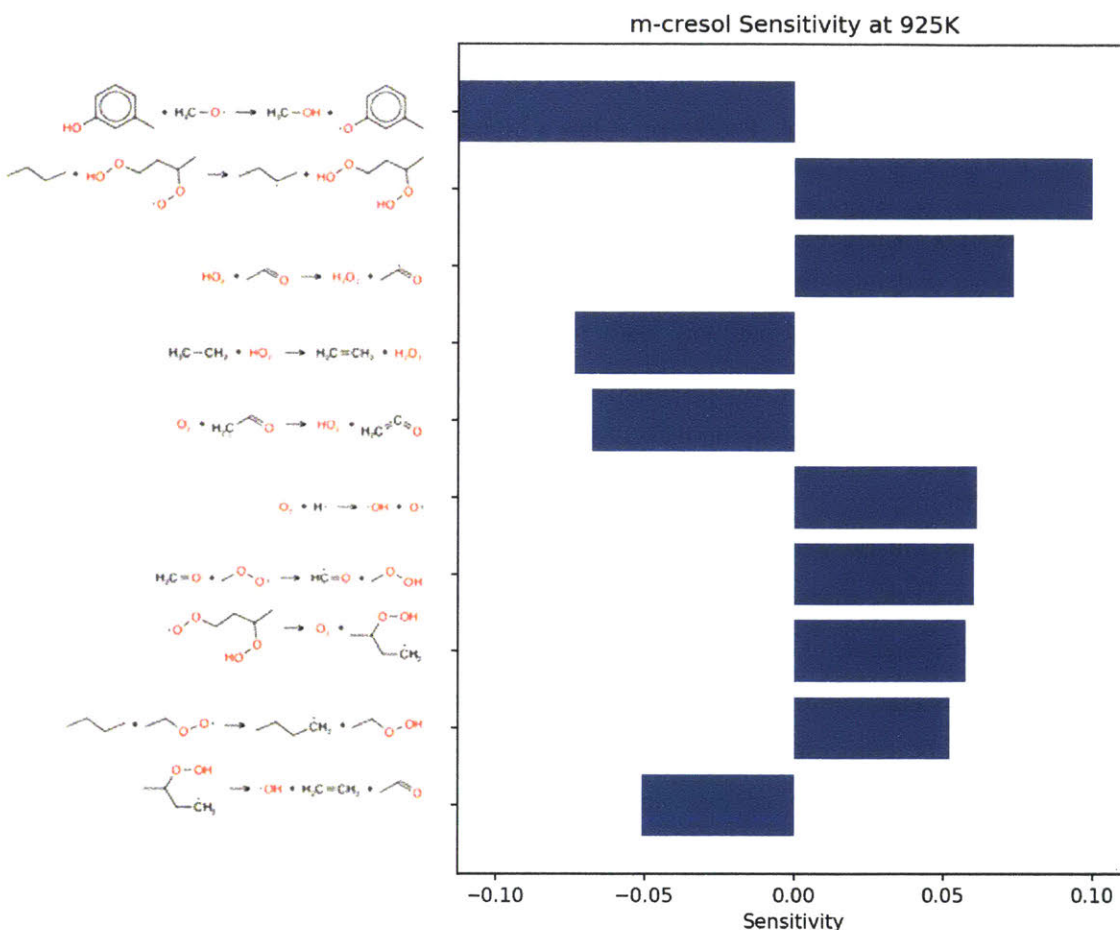
Figure 4-37 Sensitivity analysis for OH in a 2% mol m-cresol blend in butane for the engine-like simulation

Time point taken at t = 4.62 ms and T = 925K. The top 50 sensitive reactions of pure butane were filtered out to underscore the reactions involving m-cresol.

OH radical is the most important intermediate species in the ignition process. The anti-knock ability of additives mainly originates from the fact that they can quench OH radicals or precursors effectively. The reaction path analysis shown in Figure 4-28 - Figure 4-36 reveals the importance of conjugated ketone in the anti-knock behavior of substituted phenols. Two active radicals, one during initial H-abstraction and a second during subsequent disproportionation, are consumed in the formation of the conjugated ketone through the first two steps (P0). Most of the produced conjugated ketone will stay relatively inert and not be consumed until hot ignition. Therefore, the formation of the conjugated ketone is the key to understand the anti-knock ability of these additives. P-cresol and o-cresol have similar P0 pathways thus they have similar anti-

knock tendency. 2,4-xylenol has three channels for the hydrogen abstraction reaction and two conjugated ketones as the products of the pathway P0, which means it consumes active radicals faster than p-cresol and o-cresol. Therefore, it has a higher anti-knock tendency. Guaiacol has a decomposition channel which creates methyl radicals on the way to its conjugated ketone. M-cresol cannot do the P0 pathway at all, giving it the smallest effect of any of the additives.

The above understanding, which is that the formation of conjugated ketone radical and radical consumption via the P0 pathway leads to the anti-knock ability of substituted phenols, can help to find better additives. For example, we speculate that 2,4,6-trimethylphenol will have better anti-knock ability than 2,4-xylenol according to the above analysis.

4.4 Conclusion

A detailed kinetic model was automatically built using the Reaction Mechanism Generator (RMG) for the study of anti-knock tendency of n-butane blended with six additives: p-cresol, o-cresol, m-cresol, 2,4-xylenol, 2-ethylphenol, and guaiacol. Ignition delays were simulated in a constant volume batch reactor. It was found that the additives have different reactivity in different temperature ranges. Therefore, engine-like simulations were performed to investigate the ignition timing of the blends at end gas condition. These simulations were conducted by specifying a volume history, which is derived from a pressure history obtained in a RON test of PFR100, to a batch reactor. Based on the predicted ignition timing in the engine-like simulation, the anti-knock tendency of the additives can be arranged as: 2,4-xylenol > p-cresol = o-cresol > m-cresol> 2-ethylphenol > guaiacol. Quantitative predictions of RON change induced by the additives were made by interpolating the ignition timings of the additives into those of PRFs. The procedure for predicting the increase in RON agrees with experimental measurements on blends of the additives in real gasoline in a standard RON test almost within experimental uncertainty.

The key mechanism determining the anti-knock behavior was found to be the consumption of radicals as the phenol is converted into a conjugated ketone. This pathway net consumes two radical and consists of a two-step pathway: hydrogen abstraction reactions of additives followed by disproportionation. The differences in the formation of conjugated ketone and subsequent secondary chemistry were used to explain the anti-knock ranking of p-cresol, o-cresol, 2,4-xylenol, 2-ethylphenol, and guaiacol.

This study is a first attempt to apply the automated mechanism generation technique to the anti-knock study of additives with more realistic engine-like conditions. The good consistency of the prediction and the experiment result shows this method is a promising way to rank proposed anti-knock additives even before performing any experiments

4.5 References

[1]   Heywood, J. B., 1988, *Internal Combustion Engines Fundamentals*, McGraw-Hill, New York.

[2]   ASTM International, 2015, "Standard Test Method for Research Octane Number of Spark-Ignition Engine Fuel," ASTM D2699.

[3]   ASTM International, 2016, "Standard Test Method for Motor Octane Number of Spark-Ignition Engine Fuel," ASTM D2700.

[4]   Daly, S. R., Niemeyer, K. E., Cannella, W. J., and Hagen, C. L., 2016, "Predicting Fuel Research Octane Number Using Fourier-Transform Infrared Absorption Spectra of Neat Hydrocarbons," Fuel, **183**, pp. 359–365.

[5]   Mendes, G., Aleme, H. G., and Barbeira, P. J. S., 2012, "Determination of Octane Numbers in Gasoline by Distillation Curves and Partial Least Squares Regression," Fuel, **97**, pp. 131–136.

[6]   Guan, L., Feng, X. L., Li, Z. C., and Lin, G. M., 2009, "Determination of Octane Numbers for Clean Gasoline Using Dielectric Spectroscopy," Fuel, **88**(8), pp. 1453–1459.

[7]   Mittal, V., and Heywood, J. B., 2008, "The Relevance of Fuel RON and MON to Knock Onset in Modern SI Engines," SAE Tech. Pap.

[8]   Mittal, V., Heywood, J. B., and Green, W. H., 2010, "The Underlying Physics and Chemistry behind Fuel Sensitivity," SAE Int. J. Fuels Lubr., **3**(1), pp. 256–265.

[9]   Liu, Z., and Chen, R., 2009, "A Zero-Dimensional Combustion Model with Reduced Kinetics for SI Engine Knock Simulation," Combust. Sci. Technol., **181**(6), pp. 828–852.

[10]   Tanoue, K., Chado, Y., Jimoto, T., Nomura, T., Shimada, F., and Hashimoto, J., 2015, "Effect of Autoignition Characteristics of Fuels on Knocking Properties," Int. J. Engine Res., p. 1468087415601785.

[11]   Wang, Z., Qi, Y., He, X., Wang, J., Shuai, S., and Law, C. K., 2015, "Analysis of Pre-Ignition to Super-Knock: Hotspot-Induced Deflagration to Detonation," Fuel, **144**, pp. 222–227.

[12]   Gao, C. W., Allen, J. W., Green, W. H., and West, R. H., 2016, "Reaction Mechanism Generator: Automatic Construction of Chemical Kinetic Mechanisms," Comput. Phys. Commun., **203**, pp. 212–225.

[13]   Gao, C. W., Vandeputte, A. G., Yee, N. W., Green, W. H., Bonomi, R. E., Magoon, G. R., Wong, H.-W., Oluwole, O. O., Lewis, D. K., Vandewiele, N. M., and Van Geem, K. M., 2015, "JP-10 Combustion Studied with Shock Tube Experiments and Modeled with Automatic Reaction Mechanism Generation," Combust. Flame, **162**(8), pp. 3115–3129.

[14]   Class, C. A., Liu, M., Vandeputte, A. G., and Green, W. H., 2016, "Automatic Mechanism Generation for Pyrolysis of Di-Tert-Butyl Sulfide," Phys. Chem. Chem. Phys., **18**(31), pp. 21651–21658.

[15]   Allen, J. W., Scheer, A. M., Gao, C. W., Merchant, S. S., Vasu, S. S., Welz, O., Savee, J. D., Osborn, D. L., Lee, C., Vranckx, S., Wang, Z., Qi, F., Fernandes, R. X., Green, W. H., Hadi, M. Z., and Taatjes, C. A., 2014, "A Coordinated Investigation of the Combustion Chemistry of Diisopropyl Ketone, a Prototype for Biofuels Produced by Endophytic Fungi," Combust. Flame, **161**(3), pp. 711–724.

[16]   Mehl, M., Chen, J. Y., Pitz, W. J., Sarathy, S. M., and Westbrook, C. K., 2011, "An Approach for Formulating Surrogates for Gasoline with Application toward a Reduced Surrogate Mechanism for CFD Engine Modeling," Energy Fuels, **25**(11), pp. 5215–5223.

[17]   Sarathy, S. M., Javed, T., Karsenty, F., Heufer, A., Wang, W., Park, S., Elwardany, A., Farooq, A., Westbrook, C. K., Pitz, W. J., Oehlschlaeger, M. A., Dayma, G., Curran, H. J., and

Dagaut, P., 2014, "A Comprehensive Combustion Chemistry Study of 2,5-Dimethylhexane," Combust. Flame, 161(6), pp. 1444–1459.

[18]   Badra, J. A., Bokhumseen, N., Mulla, N., Sarathy, S. M., Farooq, A., Kalghatgi, G., and Gaillard, P., 2015, "A Methodology to Relate Octane Numbers of Binary and Ternary N-Heptane, Iso-Octane and Toluene Mixtures with Simulated Ignition Delay Times," Fuel, 160, pp. 458–469.

[19]   Westbrook, C. K., Mehl, M., Pitz, W. J., and Sjöberg, M., 2017, "Chemical Kinetics of Octane Sensitivity in a Spark-Ignition Engine," Combust. Flame, 175, pp. 2–15.

[20]   Ratcliff, M. A., Burton, J., Sindler, P., Christensen, E., Fouts, L., Chupka, G. M., and McCormick, R. L., 2016, "Knock Resistance and Fine Particle Emissions for Several Biomass-Derived Oxygenates in a Direct-Injection Spark-Ignition Engine," SAE Int. J. Fuels Lubr., 9(1), pp. 59–70.

[21]   McCormick, R. L., Ratcliff, M. A., Christensen, E., Fouts, L., Luecke, J., Chupka, G. M., Yanowitz, J., Tian, M., and Boot, M., 2015, "Properties of Oxygenates Found in Upgraded Biomass Pyrolysis Oil as Components of Spark and Compression Ignition Engine Fuels," Energy Fuels, 29(4), pp. 2453–2461.

[22]   Baumgardner, M. E., Vaughn, T. L., Lakshminarayanan, A., Olsen, D., Ratcliff, M. A., McCormick, R. L., and Marchese, A. J., 2015, "Combustion of Lignocellulosic Biomass Based Oxygenated Components in a Compression Ignition Engine," Energy Fuels, 29(11), pp. 7317–7326.

[23]   Cohen, N., and Benson, S. W., 1993, "Estimation of Heats of Formation of Organic Compounds by Additivity Methods," Chem. Rev., 93(7), pp. 2419–2438.

[24]   Susnow, R. G., Dean, A. M., Green, W. H., Peczak, P., and Broadbelt, L. J., 1997, "Rate-Based Construction of Kinetic Models for Complex Systems," J. Phys. Chem. A, 101(20), pp. 3731–3740.

[25]   Ince, A., Carstensen, H.-H., Reyniers, M.-F., and Marin, G. B., 2015, "First-Principles Based Group Additivity Values for Thermochemical Properties of Substituted Aromatic Compounds," AIChE J., 61(11), pp. 3858–3870.

[26]   Ince, A., Carstensen, H.-H., Sabbe, M., Reyniers, M.-F., and Marin, G. B., 2016, "Group Additive Modeling of Substituent Effects in Monocyclic Aromatic Hydrocarbon Radicals," AIChE J., p. n/a-n/a.

[27]   Demirbas, A., Balubaid, M. A., Basahel, A. M., Ahmad, W., and Sheikh, M. H., 2015, "Octane Rating of Gasoline and Octane Booster Additives," Pet. Sci. Technol., 33(11), pp. 1190–1197.

[28]   Smith, G. P., Tao, Y., and Wang, H., "Foundational Fuel Chemistry Model 1.0" [Online]. Available: http://web.stanford.edu/group/haiwanglab/FFCM1/pages/download.html. [Accessed: 05-Jan-2017].

[29]   Burke, M. P., Chaos, M., Ju, Y., Dryer, F. L., and Klippenstein, S. J., 2012, "Comprehensive H2/O2 Kinetic Model for High-Pressure Combustion," Int. J. Chem. Kinet., 44(7), pp. 444–474.

[30]   "Methyl Formate Oxidation: Speciation Data, Laminar Burning Velocities, Ignition Delay Times, and a Validated Chemical Kinetic Model - Dooley - 2010 - International Journal of Chemical Kinetics - Wiley Online Library" [Online]. Available: http://onlinelibrary.wiley.com/doi/10.1002/kin.20512/full. [Accessed: 20-Jun-2017].

[31]   Brezinsky, K., Pecullan, M., and Glassman, I., 1998, "Pyrolysis and Oxidation of Phenol," J. Phys. Chem. A, 102(44), pp. 8614–8619.

[32] Long, A. E., Grambow, Colin A., Vandeputte, Aäron G., Merchant, Shamel S., and Green, William H., 2017, "New and Realistic Pathways from Cyclopentadiene (CPD) to Naphthalene, Phenanthrene, and Other Soot Precursors," p. paper 1A14.

[33] Sung, C.-J., and Curran, H. J., 2014, "Using Rapid Compression Machines for Chemical Kinetics Studies," Prog. Energy Combust. Sci., **44**, pp. 1–18.

[34] 2013, *Chemkin-PRO 15151*, Reaction Design, San Diego.

[35] Mehl, M., Pitz, W. J., Westbrook, C. K., and Curran, H. J., 2011, "Kinetic Modeling of Gasoline Surrogate Components and Mixtures under Engine Conditions," Proc. Combust. Inst., **33**(1), pp. 193–200.

[36] Egolfopoulos, F. N., Hansen, N., Ju, Y., Kohse-Höinghaus, K., Law, C. K., and Qi, F., 2014, "Advances and Challenges in Laminar Flame Experiments and Implications for Combustion Chemistry," Prog. Energy Combust. Sci., **43**, pp. 36–67.

[37] Healy, D., Donato, N. S., Aul, C. J., Petersen, E. L., Zinner, C. M., Bourque, G., and Curran, H. J., 2010, "N-Butane: Ignition Delay Measurements at High Pressure and Detailed Chemical Kinetic Simulations," Combust. Flame, **157**(8), pp. 1526–1539.

[38] Goodwin, D., *"Cantera: An Object-Oriented Software Toolkit for Chemical Kinetics, Thermodynamics, and Transport Processes*, Caltech, Pasadena, 2009.

[39] Merchant, S. S., Goldsmith, C. F., Vandeputte, A. G., Burke, M. P., Klippenstein, S. J., and Green, W. H., 2015, "Understanding Low-Temperature First-Stage Ignition Delay: Propane," Combust. Flame, **162**(10), pp. 3658–3673.

Chapter 5

Pre-experimental Framework for the

Broad Screening of Drop-in Fuel Additives

5.1 Introduction

The deployment of drop-in additives for on-the-road engine fuels, such as the now commonly used ethanol, requires that the resulting additive+fuel blend have a large number of favorable attributes. These attributes include: high heating value, favorable auto-ignition performance, low emissions, materials compatibility, miscibility with existing fuels, low toxicity, and many other considerations. Because experiments to measure all these attributes for all potential additives is extremely time intensive and expensive, in part because a large amount of the proposed fuel additive must be synthesized to facilitate the testing, a methodology for computational screening would be very valuable. The current study focuses on development of

pre-experimental screens for these important fuel properties: ignition, polycyclic aromatic hydrocarbon (PAH) formation, fuel/water solubility, and elastomer compatibility.

Knock, an undesired phenomenon in spark ignition engines, is caused when the unburned fuel gas auto-ignites. Knock limits the efficiency of SI engines, and this limit is even more severe for modern turbo-charged engines [1]. The research octane number (RON) is an industry standard used to quantify anti-knock behavior [2]. It would be helpful to be able to predict the RON for proposed novel fuel compositions. There are many studies which try to correlate RON other observables such as infrared spectroscopy [3], distillation curve [4], dielectric spectroscopy [5], and structural group contribution methods [6]. However, the most rigorous test involves studying the detailed chemical kinetics [7]. Unfortunately, the difficulty in manual generation of accurate chemical mechanisms, limits this approach.

Another concern in new fuel compositions is the PAH growth leading to the formation of soot, which has been concluded to cause increased mortality due to heart and lung disease [8,9]. Typically, soot formation occurs from the decomposition of fuels to small molecules, formation of the first aromatic ring, and subsequent addition of aromatic rings until reaching particulate size [10]. Although much study has been accomplished bridging the mechanistic gap between small molecules and 1-2 aromatic rings [10,11], there is less focus on the mechanism of specific additives in fuels. Curran et al [12] used detailed kinetic models to conclude oxygenated additives reduced the amount of sooting in diesel flames. High throughput experimental screening has been performed using the smoke point of pure additives in an open flame [13], which, although experimental, is more in line with the goals of this study.

Both of these attributes require an accurate chemical mechanism for sufficient testing. This can be provided by the reaction mechanism generator (RMG) [14], which is an open-source software package designed to automatically construct kinetic models using a flux-based algorithm for model expansion. It is feasible to quickly study a series of molecules with RMG because a chemical mechanism can be created with a minimal amount of effort, as demonstrated in previously published papers [15–17]. Additionally, these mechanisms can offer insight into reaction pathways involved with ignition or PAH growth.

The drinking-water contamination of methyl tert-butyl ether (MTBE), an anti-knocking oxygenate additive used in gasoline, underscores the need for environmental transport models. These models rely on fuel-water partition coefficients values defined as

$$K_{i,fw} = \frac{c_{i,f}}{c_{i,w}} \tag{1}$$

where $K_{i,fw}$ is the partition coefficient and c is the molarity of species i in the fuel phase, f, and the water phase, w. The standard state of the partition coefficient assumes $T = 298.15K$ and dilute conditions such that $K_{i,fw}$ is independent of overall concentrations of solute and solvents. Yalkowsky and Banerjee [18] outline several methods for the estimation of partition coefficients including: group activity coefficients [19], correlations to octanol-water partition coefficient [20], UNIFAC [21], free energy relationships [22], and many others. The authors argue that UNIFAC and free energy relationships have potential for universality. UNIFAC is easily generalized using a few group contribution values, and can just as easily generalize mixtures of many compounds. Meanwhile poly-parameter linear free energy relationships (pp-LFERs) capture more effects of molecule interaction, having separate terms for polarizability, acidic and basic hydrogen bonds. Although, the pp-LFERs are more limited to binary systems, some work has been done to develop mixing rules [23].

Elastomers used in storage and transport of fuels are known to swell with changing fuel composition, as shown by the comprehensive experimental study for the addition of ethanol to gasoline [24]. Too much swelling of the elastomers when in contact with fuel can reduce the elasticity of the O-rings and other gaskets, leading to fuel leaks and other problems. Flory developed a theory that treated polymer-solution mixtures as regular solutions, defining the interaction parameter to account for enthalpy changes [25]. The Flory-Rehner equation [26] describes elastomer swelling by equating the work of isotropic stretching (per mole) with change in chemical potential of mixing derived from Flory-Huggins. The calculation relies on accurate estimates of interaction parameter. Interaction parameters are related to differences in solubility parameter, which were first correlated to cohesive energies by Hildebrand [27]. Later, Hansen refined the solubility parameter to include separate terms for dispersion forces, dipolar forces, and hydrogen bonding forces [28].

In the following sections, a computational screen is proposed for the ignition behavior, growth of PAH precursors during ignition, liquid solubility in fuels and water, and elastomer swelling. First, the methodology for each screen is described. For ignition behavior and PAH precursor growth, additive mixtures and base fuel are compared. Then reaction pathways which

mechanistically explain the predicted behavior are discussed. Next several theoretical methods to predict fuel solubility and fuel/water partition coefficient are compared with phase separation experiments. Finally, an implementation of the Flory-Rehner theory is compared to swelling experiments for the additives.

5.2 Methods

The model compounds, phenol, anisole, furfural, and furan, shown in Figure 5-38 were chosen for this study because they represent common functional groups found in bio-oil formed by fast pyrolysis of biomass.
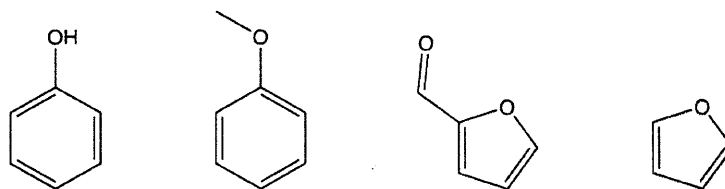
Figure 5-38 Model compounds selected to represent relevant species and functional groups in bio-oils derived from the fast pyrolysis of biomass.
The four compounds from left to right are phenol, anisole, furfural, and furan

5.2.1 Screen for ignition behavior

To investigate the effect of drop-in fuels on ignition delay, RMG was used to generate mechanisms of each additive with the LLNL gasoline surrogate mechanism [29] used as the model for the base fuel. Other chemistry included as thermochemistry or reaction libraries include: H2/O2 oxidation [30], cyclopentadienyl chemistry [31], and phenol pyrolysis [32]. Conditions for the model generation were P = 20 bar, T = 650K – 2000K, and ϕ = 1 for 10% mol fraction additive in 90 PRF in air. After automatic generation, the six individual mechanisms were combined into one master mechanism.

First ignition simulations were run in adiabatic batch reactors with 2% mole additive in pure heptane at P_0 = 20 bar, T_0 = 650 K, and ϕ = 1 using Cantera [33]. Next, the additives were tested in conditions for spark-ignition engine. Because the mechanism is too large for a full CFD simulation, a simplified engine-like simulation was created for predicting the RON number measured by a CRF engine [34]. Pressure traces, fitted from five runs of CFR engine runs of PRF 90 were used to calculate a volume profile. Because the ASTM procedure [2] only specifies intake air temperature of 375K, the initial cylinder temperature was fitted such that the end gas's

ignition time approximately matched the maximum pressure. These fitting simulations were conducted using only LLNL mechanism and resulted in an initial temperature of 400 K. CFR simulations were conducted using adiabatic variable-volume batch reactors in Chemkin-Pro [35], using the specified volume profile, P_0 = 20 bar, T_0 = 400K, and ϕ = 1 for 2% mol fraction additive in PRF 90 in air.

The two equations used to convert a pressure profile to volume were:

$$\int_{T_0}^{T_c} \frac{\gamma}{\gamma - 1} \frac{dT}{T} = \ln\left(\frac{P_c}{P}\right)$$

(2)

$$\int_{T_0}^{T_c} \frac{1}{\gamma - 1} \frac{dT}{T} = \ln\left(\frac{V_c}{V}\right)$$

(3)

Complete volume profile used in the simulation is given in Appendix A.

5.2.2 Screen for generation of PAH precursors

A screen to test each blends tendency to create PAH's was also performed. Conditions for RMG-aided mechanism generation and Chemkin-Pro simulations were based on the first two stages of diesel combustion presented in Dec et al [36]. After fuel is sprayed into the cylinder, the first region is composed of cold fuel and hot entrained air reacting at rich conditions, ϕ = 4. This mixture begins to react significantly at about 650 K and reaches approximately 1600 K after 0.25 ms when all the entrained oxygen has been consumed. In the second stage, the remaining rich oxidation products are left in essentially pyrolysis conditions for 0.5 ms at 1600 K. Finally, the products from pyrolysis reach the diffusion flame that surrounds the fuel jet, resulting in close to complete combustion (though some soot makes it past the flame and needs to be trapped/destroyed in the exhaust system, or else it will be emitted to the environment).

RMG was used to generate mechanisms to explore the sooting tendency of each additive. Butane was chosen as the base fuel to reduce the computational cost. These mechanisms were developed over two stages. First, a base butane model was created in RMG using GRI-Mech 3.0 [37]. This model was simulated in an adiabatic batch reactor starting at various initial temperatures T_0, with P_0 = 20 bar, and residence time of t = 0.25 ms, conditions consistent with the first oxidative region composed of cold fuel and entrained air. Major products with a mole fraction of greater than 10 ppm were taken from this simulation. Then a second mechanism was generated, using the additive of interest (mole fraction calculated for 5% mol of original

105

unreacted butane) and the oxidative products using their end-time mole fractions from the previous simulation. Conditions were chosen to be similar to the second stage of diesel flame: 1600K, P = 20 bar, no oxygen, and nitrogen diluent. During the second RMG generation, additional chemistry [38], [39], [40] for reacting small molecules to benzene and naphthalene were in addition to those in from butane.

The first two stages of the diesel flame were simulated using two reactor objects in Chemkin-Pro [35] as shown in Figure 5-39. The first reactor was constant-volume with conditions $T_0 = 600K$, $P_0 = 20$ bar, and $\phi = 4$. Additionally, a heat flux was fitted to approximate the heat from the entrained air such that the temperature of the reactor reached 1600K after 0.25 ms. A second isothermal, constant-volume reactor was used to simulate the second region, where chemistry that can form PAH is more likely to occur. Conditions were 1600K, 20 bar, and residence time of 0.5 ms. After the two-stage reactor simulation, the final mole fractions of key PAH precursors: benzene, indene, cyclopentadiene, and propargyl were compared.
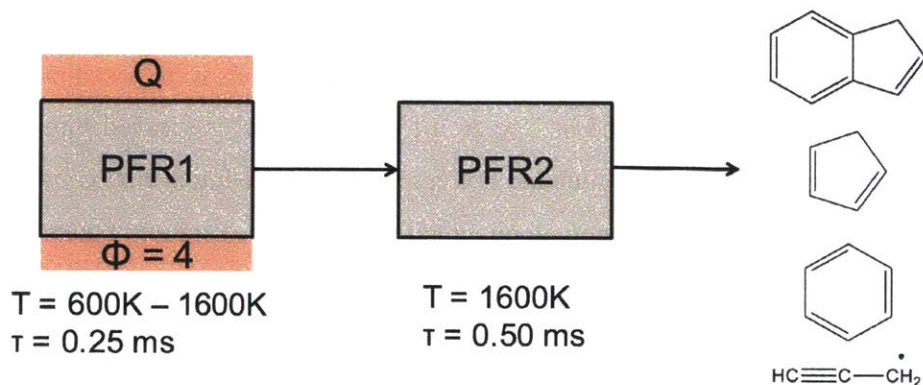
Figure 5-39 Diagram of two-stage reactor model used for predicting formation of PAH precursors.

5.2.3 Screen for solubility of the additive in fuel and water

It is inconvenient if a fuel additive is not soluble in the base fuel (since then a surfactant or co-solvent would be need to be added, to keep the additive in the fuel). Also, fuels are exposed to water in pipelines and in tanks (both at the gas station and in the vehicle). If a fuel component is too soluble in water, it will significantly partition into the aqueous phase, altering the fuel composition and potentially leading to groundwater pollution. Two different methods were used to estimate the partitioning of the proposed fuel additives between base fuel and water. First, the UNIFAC group additive method [41] as implemented in AspenTech [42], was used to

106

calculate if the fuel additives would separate from a widely used surrogate fuel mixture, Fuels for Advanced Combustion Engines (FACE) #9 [43]. The nine FACE fuels were created to represent typical values of aromatic composition, and cetane number. FACE #9 was chosen for this study because it has median values for each of these attributes. Composition for FACE #9 is given in Table 5-7.

Table 5-7 Composition of surrogate fuel FACE #9 used in simulations of liquid-liquid solubility

Component	Mass fraction	Mole fraction
n-decane	0.050	0.054
n-tetradecane	0.050	0.039
n-hexadecane	0.181	0.123
n-eicosane	0.061	0.033
Cyclohexane	0.008	0.146
Decalin	0.026	0.289
m-xylene	0.010	0.014
tetralin	0.069	0.080
phenanthrene	0.055	0.047
m-cymene	0.020	0.023
n-pentylbenzene	0.040	0.042
n-heptylbenzene	0.124	0.108

To test the predictions, each additive was tested for its solubility in FACE #9 and for phase separation in the case of water contamination. A group additive method, such as UNIFAC has the advantage that it can be used for almost any fuel additive where the necessary functional groups are available. The UNIFAC results were compared to results of pp-LFERs [44], which can be more accurate if some parameters have been empirically derived for the specific chemical species and solvents of interest. The pp-LFER employed was the Abraham correlation (Eq. 2)

$$\log K_{i,jw} = c + eE + sS + aA + bB + vV \qquad (4)$$

where K is the partition coefficient for solute i in a bi-phasic mixture of the two solvents j and w, C is a fitted constant, e is the excess molar refractivity, S is the polarizability parameter, A is H-bond acidity, B is the H-bond basicity, and V is the McGowen molar volume of the solute. The

corresponding lower-case letters are complementary parameters for the solvent pair, e.g. a is related to the difference in the H-bond accepting abilities of the two solvents, b is related to the difference in the H-bond donating abilities of the solvent, and s is related to the difference in how the two solvents interact with polarizable solutes. Although parameters for each solvent and solute were not available on the UFZ-LSER database [45], comparisons were made for solutes of phenol, anisole, and furfural in representative solvents, some of which are components of FACE #9: octanol, n-dodecane, cyclohexane, iso-octane, and toluene vs water.

To test the accuracy of the predicted partition coefficients, K_{fw} was experimentally measured for each of the four fuel additives: anisole, phenol, furan, and furfural. For each of these additives, dilute solutions were prepared in FACE 9 at a concentration of 1 mg additive/ g FACE 9. A solution of 3-chlorothiophene (Sigma Aldrich, 98%) in toluene was also prepared at a concentration of 12 mg 3-chlorothiophene / g toluene for use as an internal standard for quantification of the fuel additives. The initial concentration of additive in the FACE 9 + additive solutions were verified prior to determining the partition coefficient with water. (0.25 grams of each FACE 9 + additive solution was mixed with 0.1 grams of the standard solution and analyzed by GC-FID as described below) To determine the partition coefficient with water, 1.75 grams of each FACE 9 + additive solution were mixed with 1.75 grams of deionized water in a small vial at 21°C. The contents of the vials were mixed vigorously by hand for 10 minutes to try to reach phase equilibrium. The resulting organic and aqueous phases were then separated, and 1.3 grams of the organic phase was mixed with 0.1 grams of standard solution to quantify the amount of additive remaining in the FACE 9 phase.

Solutions were analyzed using an Agilent 7890 GC-FID with an RXi-5HT column (30m length, 250 μm ID, 0.25 μm film thickness). Calibration standards using 3-chlorothiophene as the internal standard were prepared in acetone for anisole, phenol, and furfural and in toluene for furan. 5 standards were prepared for each additive by fixing the additive concentration at 1 mg/ g solution and varying the amount of 3-chlorothiophene in ratios of 1.5, 1, 0.5, 0.25, and 0.125 grams additive per gram 3-chlorothiophene. For all runs a temperature ramp of 40 °C to 80 °C by 5 °C/min, followed by a 15 °C/min ramp to 280 °C, followed by a 20 °C/min ramp to 325 °C was used, with a 10-minute hold time at 325°C. An attached Agilent 5975C inert XL mass spec was also used to confirm the identity of the compounds in the resulting chromatograms.

5.2.4 Screen for elastomer swelling

For a mono-solvent, equilibrium elastomer swelling can be calculated using the Flory-Rehner equations [26]:

$$-\left[\ln(1 - \phi_e) + \phi_e + \chi_{1e}\phi_e^2\right] = V_1 n \left(\phi_e^{\frac{1}{3}} - \frac{\phi_e}{2}\right) \tag{5}$$

where ϕ_e is the volume fraction of the elastomer, χ_{1e} is the Flory-Huggins interaction parameter between solvent and elastomer, and V_1 is the molar volume of the solvent, and n is the cross-link density of the elastomer. The equilibrium degree of swelling is defined as the inverse of elastomer volume fraction.

$$Degree\ of\ Swelling = \frac{V_{final}}{V_{initial}} = \frac{1}{\phi_e} \tag{6}$$

The interaction parameter, χ_{1e}, is derived from the difference of solubility parameters.

$$\chi_{1e} = V_1 \frac{(\delta_1 - \delta_e)^2}{RT} \tag{7}$$

where δ_i is the solubility parameter for phase i. This definition for χ_{1e} quantifies the adage "like-dissolves-like", such that two materials with similar solubility parameters would be perfectly miscible. Solubility parameters for each additive were calculated using the Hildebrand equation [27], which only requires heat of vaporization and density of the pure substance.

$$\delta_i = \sqrt{\frac{\Delta H_{vap,i} - RT}{V_i}} \tag{8}$$

Table 5-8 gives the physical values used to calculate the solubility parameter for all solvents used in testing.

Table 5-8 Physical parameters used to calculate solubility parameters in this study. Densities were measured while heats of vaporization were taken from literature [46].

Solvent	Density at 25°C (g/ml)	Molecular Weight (g/mol)	ΔH_{vap} (kJ/mol)	V (cm³/mol) at 25°C (g/ml)	δ (Mpa$^{0.5}$) at 25°C (g/ml)
iso-octane	0.71	114.23	35.1	162.48	14.17
Toluene	0.87	92.14	37	106.27	18.02
Anisole	1.00	108.14	44	108.62	19.55
Phenol	1.04	94.11	58.8	90.49	24.95
Furan	0.94	68.08	27.81	72.64	18.68
Furfural	1.16	96.09	50.07	82.83	23.97

Unfortunately, these equations cannot be applied directly to fuel systems, which are composed of hundreds of different species, not a single solvent. Additionally, it is known that interaction parameters vary with concentration [47]; it is not clear if this system is in the dilute limit or not. One simple method used in this work is to calculate effective interaction parameters and molar volumes by taking a volume average of all species in the solvent.

The Flory-Rehner model has been generalized to a system of equations for multi-component solvents [48]:

$$W_i = \mu_{stretching,i} = V_i n \left(\phi_e^{\frac{1}{3}} - \frac{\phi_e}{2} \right) \tag{9}$$

where W_i is the work done during swelling, or chemical potential of stretching, by component i in the elastomer. In this theory, the chemical potential can be written:

$$\mu_{mix,i} = \ln \phi_i + (1 - \phi_i) - \sum_{i \neq j, j \neq e} \frac{V_i}{V_j} \phi_j + \sum_{i < j} \chi_{ij} \phi_j (1 - \phi_j)$$
$$- \sum_{p < q, p \neq i, q \neq i} \frac{V_i}{V_p} \chi_{pq} \phi_p \phi_q + \sum_{h < i} \frac{V_i}{V_h} \chi_{hi} \phi_h (1 - \phi_i) \tag{10}$$

where $\mu_{mix,i}$ is the chemical potential of mixing for species i and all sums indicate pairwise cross-terms (within stated constraints) that include all solvents and elastomer e. Finally, a system of

110

equations is derived by setting the chemical potential of each species equal across the liquid phase and elastomer. The system of equations was solved using the optimization implemented in Sci-Py [49].

$$\mu_{mix,i}\big|_{liquid} = \mu_{mix,i}\big|_{elastomer} + W_i \tag{11}$$

$$\sum_i \phi_i \Bigg|_{elastomer} = 1 \tag{12}$$

To test the accuracy of this computational screen, experiments for O-ring expansion are conducted where O-rings (OD 1/4 inch, ID 1/8 inch) are immersed in 1 mL of solvent and kept in room temperature for seven days. The O-rings used in this experiment are composed of Buna-N rubber, which is a co-polymer of butadiene and acrylonitrile. Mass of solvent, O-ring, and solute is measured using a Metter Toledo XS204 analytical balance. The size of individual O-rings for each experimental condition is measured using Mitutoyo Absolute Digimatic Vernier calipers before immersion to solvent and after seven days of immersion.

Trials with several pure solvents: toluene, iso-octane, anisole, furan, and furfural, were used to calculate the solubility parameter cross-link density of Buna-N. Fuel C, a 50/50 volume blend of toluene and iso-octane [24], was chosen as a surrogate for gasoline. Regular grade gasoline (octane rating 87) was purchased from Sunoco Gas Station (Cambridge, MA 02139) and tested as a control. Trials using blends of phenol, anisole, furan, and furfural in fuel C were then used to validate the model. Volumes for the O-rings were calculated using the following formula:

$$V = \frac{\pi^2}{4}(D_{outer} - D_{inner})^2(D_{outer} + D_{inner}) \tag{13}$$

5.3 Results and Discussion

5.3.1 Screen for ignition behavior

Figure 5-40 shows comparisons of predicted ignition delay for 2% additives in PRF 90 with conditions: $P_0 = 20$ bar, $\phi = 1$, and various initial temperatures. It can be seen at this condition that furfural enhances the ignition. The behavior of phenol is more complicated: it

111

accelerates ignition when the initial temperature is low but slows ignition at higher temperatures. Both furan and anisole appear to have a negligible effect at most conditions, although the furan may very slightly slow down the ignition.
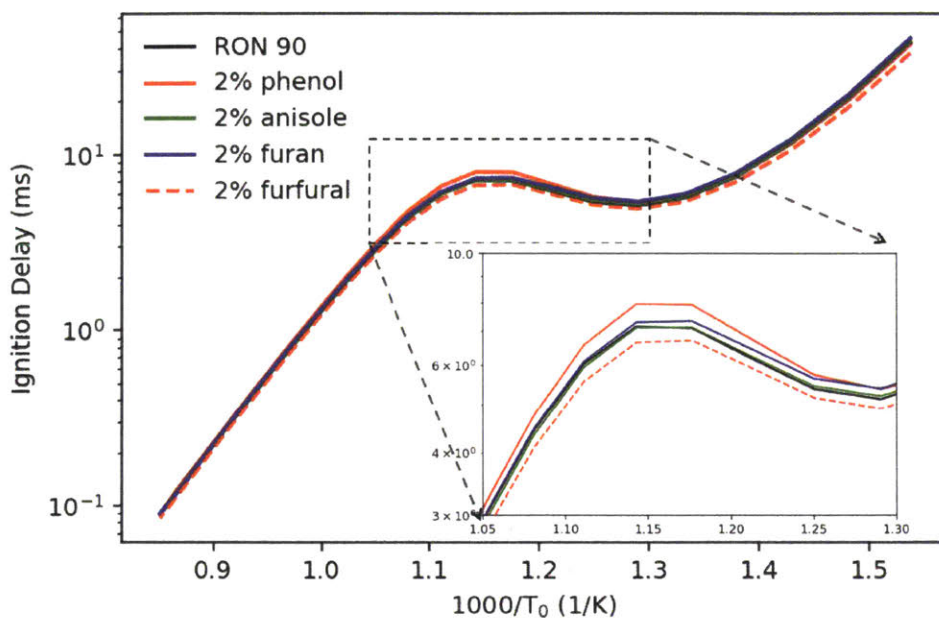
Figure 5-40 Computed effect of fuel additives on ignition delay of PRF90 in constant-volume adiabatic batch reactor.
Conditions: P_0= 20 bar, and ϕ = 1. The overlapped plot shows a zoomed in view for temperatures between 750K and 950K.

A simple constant-volume batch reactor, while placing strong emphasis on chemical effects, is not a good approximate of the end gas conditions in a combustion engine, where pressure and temperature continuously increase, first due to compression by the piston motion, then due burning of the rest of the fuel-air mixture. To address conditions more relevant to gasoline, CFR engine-like simulations following the methodology outlined in section 2.1 were performed to investigate the ignition timing of the mixture when being exposed to the end gas condition. From Figure 5-41, it can be seen that that furan had the largest octane-boosting effect in the RON test conditions, although furan had almost no discernable effect in the constant-volume adiabatic reactor case. This emphasizes the importance of the physical compression toward predicting RON. Phenol has smaller, but still significant octane-boosting effect. Anisole seems to have very insignificant effects. Finally, furfural enhances the ignition (i.e. reduces the

112

RON). Estimated change in the RON of the mixtures is given in Table 5-9 by interpolating between PRF85 and PRF95.
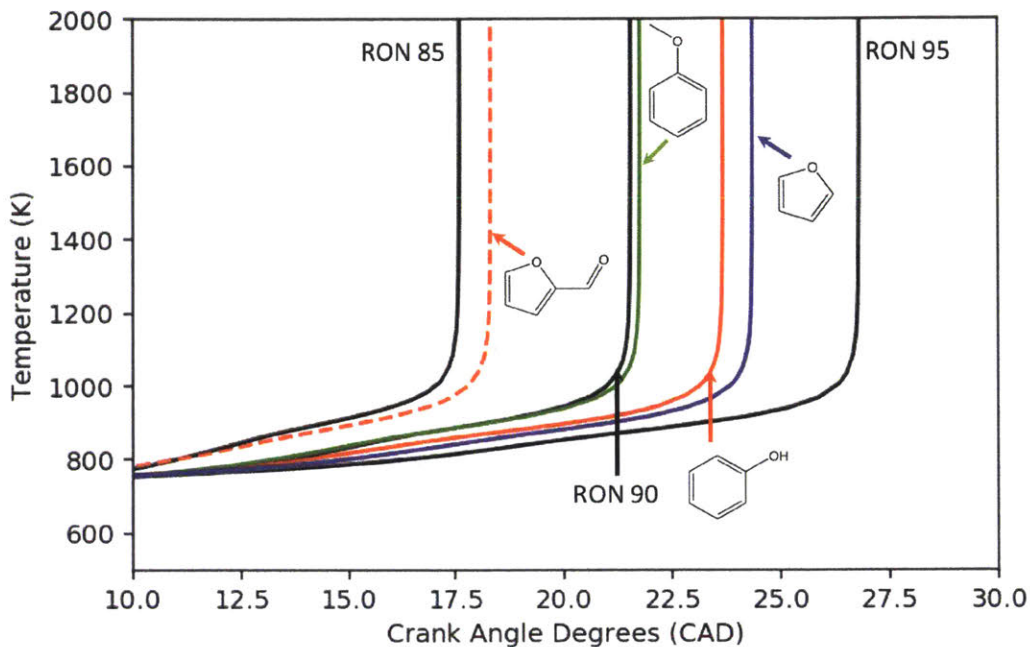
Figure 5-41 CFR-like simulations of additives mixtures in PRF90, with PRF fuels
Conditions $T_0 = 400K$, $P_0 = 1.06$ bar, $\phi = 1$. Enforced volume profile were calculated using pressure traces from 5 runs of PRF 90 in CRF engines.

Table 5-9 Estimated blending RON numbers for 2% mixtures of additives with PRF 90.
Linearly interpolated from runs of 85 - 95 PRF.

Base "RON"	90.0	90.0	90.0	90.0
Blended "RON"	92.6	91.9	89.8	86.0
Δ"RON"	2.6	1.9	-0.2	-4.0

Because the regression for PRF is not perfectly linear, the anisole blend was calculated to have a negative effect on RON, despite having a slightly larger ignition delay than PRF 90. We

were unable to find comparisons in literature for any of the additives except anisole. Ratcliff et al report a blend RON of 95.0 for a 19.6% volume blend of anisole in gasoline base fuel (RON= 87.9) [50]. The authors used this value to calculate a blending RON of 123.4, metric commonly used to linearly interpolate RON of blends, using the formula:

$$Blending\ RON = \frac{Blend\ RON - Base\ fuel\ RON * \phi_f}{1 - \phi_f} \qquad (14)$$

where blend RON is the experimentally measured value of RON of blend and ϕ_f is the volume fraction of base fuel. Using this Eq (9), we would calculate a blend RON of 90.6. This is higher than our simulated value of 89.8; the discrepancy may be caused by Ratcliff's much higher blending volume.

Chemical pathway analysis for each additive's initial chemistry was performed to determine the model compound's effect on auto-ignition behavior. It is known that the concentration of reactive radicals, specifically OH, is the key attribute governing the ignition delay of a fuel [51]. Therefore, most analysis was focused on how the additives affect the build-up of OH concentration.

In the main pathway for furan, an OH radical adds ortho to the oxygen atom. The adduct radical ring-opens via beta scission to an allylic-like radical as shown in Figure 5-42. This species undergoes further hydrogen-abstraction, mostly by oxygen, to form a conjugated dione. Because of the conjugated double bonds, the resulting dione is relatively stable compared to other fuel compounds in the system and does not have any low-barrier reaction paths leading to radical chain branching at pre-ignition temperatures. The net effect of this pathway is the conversion of a highly reactive OH radical into a relatively unreactive allylic radical, which later becomes a relatively unreactive HO_2 radical.

The main terminating effect of phenol is shown in Figure 5-42. Phenol has a similar chain-terminating effect to furan, although its mechanism is much simpler. In agreement with Brezinsky et al [32], this study's simulation predicts phenol mainly being hydrogen abstracted to phenoxy radical. Given that phenoxy is also highly resonantly stabilized, this radical has a difficult time abstracting from other fuel molecules to carry on the chain reaction, and stays relatively inert for the rest of pre-ignition chemistry.

Furan Pre-Ignition
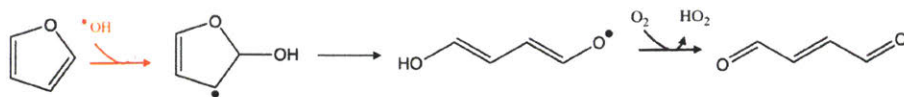
Phenol Pre-ignition
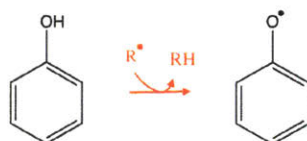
Figure 5-42 Main steps in pre-ignition chemistry for furan and phenol at T < 850K.
Chain terminating reactions are shown in red. The terminal species in each reaction sequence was not found to have significant product channels prior to the ignition.

Anisole has a negligible effect on ignition for all conditions tested. In Figure 5-43, it can be seen that the terminal carbon on the ether group is the main target of hydrogen abstraction. This can then combine with oxygen forming a peroxy. The peroxy abstracts a hydrogen predominantly from HO_2, but some from fuel. Then, weak O-O bond cleaves, creating formaldehyde, an OH radical, and phenoxy radical. As before, the phenoxy radical is relatively unreactive. If HO_2 donates the hydrogen, the pathway is radical neutral converting the original radical used to initiate the reaction pathway into an OH. In the case where fuel donates that hydrogen, we would expect a slightly faster ignition. However, the reaction of the peroxy with fuel has a significant barrier, while the reaction of the peroxy with HO2 is very fast, so it is likely that this side channel is too minor to have a significant effect in the simulation.
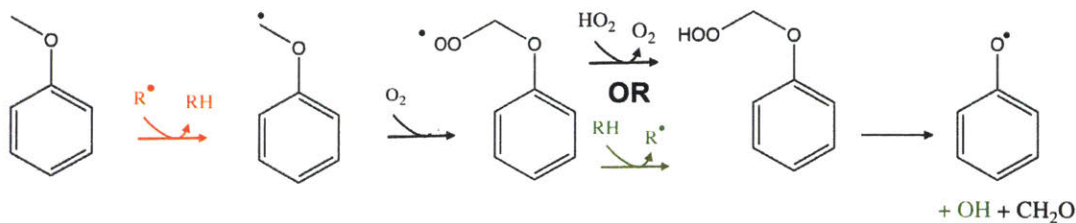
Figure 5-43 Main steps in pre-ignition chemistry for anisole at T < 850K.
In the third step, the peroxy can abstract from either HO_2 or the fuel.

Furfural was the only additive which showed consistent cetane-boosting effects for all conditions. The main pathway found for furfural is shown in Figure 5-44, and begins with hydrogen abstraction from the aldehyde group leading to a peroxy radical. This peroxy then adds back onto the furan ring creating a highly-strained polycyclic species. Beta-scission on this

115

structure results in a seven-membered ring with a radical. This can further beta-scission to give a conjugated linear molecule with a radical on a carboxylic acid. The carboxylic acid will decompose into CO_2 and the radical, ultimately forming a radical version of the same conjugated dione formed from furan. However, the formation of CO_2 in this case is highly exothermic which pre-emptively increases the temperature of the system and allows the other ignition reactions to occur faster. Although furfural does not directly aid in radical formation, it does speed up the ignition through temperature rise.
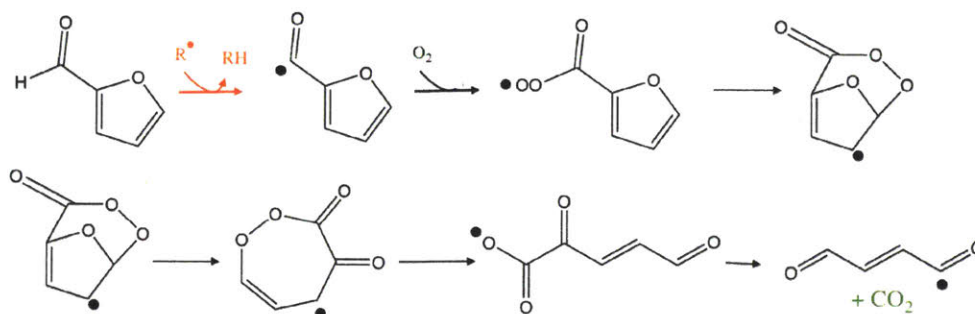
Figure 5-44 Main steps in pre-ignition chemistry for furfural at T < 850K.
Although the total reaction pathway is radical neutral, the production of CO_2 is a highly exothermic process. Overall furfural promotes the ignition of the fuel.

5.3.2 Screen for generation of PAH precursors

After the two-stage simulation described in Section 2.2, comparisons for the concentration of known PAH precursors were made between blends of butane + additives. Figure 5-45 shows mole fraction of PAH precursors versus time during the constant temperature pyrolysis stage, which begins at 0.25 ms. Of the PAH precursors: benzene, cyclopentadiene, indene, and propargyl, the pure butane simulation only showed a significant amount of propargyl. As one would expect, the direct addition of aromatics tends to increase the PAH precursors. Phenol primarily leads to an increase in the amount of benzene and propargyl. Anisole leads predominantly to cyclopentadiene, propargyl and indene. Finally, furan and furfural had exactly the same effect: increasing all PAH precursors studied. Pathways to these PAH precursors found by the automatically-generated mechanism are discussed below. Note that the discussed pathways are not necessarily the main reaction pathways of the additives. Because butane is predicted to produce only a very small amount of PAH precursors, even small side channels for the additives can give large increases in PAH precursors.

116
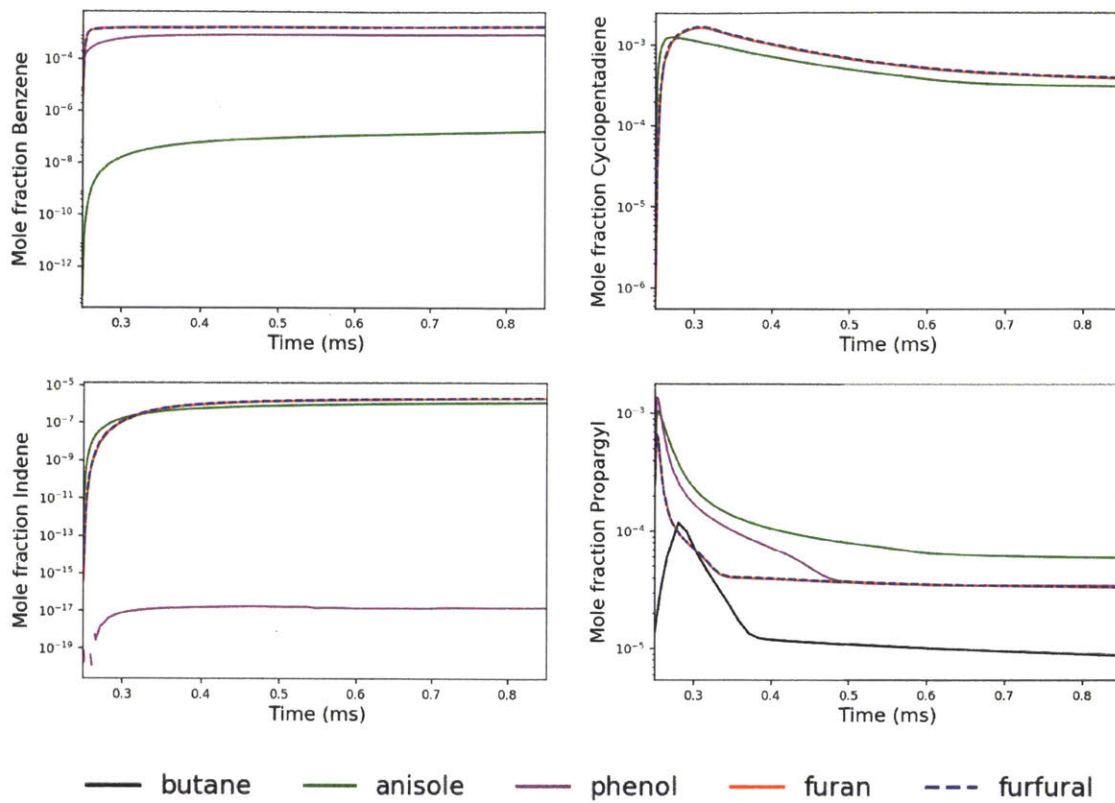
Figure 5-45 Comparisons between mole fractions of PAH precursors between blends of 2% mole additive in butane.
The x-axis gives the total simulation time, with the second reactor, which represents the pyrolysis region of a diesel flame, beginning at t = 0.25 ms. Conditions in the second reactor are T = 1600K, P = 20 bar, and pyrolysis conditions with products with partial oxidation. Note that not all fuel blends produce every PAH precursor.

The main pathways for anisole and phenol are shown in Figure 5-46. In the simulation of the pyrolysis conditions, anisole directly dissociates giving phenoxy and methyl radical. Phenoxy radical creates a bridged species through intra-addition, ring breaks, and beta scissions into cyclopentadiene [32]. One reaction pathway included in the mechanism has cyclopentadiene combining with cyclopentadienyl eventually forming indene [31]. Because the main product of phenol during oxidation is also phenoxy radical, one would expect it to go through the same pathways as anisole. However, the mechanism proposes that addition of methyl radical to the benzene ring out-competes the creation of the bridged species. Additionally, another competing

117

pathway through a different radical is present. H-addition alpha to the alcohol group followed by subsequent beta scission directly produces benzene and OH radical.

Anisole Pyrolysis Pathway

+ CH₃   + CO
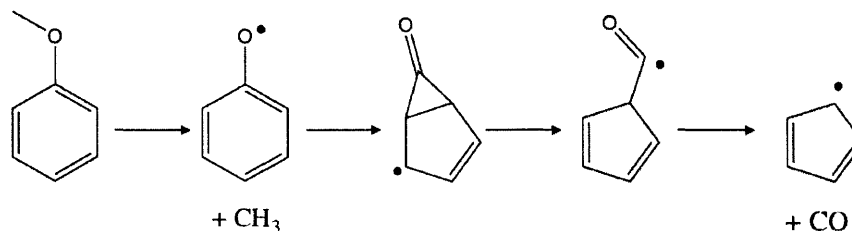
Phenol Pyrolysis Pathway

+ OH
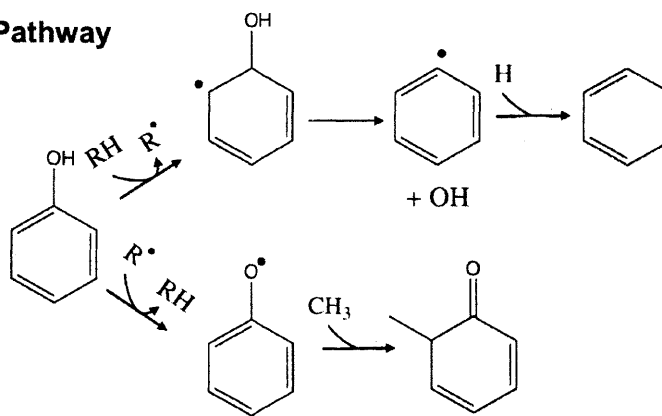
Figure 5-46 Pyrolysis pathways at 1600K of anisole and phenol relevant to PAH precursors

After H-abstraction from the carbonyl group, furfural quickly decomposes to a 2-furanyl radical and carbon monoxide as shown in Figure 5-47. This radical can then H-abstract back to furan explaining the similarity in the furan and furfural products. RMG explored decomposition pathways for various radicals of furan. The decomposition of the 3-furanyl radical leads directly to the production of propargyl. 3-furanyl radical beta scission to give a resonantly stabilized alkoxy radical. This radical can perform an intra-H migration to give a radical on the carbonyl. Finally, the carbonyl decomposes to CO and propargyl.

Furfural Pyrolysis Pathway
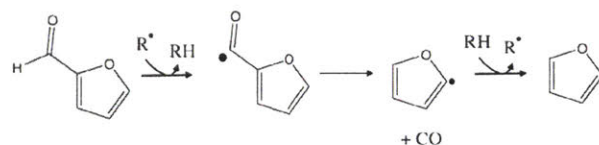
Furan to Propargyl Pathway
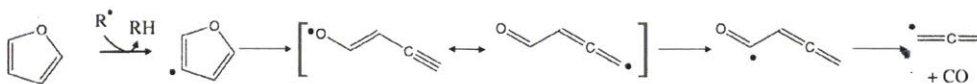
Figure 5-47 Pyrolysis pathways at 1600K of furan and furfural relevant to PAH precursors.
Bracketed species indicate a resonance structure rather than chemical reaction.

To keep mechanisms to a tractable size, all mechanisms were generated with a loose flux tolerance in RMG. This makes it almost certain that some relevant pathways were not included in the mechanisms. For example, the methyl addition to phenoxy should also appear in the anisole mechanism. Additionally, RMG struggles with polycyclic and aromatic chemistry, often predicting thermochemistry or misapplying reaction analogies intended for more linear species.

5.3.3 Screen for fuel solubility

Of the model compounds, UNIFAC group additive values were found for phenol, anisole furfural, and all components of the FACE #9 fuel shown in Table 5-7. A simple chemical flowsheet consisting of a single stream input stream and a decanter object was created in ASPEN-PRO [42] using the UNIFAC-LL model. For all three additives, no separation was found between additive and surrogate fuel for any mixture with as much as 10% mol additive, which is typically a much higher fraction than one would use in practice.

The same decanter module was used with 5% mole additive in FACE #9 and varying volume fractions of water up to 10% at T = 298.15K. This UNIFAC model predicts an average value of K_{fw} = 2.23 x 10^4 for phenol, K_{fw} = 4.43 x 10^2 for anisole, and K_{fw} = 0.644 for furfural. The partition coefficient depends strongly on the identity of the additive, but only drops slightly with the addition of water. These are compared with experiments at the same condition shown denoted with stars in the parity plot shown in Figure 5-48. Finally, pp-LFER parameters were found for all additives, but for only some binary systems. The systems chosen for comparison were water with octanol, n-dodecane, iso-octane, cyclohexane, and toluene. Values of pp-LFER parameters are given in Table 5-10.

119

Table 5-10 Parameters for pp-LFER used in this study.
All solvent parameters are for a binary mixture of the organic solvent and water.

Solute	E	S	A	B	V	
Phenol	0.81	0.89	0.6	0.3	0.775	
Anisole	0.71	0.75	0	0.29	0.916	
Furan	0.37	0.51	0	0.13	0.536	
Furfural	0.69	1.13	0	0.45	0.693	
Solvent	e	s	a	b	v	c
Octanol	0.49	-1.04	-0.02	-4.24	4.22	-0.03
n-dodecane	0.57	-1.64	-3.55	-5.01	4.46	0.11
iso-octane	0.56	-1.74	-3.68	-4.86	4.42	0.32
Toluene	0.53	-0.72	-3.01	-4.82	4.55	0.14
Cyclohexane	0.78	-1.68	-3.74	-4.93	4.58	0.16

Comparison between predicted K_{fw} for the pp-LFER and UNIFAC are compared with dots in Figure 5-48.

Figure 5-48 Comparisons between UNIFAC predictions and pp-LFER prediction or experimental measurements of partition coefficient.
The color of each point denotes the additive, while the shape of the point describes if pp-LFER predictions or experimental measurements are plotted on the y-axis.

The UNIFAC predictions agree reasonably well with pp-LFER for anisole and furfural, but are very different for phenol. For phenol, UNIFAC predicts a much higher fuel solubility than the pp-LFERS. In UNIFAC, the activity coefficient is calculated by adding the

120

combinatorial component, which accounts for surface area and molar volume, and the residual component, which accounts for interactions between groups. The combinatorial component is more similar to the fuel components than water. It is possible that the combinatorial component is over-represented and the hydrogen bonding that can occurs with water and the alcohol group are under-represented in UNIFAC. Interestingly, the experimental results for FACE #9 tend to agree more with pp-LFER predictions than UNIFAC's, despite the fact that pp-LFER are for binary systems instead of a fuel blend. The solubility of the anisole is predicted higher than experimentally observed. Because the experiments measured the additive remaining in the fuel (but not the amount of additive in the water), there is a large experimental error if Kfw>1. For this reason, it is believed that the anisole measurement has significant error. It is planned to re-measure this data point by fluorescence in the near future.

5.3.4 Screen for elastomer compatibility

Table 5-11 shows the experimentally determined degree of swelling in buna-N rubber as well as physical parameters for the pure solvents and base fuels. No experiment was attempted for phenol, which is solid at room temperature. Iso-octane actually showed a slight amount of shrinkage, indicating that very little iso-octane was absorbed into the elastomer. The shrinkage may indicate that some leaching of rubber components has occurred. Experiments of the remaining system of pure solvents: toluene, anisole, furan, and furfural, were used to calculate the cross-link density n and the elastomer solubility parameter δ_e using a least squares fit with Eq 3. These values were calculated as $n = 1.17 \times 10^{-3}$ mol/cm^3 and $\delta_e = 21.2$ MPa$^{1/2}$. The calculated elastomer solubility parameter agrees well with literature which gives a range of 18 MPa$^{1/2}$ to 28 MPa$^{1/2}$ [52] depending on the percentage of acrylonitrile in the co-polymer. Finally, fuel C and gasoline are shown to have very similar degrees of swelling in buna-N, justifying fuel C as an appropriate base fuel for this experiment.

Table 5-11 Experimental results for the swelling of Buna-N rubber

Sample Name	Volume (mm³) Before	Volume (mm³) After	Weight (g) O-Ring	Weight (g) Solvent	Weight (g) Solute	O-Ring After	Degree of swelling
Toluene	31.7	74.1	0.0439	0.773		0.0655	2.35
Iso-octane	36.7	35.7	0.044	0.670		0.043	0.98
Fuel C	37.1	48.7	0.046	0.726		0.0539	1.38
Fuel C	36.0	53.5	0.0444	0.654		0.0539	1.50
Fuel C	35.5	48.1	0.0454	0.699		0.0549	1.38
Gasoline	36.9	49.4	0.0455	0.664		0.0532	1.36
Anisole	36.4	106.4	0.046	0.904		0.1134	2.93
Furan	32.7	73.2	0.0455	0.782		0.0758	2.23
Furfural	35.7	82.7	0.0451	1.106		0.1014	2.38
Fuel C Anisole 20%	37.7	61.6	0.0456	0.674	0.274	0.0626	1.66
Fuel C Anisole 2%	37.4	50.4	0.0457	0.739	0.0189	0.0553	1.36
Fuel C Phenol 20%	38.4	99.2	0.0449	0.701	0.193	0.1005	2.62
Fuel C Phenol 2%	35.9	61.7	0.0454	0.682	0.0155	0.0621	1.77
Fuel C Furan 20%	38.0	53.4	0.0457	0.659	0.0944	0.0566	1.44
Fuel C Furan 2%	38.7	47.9	0.0468	0.659	0.0166	0.0561	1.27
Fuel C Furfural 20%	39.9	93.1	0.0467	0.669	0.231	0.1041	2.42
Fuel C Furfural 2%	33.7	50.5	0.0453	0.665	0.0209	0.0583	1.51
Diesel	36.2	38.6	0.0458	0.754		0.0464	1.66

The results from the Flory-Rehner model quantifies the intuition that "like dissolves like", such that identical solubility parameters δ_e and $\delta_{solvent}$ lead to maximum swelling. Because the Buna-N rubber has a much higher solubility parameter than the base fuel C, additives which have a higher solubility parameter than fuel C also have a higher degree of swelling. The next set of experiments tested swelling due to blends of fuel C with approximately 2% and 20% volume fractions of one additive from the model compounds: phenol, anisole, furan, and furfural. Two different models were compared to experiments

122

with blends. In the first, the single-component Flory-Rehner (Eq 3) was used with volume averaged values for interaction parameters and molar volumes. The second model applies the multi-component Flory-Rehner shown in Eq 6-8. A parity plot showing the comparison is shown in Figure 5-49.
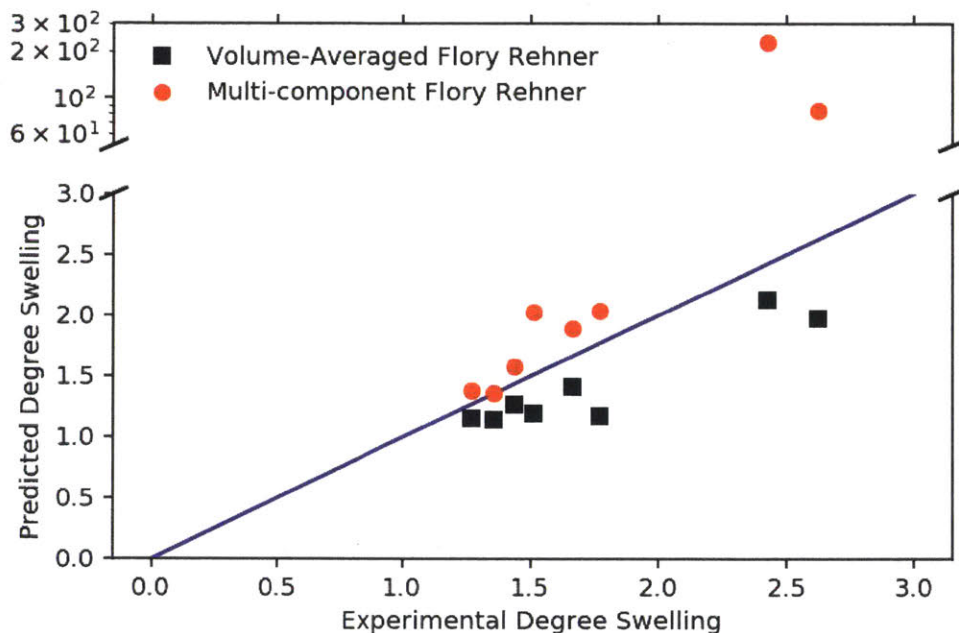
Figure 5-49 Comparison between two volume-averaged and multi-component Flory-Rehner models with experiment for blends of fuel C and additive

Both models generally capture the effect that increasing additive concentration increases the degree of swelling. The volume-averaged Flory-Rehner equation systematically under-predicts the degree of swelling. This method inherently ignores the interaction between solvent species. The under-prediction may occur from ignoring the phase separation between additives and iso-octane because the additives have closer values of solubility parameters with the elastomer than iso-octane. On the other hand, the multi-component Flory-Rehner generally over-predicts the degree of swelling. One mechanism uncaptured by this model is the presence of hydrogen bonding. However, it is unclear how hydrogen bonding would affect the swelling, as both several additives and the acrylonitrile component in the elastomer can potentially participate in hydrogen bonding. The use of Hansen parameters [28] would capture hydrogen bonding, but

these are harder to estimate than Hildebrand which only rely on heat of vaporization. Despite these limitations, both mechanisms give reasonable accuracy and could be used to eliminate additive which greatly swell elastomers.

For 20% phenol and 20% furfural in fuel C, the multi-component Flory-Rehner vastly over-predicts the swelling by at least an order of magnitude. For the purposes of screening drop-in fuels, this is still acceptable as this only occurs when there is also large amount of experimental swelling. Additionally, these volume fractions of phenol and furfural are well outside the range of what would be considered for a drop-in fuel. Still, it is worth investigating the deficiencies in the model which lead to this poor comparison. The primary reason is that Flory-Rehner equation has no limitation on the maximum stretching that can occur in the elastomer. In fact, Eq 5 predicts that the work required to stretch the elastomer approaches 0 as ϕ_e approaches 0, the limit of infinite stretching. Clearly, this prediction is unphysical as one would expect more work for greater stretching and eventual breakage of the cross-links. Also, the liquid phase was assumed to be an infinite reservoir to reduce the number of coupled equations, but that may not be a good assumption when there is a high degree of swelling. The iso-octane is typically the least soluble fuel component in the elastomer. However, it is even less soluble with phenol and furfural, such that it prefers the elastomer. In these outlier cases, when the liquid phase has large amounts of phenol or furfural, the elastomer phase becomes more akin to a pool of iso-octane with some rubber ($\phi_e < 0.02$). Combined with the infinite reservoir assumptions and unlimited stretching, this effect leads to the extreme overestimate of swelling.

5.4 Conclusions

Several computational methods were compiled for the screening of four attributes desirable with fuel components: ignition properties, growth of PAH, liquid solubility, and elastomer compatibility. These tests were then applied to a test case of fuels blended with additives based on the model compounds: phenol, anisole, furan, and furfural, found in bio-oil from the fast pyrolysis of lignin. To test the ignition properties, detailed kinetic mechanisms were automatically generated by RMG. These mechanisms were then simulated at engine-like conditions using butane as a base fuel. It was found that that furan and phenol slowed down auto-ignition, anisole had a negligible effect, and furfural sped up auto-ignition compared to butane. Relevant radical or heat producing pathways were discussed for each model compound.

RMG-generated mechanisms were also created for pyrolysis conditions pertaining to the PAH growth. These mechanisms were simulated in a two-stage PFR system to approximate a diesel flame. It was found that phenol quickly broke down to benzene, while the other additives created cyclopentadiene, which can eventually react to indene. Additionally, all additives created more propargyl. Some pathways toward PAH precursors were presented. Although this methodology was successful in discovering some correct pathways, it was clear that many suggested pathways were unlikely due to poor estimation of thermochemistry or kinetic parameters for aromatics. Additionally, it was impossible to explore all relevant chemical pathways because of the relatively large size of the additives.

The partition coefficient of each additive between FACE #9 and water were estimated using both UNIFAC, a group contribution method, and pp-LFER, which uses fitted empirical parameters. These results were then compared to experimentally measured partition coefficients measured by GC and mass spectrometry. It was found that pp-LFERs were more in agreement with experimentally measured results. In particular, UNIFAC seemed to over-estimate phenol's fuel solubility. Unfortunately, the UNIFAC is more easily generalized than pp-LFERS.

Estimates for elastomer swelling were obtained using Flory-Rehner theory and compared against experimental measurements. Solubility parameters were determined using the Hildebrand definition, which is the most easily estimated for novel compounds. Although the cross-link density and solubility parameter for the rubber was unknown, they were determined to be 1.17×10^{-3} mol/cm^3 and 21.2 $MPa^{1/2}$, respectively, using experiments with pure solvents. Two modifications to the Flory-Rehner equations were proposed to estimate fuel blends: the use of volume-averaged parameters and generalization for multi-component solvents. It was found that the volume-averaged method generally under-predicted elastomer swelling, while the multi-component solvents over-estimated swelling.

This study presents several methodologies for screening desirable attributes of drop-in fuel additives. While none of methods yield results accurate enough to certify additives for use, they are accurate enough to eliminate molecules which fall outside the acceptable range. These computational screens provide a broad, useful, and cheap framework for evaluation for a species potential as a fuel even before performing experiments.

5.5 References

[1]   Heywood, J. B., 1988, *Internal Combustion Engines Fundamentals*, McGraw-Hill, New York.

[2]   ASTM International, 2015, "Standard Test Method for Research Octane Number of Spark-Ignition Engine Fuel," ASTM D2699.

[3]   Daly, S. R., Niemeyer, K. E., Cannella, W. J., and Hagen, C. L., 2016, "Predicting Fuel Research Octane Number Using Fourier-Transform Infrared Absorption Spectra of Neat Hydrocarbons," Fuel, **183**, pp. 359–365.

[4]   Mendes, G., Aleme, H. G., and Barbeira, P. J. S., 2012, "Determination of Octane Numbers in Gasoline by Distillation Curves and Partial Least Squares Regression," Fuel, **97**, pp. 131–136.

[5]   Guan, L., Feng, X. L., Li, Z. C., and Lin, G. M., 2009, "Determination of Octane Numbers for Clean Gasoline Using Dielectric Spectroscopy," Fuel, **88**(8), pp. 1453–1459.

[6]   Albahri, T. A., 2003, "Structural Group Contribution Method for Predicting the Octane Number of Pure Hydrocarbon Liquids," Ind. Eng. Chem. Res., **42**(3), pp. 657–662.

[7]   Ghosh, P., Hickey, K. J., and Jaffe, S. B., 2006, "Development of a Detailed Gasoline Composition-Based Octane Model," Ind. Eng. Chem. Res., **45**(1), pp. 337–345.

[8]   Pope, C. A., Burnett, R. T., Thun, M. J., Calle, E. E., Krewski, D., Ito, K., and Thurston, G. D., 2002, "Lung Cancer, Cardiopulmonary Mortality, and Long-Term Exposure to Fine Particulate Air Pollution | Lung Cancer | JAMA | The JAMA Network," J. Am. Medicial Assoc., **287**(9), pp. 1132–1141.

[9]   Dockery, D. W., Pope, C. A., Xu, X., Spengler, J. D., Ware, J. H., Fay, M. E., Ferris, B. G. J., and Speizer, F. E., 1993, "An Association between Air Pollution and Mortality in Six U.S. Cities," N. Engl. J. Med., **329**(24), pp. 1753–1759.

[10]   McEnally, C. S., Pfefferle, L. D., Atakan, B., and Kohse-Höinghaus, K., 2006, "Studies of Aromatic Hydrocarbon Formation Mechanisms in Flames: Progress towards Closing the Fuel Gap," Prog. Energy Combust. Sci., **32**(3), pp. 247–294.

[11]   Mebel, A. M., Landera, A., and Kaiser, R. I., 2017, "Formation Mechanisms of Naphthalene and Indene: From the Interstellar Medium to Combustion Flames," J. Phys. Chem. A, **121**(5), pp. 901–926.

[12]   Curran, H. J., Fisher, E. M., Glaude, P.-A., Marinov, N. M., Pitz, W. J., Westbrook, C. K., Layton, D. W., Flynn, P. F., Durrett, R. P., Zur Loye, A. O., Akinyemi, O. C., and Dryer, F. L., 2001, "Detailed Chemical Kinetic Modeling of Diesel Combustion with Oxygenated Fuels."

[13]   McEnally, C. S., and Pfefferle, L. D., 2011, "Sooting Tendencies of Oxygenated Hydrocarbons in Laboratory-Scale Flames," Environ. Sci. Technol., **45**(6), pp. 2498–2503.

[14]   Gao, C. W., Allen, J. W., Green, W. H., and West, R. H., 2016, "Reaction Mechanism Generator: Automatic Construction of Chemical Kinetic Mechanisms," Comput. Phys. Commun., **203**, pp. 212–225.

[15]   Gao, C. W., Vandeputte, A. G., Yee, N. W., Green, W. H., Bonomi, R. E., Magoon, G. R., Wong, H.-W., Oluwole, O. O., Lewis, D. K., Vandewiele, N. M., and Van Geem, K. M., 2015, "JP-10 Combustion Studied with Shock Tube Experiments and Modeled with Automatic Reaction Mechanism Generation," Combust. Flame, **162**(8), pp. 3115–3129.

[16]   Class, C. A., Liu, M., Vandeputte, A. G., and Green, W. H., 2016, "Automatic Mechanism Generation for Pyrolysis of Di-Tert-Butyl Sulfide," Phys. Chem. Chem. Phys., **18**(31), pp. 21651–21658.

[17]   Allen, J. W., Scheer, A. M., Gao, C. W., Merchant, S. S., Vasu, S. S., Welz, O., Savee, J. D., Osborn, D. L., Lee, C., Vranckx, S., Wang, Z., Qi, F., Fernandes, R. X., Green, W. H., Hadi, M. Z., and Taatjes, C. A., 2014, "A Coordinated Investigation of the Combustion Chemistry of Diisopropyl Ketone, a Prototype for Biofuels Produced by Endophytic Fungi," Combust. Flame, 161(3), pp. 711–724.

[18]   Yalkowsky, S. H., and Banerjee, S., 1992, *Aqueous Solubility : Methods of Estimation for Organic Compounds*, New York : Marcel Dekker, c1992.

[19]   Fühner, H., 1924, "Die Wasserlöslichkeit in Homologen Reihen," Berichte Dtsch. Chem. Ges. B Ser., 57(3), pp. 510–515.

[20]   Hansch, C., Quinlan, J. E., and Lawrence, G. L., 1968, "Linear Free-Energy Relationship between Partition Coefficients and the Aqueous Solubility of Organic Liquids," J. Org. Chem., 33(1), pp. 347–350.

[21]   Fredenslund, A., Gmehling, J., and Rasmussen, P., 1977, *Equilibria Using UNIFAC a Group-Contribution Method*, Elsevier, Amsterdam.

[22]   J. Kamlet, M., Doherty, R., H. Abraham, M., Carr, P., F. Doherty, R., and W. Taft, R., 1987, "Linear Solvation Energy Relationships. 41. Important Differences between Aqueous Solubility Relationships for Aliphatic and Aromatic Solutes," J. Phys. Chem., 91.

[23]   Arey, J. S., and Gschwend, P. M., 2005, "Estimating Partition Coefficients for Fuel–Water Systems: Developing Linear Solvation Energy Relationships Using Linear Solvent Strength Theory To Handle Mixtures," Environ. Sci. Technol., 39(8), pp. 2702–2710.

[24]   Kass, M., Theiss, T., Janke, C., Pawel, S., Chapin, J. T., Yang, E., and Boyce, K., 2012, "Compatibility of Elastomers with Test Fuels of Gasoline Blended with Ethanol," Seal. Technol., 2012(12), pp. 7–12.

[25]   Flory, P. J., 1942, "Thermodynamics of High Polymer Solutions," J. Chem. Phys., 10(1), pp. 51–61.

[26]   Flory, P. J., and Rehner, J., 1943, "Statistical Mechanics of Cross- Linked Polymer Networks II. Swelling," J. Chem. Phys., 11(11), pp. 521–526.

[27]   Hildebrand, J. H., 1929, "Intermolecular Forces in Liquids," Phys. Rev., 34(6), pp. 984–993.

[28]   Hansen, C. M., 2004, "50 Years with Solubility Parameters—past and Future," Prog. Org. Coat., 51(1), pp. 77–84.

[29]   Mehl, M., Pitz, W. J., Westbrook, C. K., and Curran, H. J., 2011, "Kinetic Modeling of Gasoline Surrogate Components and Mixtures under Engine Conditions," Proc. Combust. Inst., 33(1), pp. 193–200.

[30]   Burke, M. P., Chaos, M., Ju, Y., Dryer, F. L., and Klippenstein, S. J., 2012, "Comprehensive H2/O2 Kinetic Model for High-Pressure Combustion," Int. J. Chem. Kinet., 44(7), pp. 444–474.

[31]   Long, A. E., Grambow, Colin A., Vandeputte, Aäron G., Merchant, Shamel S., and Green, William H., 2017, "New and Realistic Pathways from Cyclopentadiene (CPD) to Naphthalene, Phenanthrene, and Other Soot Precursors," p. paper 1A14.

[32]   Brezinsky, K., Pecullan, M., and Glassman, I., 1998, "Pyrolysis and Oxidation of Phenol," J. Phys. Chem. A, 102(44), pp. 8614–8619.

[33]   Goodwin, D., *"Cantera: An Object-Oriented Software Toolkit for Chemical Kinetics, Thermodynamics, and Transport Processes*, Caltech, Pasadena, 2009.

[34]   Zhang, P., Yee, N. W., Filip, S. V., Hetrick, C. E., Yang, B., and Green, W. H., (submitted), "Modeling Study of the Anti-Knock Tendency of Substituted Phenols as Additives: An Application of the Reaction Mechanism Generator (RMG)," Phys. Chem. Chem. Phys.

[35]   2013, *Chemkin-PRO 15151*, Reaction Design, San Diego.

[36]   Dec, J. E., 1997, "A Conceptual Model of DI Diesel Combustion Based on Laser-Sheet Imaging*."

[37]   Gregory P. Smith, David M. Golden, Michael Frenklach, Nigel W. Moriarty, Boris Eiteneer, Mikhail Goldenberg, C. Thomas Bowman, Ronald K. Hanson, Soonho Song, William C. Gardiner, Vitali V. Lissianski, and Zhiwei Qin, "GRI-Mech 3.0" [Online]. Available: http://combustion.berkeley.edu/gri-mech/version30/text30.html#cite. [Accessed: 05-Jan-2017].

[38]   Senosiain, J. P., Klippenstein, S. J., and Miller, J. A., 2005, "The Reaction of Acetylene with Hydroxyl Radicals," J. Phys. Chem. A, **109**(27), pp. 6045–6055.

[39]   Stewart, P. H., Larson, C. W., and Golden, D. M., 1989, "Pressure and Temperature Dependence of Reactions Proceeding via a Bound Complex. 2. Application to 2CH3 → C2H5 + H," Combust. Flame, **75**(1), pp. 25–31.

[40]   Joshi, A. V., and Wang, H., 2006, "Master Equation Modeling of Wide Range Temperature and Pressure Dependence of CO + OH → Products," Int. J. Chem. Kinet., **38**(1), pp. 57–73.

[41]   Fredenslund, A., Jones, R. L., and Prausnitz, J. M., 1975, "Group-Contribution Estimation of Activity Coefficients in Nonideal Liquid Mixtures," AIChE J., **21**(6), pp. 1086–1099.

[42]   2013, *Aspen-Tech*, Reaction Design, San Diego.

[43]   Anand, K., Ra, Y., Reitz, R. D., and Bunting, B., 2011, "Surrogate Model Development for Fuels for Advanced Combustion Engines," Energy Fuels, **25**(4), pp. 1474–1484.

[44]   Abraham, M. H., Andonian-Haftvan, J., Whiting, G. S., Leo, A., and Taft, R. S., 1994, "Hydrogen Bonding. Part 34. The Factors That Influence the Solubility of Gases and Vapours in Water at 298 K, and a New Method for Its Determination," J. Chem. Soc. Perkin Trans. 2, **0**(8), pp. 1777–1791.

[45]   Ulrich, N. . E., S. ..Brown, T. N. ..Watanabe, N. ..Bronner, G. ..Abraham, M. H. ..Goss, K. U., 2017, "UFZ-LSER Database v 3.2 [Internet]."

[46]   "NIST Chemistry WebBook" [Online]. Available: http://webbook.nist.gov/chemistry/. [Accessed: 19-Oct-2017].

[47]   Okeowo, O., and Dorgan, J. R., 2006, "Multicomponent Swelling of Polymer Networks," Macromolecules, **39**(23), pp. 8193–8202.

[48]   Godbole, R. V., Khabaz, F., Khare, R., and Hedden, R. C., 2017, "Swelling of Random Copolymer Networks in Pure and Mixed Solvents: Multi-Component Flory–Rehner Theory," J. Phys. Chem. B, **121**(33), pp. 7963–7977.

[49]   Oliphant, T. E., 2007, "Python for Scientific Computing," Comput. Sci. Eng., **9**(3), pp. 10–20.

[50]   Ratcliff, M. A., Burton, J., Sindler, P., Christensen, E., Fouts, L., Chupka, G. M., and McCormick, R. L., 2016, "Knock Resistance and Fine Particle Emissions for Several Biomass-Derived Oxygenates in a Direct-Injection Spark-Ignition Engine," SAE Int. J. Fuels Lubr., **9**(1), pp. 59–70.

[51]   Westbrook, C. K., 2000, "Chemical Kinetics of Hydrocarbon Ignition in Practical Combustion Systems," Proc. Combust. Inst., **28**(2), pp. 1563–1577.

[52]   Barton, A. F. M., 1990, *CRC Handbook of Polymer-Liquid Interaction Parameters and Solubility Parameters*, CRC Press, Boca Raton, Florida.

Chapter 6

Conclusions and Recommendations

In this work, we have made improvements to and characterized the performance of the Reaction Mechanim Generator (RMG) database, a powerful tool for estimating the thermochemistry and kinetic parameters. We have also applied the entire RMG software to modeling the chemical kinetics of a variety of fuel blends. The primary focus in of these models was prediction the auto-ignition of fuel blends, both for better fundamental understanding of well-studied fuels and for prediction of novel fuel components. A smaller amount of this work was focused on modeling other properties that limit the feasibility of changing fuel composition: tendency to produce soot, liquid solubility, and elastomer swelling. In earlier chapters, we demonstrated state-of-the-art capabilities for predicting some of these fuel performance parameters, based on improvements we made to the database. In this chapter, we highlight areas where further improvements are needed, to guide future work in this area.

6.1 Improvements to RMG Database

We have presented updated structures and features for the database which include new atom types, corrected averaging schemes, and guidelines for writing groups for families. Validation tests were performed for the thermo database against CBS-QB3/B3LYP calculated enthalpies of formation. It was found that hydrocarbons and oxygenates have mean average enthalpy errors of 5.96 kcal/mole for non-

cyclics and 6.49 kcal/mole for cyclics. Nitrogenated compounds still lack some essential groups, causing a large amount of errors for nitrogen-containing compounds with triple bonds. This should be corrected soon.

Reaction rates at 1000K were also validated against the NIST chemical database. It was found that exact matches are typically within an order of magnitude in accuracy, while averaged matches were within a multiplicative error of about 22.

A considerable amount of time was spent removing inconsistencies in the database. A large issue was that the structure of the database was so convoluted, many users were discouraged to contribute at all. When they did, they often did so with few specific guidelines. As a result, they were prone to making mistakes, particularly when creating new groups for the various trees. To remedy the situation, various unit tests were implemented to ensure that groups were accessible when RMG descends the tree. A multitude of bugs were caught and fixed in the making of the unit tests. In addition, a simple run of the unit test will inform new contributors of any mistakes that have been encountered before. However, the status quo is probably still insufficient in terms of both testing and reducing the hurdles for users to contribute.

It is essential for the continued growth and improvement of the database that users contribute new data. The two common reasons why users do not contribute their data to the database are tediousness in making the additions and fear of destroying the accuracy of predictions. For the former problem, automated scripts should be made that not only add training reactions but suggest and create appropriate groups. Current RMG developers already have developed many tools required for this, but they should be consolidated and made official to users outside the group. The latter problem could be handled with better regression testing, and comparisons of new versions of RMG to benchmarked versions. We have already implemented RMG-tests to compare species, thermochemistry, and reaction rates between versions for specifically designed test mechanisms. However, this information is often not useful; significant changes in the database *will* change these parameters, but the user does not know if the new values are an improvement. In these regression tests, it would be better to implement automated validation, particularly with experimental data for systems previously studied by RMG. If a user could see that their additions have not changed, or perhaps even improved, predictions of these systems, they will have more confidence that their modifications to the RMG database have not "broken" RMG's estimates.

Although some thought may have been put into group placement during the creation of the tree, most new entries are added *ad hoc* for whatever model they are trying to create. This results in the current nodal placement which has little reasoning other than making each entry accessible. Ideally,

structural groups which cause the largest difference in reaction rates should be differentiated near the top of the tree. This scheme would improve the accuracy of averaged matches because templates with similar reaction rates would also have small 2-norm distance. Such a tree organization may also provide some insight on how to assign nodal distances; important differences would be at the top, and less important differences would be at the bottom. It is likely that some automated optimization would be necessary to achieve this reorganization. Training reactions are a newer and generally superior style for adding kinetic parameters when the reaction is specified. Many rules should be training reactions, but were added before training reactions were a feature. It is recommended that these rules be converted into training reaction to enable more aggressive tree restructuring.

While a great deal of work has been accomplished for estimating their thermochemistry, cyclics and polycyclics are still difficult to correctly represent in unimolecular reactions. These reactions are usually double counted because two different backbones can be matched by labeling clockwise or counter-clockwise on the ring. It is probably necessary to divide unimolecular families into a linear version and a cyclic version, if not for the backbone labelling problem, at least to separate kinetic parameters, which should be vastly different. In addition, it might be necessary to implement a new algorithm to match the backbones to prevent double counting. Finally, the rules developed in section 2.4.2 are too restrictive for these newly proposed families; some deliberation should be given to making separate rules for the cyclic families.

6.2 Low Temperature Oxidation Pathways for Small Molecules

This section of work is focused on simplifying the models for fuel ignition from full detailed kinetic mechanisms to, when possible, analytical expressions or reduced mechanisms with only reactions that effect ignition. Although alkane oxidation appears to have two stages of ignition by pressure trace, previous work has shown that there are in fact four chemically distinct stages:

1. Stage 0: a brief induction stage
2. Stage 1A: a period of exponential rise in radicals
3. Stage 1B: slowing radical production punctuated with sudden drop in radical concentration
4. Stage 2: Temperature rise until H_2O_2 decomposition leads to final ignition.

Stage 0 and Stage 1A for propane had already been reduced to analytical expressions in terms of initial conditions and rate parameters. This work reports the important heat producing reactions in stage 1B and stage 2; it then is able to give a reduced mechanism for propane. A similar approach was applied to methanol, discovering only three stages of ignition:

133

1. Stage 0: a brief induction stage

2. Stage 1A: a period of exponential rise in radicals

3. Stage 2: Temperature rise until H_2O_2 decomposition leads to final ignition.

Similar to propane, we were able to reduce the timings for stage 0 and stage 1A to an analytical expression and give a final reduced mechanism for the entire ignition. It was found that the only significant source of heat pre-ignition was the creation of formaldehyde. We had originally set out with the ultimate goal of expressing each of methanol's stages with analytical expressions, but we were unable to decouple formaldehyde mole fraction from HO_2's. This left a system of ODEs that still required numerical methods to solve. Further analysis may be able to find a correlation for the formaldehyde concentration to enable a fully analytical expression.

We recommend that this analysis be applied to other model compounds. Highly branched alkanes and aromatics are the other main components in gasoline, and ethers have been used as fuel additives. Perhaps neo-pentane, toluene, and tert-butyl ether would make good model compounds, although their larger size than propane may be a cause of concern. Studying a blend of these fuels may be a good next step in better fundamental understanding for gasoline ignition.

6.3 Detailed Kinetic Mechanisms for Auto Ignition

This work used detailed kinetic mechanisms to model the auto-ignition of fuel blended with a number of additives derived from bio-oils: p-cresol, o-cresol, m-cresol, ethylphenol, xylenol, guaiacol, phenol, anisole, furan, and furan. A special variable volume reactor was created to simulate the Cooperative Fuel Research (CFR) engine used to determine Research Octane Number (RON) number. For the first six additives, we were able to show that *a priori* predictions were able to correctly rank the RON of blends when compared with experimental measurements. Rate of production and sensitivity analysis for OH gave insight on the chemistry that leads to changes in ignition delay.

The main challenge for generation of the mechanisms was the large size, eventually causing RMG iterations to slow down significantly. The limiting factor may not simply be speed and memory of the software. Despite the recent efforts by Kehang Han and Zachary Buras to improve thermochemistry prediction, RMG still includes many species that appear to have infeasibly strained rings. As mentioned in Section 4.2.1, many of these species were manually removed from the mechanism after generation. Further improvement for estimating the thermochemistry would allow RMG to explore more relevant pathways. Perhaps additional Benson groups supplemented by heuristics is not sufficient given the large combinatorial number of polycyclics. Applying machine-learning to estimating thermochemistry is already being explored by other students and may become a necessity for these complex fuels.

Although we have been able to use variable volume reactors to predict RON's, it is becoming increasingly clear that octane numbers are a bad metric for novel engines. In the future, we should see if we can apply similar simple models to actual engines instead of the CFR engine.

6.4 Feasibility Screens for Fuel Additives

In this study, we developed or applied existing theory to test for sooting tendency, water/fuel solubility, and elastomer swelling for fuel additives. The screen for sooting tendency lacks validation, which is important to prove that our models give good predictions. As mentioned in section 5.1, experiments for smoke point in open flames performed by Dr. McEnally's research group is a good experimental set for validation. However, it might be necessary to develop a new physical model for this system. In addition, the poor estimation of polycyclic thermochemistry discussed in the previous section is even more limiting in models for PAH growth. Rate of production analysis was performed for the mechanisms, but the large size made it impossible to carry out comprehensive sensitivity analysis.

It will probably be difficult for pre-experimental screens to become a common practice without making them more expedient. As pointed out by our collaborators at BP, it is still easier for them to actually run the ASTM for RON than to create a detailed mechanism. The proposed tests for solubility and elastomer swelling also require quite a few parameters, which may or may not be available in literature. If spreading the practice is a goal, it will probably be necessary to compile all the screens into a software suite, which can automatically query literature for parameters. In particular, the multi-component Flory-Rehner model requires solving a system of equations with a large number of terms, so providing a general-purpose computer implementation would be very useful. Another necessary step would be the inclusion of feasibility tests for other parameters like heating value or toxicity.

Appendix A

Volume Profile used in Engine-Like simulation

Table A-12 Pressure and Volume profile for engine-like simulation for PRF100.
Averaged from over 500 CRF PRF100 runs

Crank Angle Degree	Time (ms)	P (bar)	V (cm^3)
-146	0.000	1.089	9.027
-145	0.278	1.088	9.027
-144	0.556	1.092	9.008
-143	0.835	1.101	8.957
-142	1.113	1.109	8.908
-141	1.391	1.108	8.913
-140	1.669	1.113	8.882
-139	1.948	1.106	8.926
-138	2.226	1.126	8.805
-137	2.504	1.129	8.790
-136	2.782	1.139	8.732
-135	3.061	1.138	8.736
-134	3.339	1.147	8.688
-133	3.617	1.156	8.636
-132	3.895	1.159	8.615
-131	4.174	1.170	8.559
-130	4.452	1.178	8.515
-129	4.730	1.195	8.424
-128	5.008	1.206	8.367

(Table continued on next page)

Crank Angle Degree	Time (ms)	P (bar)	V (cm^3)
-127	5.287	1.216	8.314
-126	5.565	1.217	8.307
-125	5.843	1.233	8.229
-124	6.121	1.239	8.196
-123	6.400	1.241	8.190
-122	6.678	1.258	8.107
-121	6.956	1.277	8.014
-120	7.234	1.284	7.981
-119	7.513	1.302	7.897
-118	7.791	1.302	7.901
-117	8.069	1.315	7.841
-116	8.347	1.335	7.752
-115	8.625	1.349	7.691
-114	8.904	1.370	7.601
-113	9.182	1.378	7.571
-112	9.460	1.396	7.495
-111	9.738	1.410	7.441
-110	10.017	1.416	7.419
-109	10.295	1.436	7.340
-108	10.573	1.455	7.265
-107	10.851	1.479	7.178
-106	11.130	1.492	7.131
-105	11.408	1.511	7.062
-104	11.686	1.535	6.981
-103	11.964	1.558	6.902
-102	12.243	1.562	6.888
-101	12.521	1.588	6.803
-100	12.799	1.609	6.736
-99	13.077	1.636	6.655
-98	13.356	1.664	6.569
-97	13.634	1.684	6.511
-96	13.912	1.720	6.409
-95	14.190	1.745	6.339
-94	14.469	1.767	6.281
-93	14.747	1.780	6.245
-92	15.025	1.820	6.141
-91	15.303	1.853	6.058
-90	15.582	1.877	6.001
-89	15.860	1.910	5.921

Crank Angle Degree	Time (ms)	P (bar)	V (cm^3)
-88	16.138	1.939	5.854
-87	16.416	1.983	5.757
-86	16.694	2.009	5.700
-85	16.973	2.053	5.608
-84	17.251	2.093	5.527
-83	17.529	2.128	5.457
-82	17.807	2.172	5.375
-81	18.086	2.206	5.312
-80	18.364	2.246	5.240
-79	18.642	2.295	5.156
-78	18.920	2.338	5.084
-77	19.199	2.397	4.990
-76	19.477	2.432	4.935
-75	19.755	2.483	4.858
-74	20.033	2.545	4.768
-73	20.312	2.605	4.685
-72	20.590	2.659	4.612
-71	20.868	2.718	4.537
-70	21.146	2.764	4.479
-69	21.425	2.843	4.385
-68	21.703	2.908	4.310
-67	21.981	2.971	4.241
-66	22.259	3.055	4.151
-65	22.538	3.127	4.079
-64	22.816	3.202	4.007
-63	23.094	3.278	3.935
-62	23.372	3.362	3.861
-61	23.651	3.446	3.789
-60	23.929	3.546	3.707
-59	24.207	3.627	3.644
-58	24.485	3.735	3.564
-57	24.763	3.829	3.497
-56	25.042	3.934	3.426
-55	25.320	4.040	3.357
-54	25.598	4.152	3.288
-53	25.876	4.275	3.216
-52	26.155	4.385	3.154
-51	26.433	4.527	3.078
-50	26.711	4.653	3.014

(Table continued on next page)

Crank Angle Degree	Time (ms)	P (bar)	V (cm^3)
-49	26.989	4.788	2.949
-48	27.268	4.937	2.881
-47	27.546	5.075	2.821
-46	27.824	5.246	2.750
-45	28.102	5.393	2.693
-44	28.381	5.559	2.631
-43	28.659	5.743	2.566
-42	28.937	5.902	2.513
-41	29.215	6.085	2.455
-40	29.494	6.289	2.394
-39	29.772	6.478	2.340
-38	30.050	6.689	2.283
-37	30.328	6.889	2.232
-36	30.607	7.113	2.178
-35	30.885	7.341	2.126
-34	31.163	7.563	2.078
-33	31.441	7.813	2.027
-32	31.720	8.044	1.981
-31	31.998	8.305	1.933
-30	32.276	8.568	1.887
-29	32.554	8.833	1.844
-28	32.832	9.102	1.802
-27	33.111	9.380	1.760
-26	33.389	9.674	1.719
-25	33.667	9.957	1.681
-24	33.945	10.244	1.644
-23	34.224	10.544	1.608
-22	34.502	10.837	1.574
-21	34.780	11.138	1.541
-20	35.058	11.441	1.510
-19	35.337	11.738	1.480
-18	35.615	12.034	1.452
-17	35.893	12.333	1.425
-16	36.171	12.622	1.399
-15	36.450	12.916	1.374
-14	36.728	13.181	1.353
-13	37.006	13.454	1.332
-12	37.284	13.711	1.312
-11	37.563	13.973	1.293

Crank Angle Degree	Time (ms)	P (bar)	V (cm^3)
-10	37.841	14.248	1.274
-9	38.119	14.529	1.255
-8	38.397	14.865	1.232
-7	38.676	15.241	1.209
-6	38.954	15.646	1.184
-5	39.232	16.095	1.159
-4	39.510	16.549	1.134
-3	39.789	17.043	1.108
-2	40.067	17.577	1.082
-1	40.345	18.161	1.055
0	40.623	18.780	1.027
1	40.902	19.443	1.000
2	41.180	20.145	0.973
3	41.458	20.878	0.946
4	41.736	21.617	0.921
5	42.014	22.389	0.896
6	42.293	23.144	0.873
7	42.571	23.899	0.851
8	42.849	24.621	0.831
9	43.127	25.354	0.813
10	43.406	26.077	0.795
11	43.684	26.799	0.778
12	43.962	27.498	0.763
13	44.240	28.189	0.748
14	44.519	28.917	0.733
15	44.797	29.679	0.718
16	45.075	30.526	0.703
17	45.353	31.371	0.688
18	45.632	32.264	0.673
19	45.910	33.363	0.655
20	46.188	34.499	0.638
21	46.466	35.376	0.626
22	46.745	36.128	0.615
23	47.023	36.504	0.610
24	47.301	36.506	0.610
25	47.579	36.243	0.614
26	47.858	35.641	0.622
27	48.136	34.987	0.631
28	48.414	34.124	0.644

Crank Angle Degree	Time (ms)	P (bar)	V (cm³)
29	48.692	33.272	0.657
30	48.971	32.342	0.671
31	49.249	31.475	0.686
32	49.527	30.484	0.703
33	49.805	29.572	0.720
34	50.083	28.667	0.738
35	50.362	27.793	0.756
36	50.640	26.928	0.775
37	50.918	26.066	0.795
38	51.196	25.230	0.816
39	51.475	24.458	0.836
40	51.753	23.702	0.857
41	52.031	22.978	0.878
42	52.309	22.252	0.900
43	52.588	21.603	0.921
44	52.866	20.947	0.944
45	53.144	20.329	0.966
46	53.422	19.745	0.988
47	53.701	19.146	1.012
48	53.979	18.604	1.035
49	54.257	18.054	1.059
50	54.535	17.535	1.084

Table A-13 Pressure and Volume profile for engine-like simulation for PFR90.
Averaged from over 500 CRF PRF90 runs

Crank Angle Degree	Time (ms)	P (bar)	V (cm^3)
-146	0.000	1.089	6.328
-145	0.278	1.093	6.311
-144	0.556	1.094	6.304
-143	0.835	1.113	6.225
-142	1.113	1.108	6.246
-141	1.391	1.106	6.257
-140	1.669	1.128	6.162
-139	1.948	1.118	6.205
-138	2.226	1.128	6.163
-137	2.504	1.127	6.166
-136	2.782	1.143	6.101
-135	3.061	1.146	6.091
-134	3.339	1.152	6.067
-133	3.617	1.156	6.051
-132	3.895	1.178	5.967
-131	4.174	1.177	5.970
-130	4.452	1.188	5.929
-129	4.730	1.186	5.935
-128	5.008	1.207	5.857
-127	5.287	1.210	5.846
-126	5.565	1.219	5.817
-125	5.843	1.231	5.774
-124	6.121	1.232	5.770
-123	6.400	1.246	5.722
-122	6.678	1.256	5.687
-121	6.956	1.268	5.645
-120	7.234	1.279	5.611
-119	7.513	1.295	5.558
-118	7.791	1.301	5.538
-117	8.069	1.322	5.473
-116	8.347	1.334	5.434
-115	8.625	1.332	5.440
-114	8.904	1.351	5.383
-113	9.182	1.372	5.323
-112	9.460	1.388	5.277
-111	9.738	1.400	5.241
-110	10.017	1.407	5.222

Crank Angle Degree	Time (ms)	P (bar)	V (cm³)
-109	10.295	1.430	5.159
-108	10.573	1.444	5.121
-107	10.851	1.459	5.081
-106	11.130	1.471	5.051
-105	11.408	1.496	4.988
-104	11.686	1.509	4.955
-103	11.964	1.530	4.904
-102	12.243	1.547	4.864
-101	12.521	1.567	4.816
-100	12.799	1.584	4.778
-99	13.077	1.617	4.705
-98	13.356	1.628	4.681
-97	13.634	1.656	4.621
-96	13.912	1.676	4.580
-95	14.190	1.706	4.518
-94	14.469	1.724	4.483
-93	14.747	1.751	4.431
-92	15.025	1.765	4.405
-91	15.303	1.793	4.352
-90	15.582	1.823	4.298
-89	15.860	1.847	4.256
-88	16.138	1.883	4.194
-87	16.416	1.917	4.139
-86	16.694	1.936	4.108
-85	16.973	1.973	4.049
-84	17.251	2.002	4.005
-83	17.529	2.044	3.943
-82	17.807	2.076	3.897
-81	18.086	2.119	3.837
-80	18.364	2.143	3.805
-79	18.642	2.207	3.722
-78	18.920	2.237	3.684
-77	19.199	2.269	3.644
-76	19.477	2.318	3.586
-75	19.755	2.356	3.542
-74	20.033	2.411	3.481
-73	20.312	2.459	3.430
-72	20.590	2.511	3.376
-71	20.868	2.560	3.326

Crank Angle Degree	Time (ms)	P (bar)	V (cm^3)
-70	21.146	2.611	3.278
-69	21.425	2.664	3.228
-68	21.703	2.727	3.171
-67	21.981	2.775	3.129
-66	22.259	2.842	3.074
-65	22.538	2.899	3.028
-64	22.816	2.971	2.972
-63	23.094	3.037	2.923
-62	23.372	3.095	2.881
-61	23.651	3.163	2.834
-60	23.929	3.251	2.776
-59	24.207	3.316	2.734
-58	24.485	3.405	2.680
-57	24.763	3.473	2.640
-56	25.042	3.565	2.588
-55	25.320	3.657	2.538
-54	25.598	3.743	2.494
-53	25.876	3.841	2.445
-52	26.155	3.935	2.401
-51	26.433	4.028	2.358
-50	26.711	4.125	2.316
-49	26.989	4.230	2.272
-48	27.268	4.339	2.229
-47	27.546	4.460	2.182
-46	27.824	4.581	2.138
-45	28.102	4.689	2.100
-44	28.381	4.804	2.062
-43	28.659	4.948	2.016
-42	28.937	5.058	1.982
-41	29.215	5.195	1.942
-40	29.494	5.337	1.903
-39	29.772	5.476	1.865
-38	30.050	5.633	1.825
-37	30.328	5.780	1.790
-36	30.607	5.939	1.753
-35	30.885	6.080	1.722
-34	31.163	6.248	1.686
-33	31.441	6.404	1.655
-32	31.720	6.570	1.623

(Table continued on next page)

Crank Angle Degree	Time (ms)	P (bar)	V (cm^3)
-31	31.998	6.735	1.592
-30	32.276	6.908	1.561
-29	32.554	7.069	1.534
-28	32.832	7.254	1.504
-27	33.111	7.433	1.476
-26	33.389	7.611	1.449
-25	33.667	7.791	1.423
-24	33.945	7.977	1.398
-23	34.224	8.154	1.374
-22	34.502	8.337	1.351
-21	34.780	8.518	1.329
-20	35.058	8.691	1.309
-19	35.337	8.869	1.288
-18	35.615	9.048	1.269
-17	35.893	9.216	1.251
-16	36.171	9.380	1.234
-15	36.450	9.558	1.216
-14	36.728	9.692	1.203
-13	37.006	9.834	1.190
-12	37.284	9.983	1.176
-11	37.563	10.112	1.164
-10	37.841	10.247	1.152
-9	38.119	10.381	1.141
-8	38.397	10.520	1.129
-7	38.676	10.665	1.117
-6	38.954	10.828	1.104
-5	39.232	11.011	1.090
-4	39.510	11.193	1.076
-3	39.789	11.393	1.062
-2	40.067	11.601	1.047
-1	40.345	11.817	1.032
0	40.623	12.055	1.016
1	40.902	12.309	1.000
2	41.180	12.584	0.983
3	41.458	12.875	0.966
4	41.736	13.195	0.948
5	42.014	13.537	0.929
6	42.293	13.898	0.910
7	42.571	14.291	0.891

Crank Angle Degree	Time (ms)	P (bar)	V (cm^3)
8	42.849	14.720	0.870
9	43.127	15.162	0.851
10	43.406	15.650	0.830
11	43.684	16.160	0.810
12	43.962	16.673	0.790
13	44.240	17.205	0.771
14	44.519	17.727	0.753
15	44.797	18.267	0.736
16	45.075	18.794	0.720
17	45.353	19.292	0.705
18	45.632	19.795	0.691
19	45.910	20.279	0.678
20	46.188	20.746	0.666
21	46.466	21.210	0.655
22	46.745	21.662	0.644
23	47.023	22.113	0.634
24	47.301	22.578	0.624
25	47.579	23.017	0.614
26	47.858	23.454	0.605
27	48.136	23.845	0.598
28	48.414	24.202	0.591
29	48.692	24.499	0.585
30	48.971	24.707	0.581
31	49.249	24.779	0.580
32	49.527	24.739	0.581
33	49.805	24.598	0.583
34	50.083	24.348	0.588
35	50.362	24.012	0.594
36	50.640	23.606	0.602
37	50.918	23.178	0.611
38	51.196	22.668	0.622
39	51.475	22.202	0.632
40	51.753	21.638	0.645
41	52.031	21.140	0.657
42	52.309	20.600	0.670
43	52.588	20.068	0.684
44	52.866	19.572	0.697
45	53.144	19.054	0.712
46	53.422	18.600	0.726

(Table continued on next page)

Crank Angle Degree	Time (ms)	P (bar)	V (cm³)
47	53.701	18.116	0.741
48	53.979	17.638	0.756
49	54.257	17.182	0.772
50	54.535	16.758	0.787